

THE UNIVERSITY OF CALGARY

**AVI Multilayer Forest Classification
Using Airborne Image Texture**

by

Ludmila Monika Moskal

**A THESIS SUBMITTED TO THE
FACULTY OF GRADUATE STUDIES IN PARTIAL
FULFILLMENT OF THE REQUIREMENTS FOR THE DEGREE OF
MASTER OF SCIENCE**

DEPARTMENT OF GEOGRAPHY

**CALGARY, ALBERTA
DECEMBER, 1999**

©Ludmila Monika Moskal 1999



**National Library
of Canada**

**Acquisitions and
Bibliographic Services**

**395 Wellington Street
Ottawa ON K1A 0N4
Canada**

**Bibliothèque nationale
du Canada**

**Acquisitions et
services bibliographiques**

**395, rue Wellington
Ottawa ON K1A 0N4
Canada**

Your file Votre référence

Our file Notre référence

The author has granted a non-exclusive licence allowing the National Library of Canada to reproduce, loan, distribute or sell copies of this thesis in microform, paper or electronic formats.

The author retains ownership of the copyright in this thesis. Neither the thesis nor substantial extracts from it may be printed or otherwise reproduced without the author's permission.

L'auteur a accordé une licence non exclusive permettant à la Bibliothèque nationale du Canada de reproduire, prêter, distribuer ou vendre des copies de cette thèse sous la forme de microfiche/film, de reproduction sur papier ou sur format électronique.

L'auteur conserve la propriété du droit d'auteur qui protège cette thèse. Ni la thèse ni des extraits substantiels de celle-ci ne doivent être imprimés ou autrement reproduits sans son autorisation.

0-612-49649-X

Canada

ABSTRACT

In this study a Compact Airborne Spectrographic Imager (*casi*) multiresolution data set, acquired over the Kananaskis Barrier Lake mix-wood forest in the Rocky Mountains of Alberta, was analyzed for classification accuracies using forest cover types outlined by the Alberta Vegetation Inventory (AVI), with special emphases on identifying multistory canopies and species composition. Seven spectral channels, existing in the three resolutions of the imagery (60 cm, 1m, 2 m), and five textural channels derived from second-order texture measures of the 'brightness' component of the imagery, were used in discriminant analysis to determine the usefulness of the textural information and compare two sample stratification schemes (six-class using only the first AVI canopy layer and thirteen-class using all AVI canopy layers) based on the AVI label. Field data used to determine classification accuracies included a plot level survey of species composition by basal area, crown closures, stem count, height, dbh and additional site descriptors such as slope and aspect. On average, the use of texture channels improved the per-plot classification accuracies by 17% compared to using the spectral channels alone. The highest per pixel resolution imagery of 60 cm outperformed the other image resolutions (1 m and 2 m) and the thirteen-class sample stratification scheme improved the classification accuracies by 14%, with results of 87% and a KHAT of 0.85, compared to the six-class sample stratification scheme results of 72% and a KHAT of 0.73.

ACKNOWLEDGEMENTS

Most importantly I would like to thank my parents for encouraging independent thinking, at an early age; their lessons have made me who I am today.

I am grateful to my supervisor, Dr. Steven E. Franklin, who provided an opportunity for me to undertake this research. Dr. Franklin's contagious enthusiasm towards science and remote sensing has been inspiring. I would also like to give a special acknowledgement and thank you to the other members of my committee, Dr. Mryka Hall-Beyer for her guidance and encouragement and Dr. Robert W. Longair for offering a biological perspective and providing a thorough review of my thesis. In addition, thank you to Dr. Derek Peddle (University of Lethbridge) for participating in my thesis proposal defense.

Enough can not be said about all the individuals assisting me during my field season, but most importantly I would like to thank Dr. Ron Hall of the Canadian Forest Service for giving freely of his time, knowledge and expertise. Thank you to all of the field research assistants: Cynthia Huculak, Mira Kunes, Beth Dickson and Glenda Samuelson and the University of Regina and University of Lethbridge research teams.

I would also like to acknowledge and thank the staff, technicians and co-op students at the University of Calgary, Kananaskis Field Station (Barrier Lake), for providing equipment, technical expertise and most importantly, Ines Kwan, field assistant extraordinaire. Likewise a special thank you to the Department of Geography, staff, faculty and students.

Last but not least I would like to thank my colleagues Median Deuling, Beth Dickson, Graham Gerylo and Al Maudie who offered friendship, assistance and critical thought (and sometimes pen) during my graduate studies.

Support for this thesis came from Dr. S.E. Franklin's NSERC Grant, Teaching Assistantships and Graduate Research Scholarships supplied by the Faculty of Graduate Studies, through the Department of Geography.

DEDICATION

W pamięci Izabeli Olejniczak

TABLE OF CONTENENTS

APPROVAL PAGE.....	ii
ABSTRACT.....	iii
ACKNOWLEDGEMENTS.....	iv
DEDICATION.....	v
TABLE OF CONTENTS.....	vi
LIST OF TABLES.....	ix
LIST OF FIGURES AND PLATES.....	xi
CHAPTER 1 INTRODUCTION AND RESEARCH OBJECTIVES.....	1
1.1 INTRODUCTION	1
1.2 RESEARCH OBJECTIVES	5
1.3 THESIS ORGANIZATION	6
CHAPTER 2 REMOTE SENSING OF FOREST STRUCTURE	8
2.1 INTRODUCTION	8
2.2 REMOTE SENSING IN FOREST INVENTORY METHODS.....	8
2.3 CHARACTERISTICS OF AVI.....	11
2.4 DIGITAL METHODS APPLIED TO IMAGERY IN FORESTRY APPLICATIONS.....	15
2.5 CHARACTERISTICS OF <i>CASI</i>	18
2.6 APPLICATION OF TEXTURE IN IMAGE CLASSIFICATION	19
2.7 CHAPTER SUMMARY	23
CHAPTER 3 STUDY AREA AND DATA COLLECTED.....	25
3.1 LOCATION AND DESCRIPTION OF THE STUDY AREA.....	25
3.2 DATA ACQUISITION	28
3.2.1 <i>Field Data</i>	28
3.2.1.1 Spectroradiometer Data.....	29
3.2.1.2 Sampling Procedure	29
3.2.1.3 GPS Data Collection	30
3.2.1.4 Forest Measurements	31
3.2.2 <i>casi Imagery</i>	36
3.3 CHAPTER SUMMARY	39
CHAPTER 4 METHODOLOGY	40
4.1 INTRODUCTION	40
4.2 BASAL AREA AND AVI PLOT LABELS.....	41

4.2.1.1	Sample Stratification Based on AVI First Canopy Layer.....	44
4.2.1.2	Sample Stratification Based on All AVI Canopy Layers	44
4.3	IMAGE PREPARATION AND STATISTICAL DATA EXTRACTION	47
4.4	PRINCIPAL COMPONENT ANALYSIS.....	49
4.5	STRUCTURE AND <i>CAS</i> /IMAGERY SHADOW	54
4.6	CREATION OF TEXTURE CHANNELS	55
4.7	TEXTURE AND <i>CAS</i> /IMAGERY SHADOW.....	58
4.8	STATISTICAL DATA EXTRACTION FROM <i>CAS</i> /IMAGERY	60
4.9	CLASSIFICATION PROCEDURE	60
4.10	ACCURACY ASSESSMENT	62
4.11	CHAPTER SUMMARY	64
CHAPTER 5	RESULTS AND ANALYSIS	65
5.1	INTRODUCTION	65
5.2	VISUAL INTERPRETATION OF IMAGE TEXTURE	66
5.3	DESCRIPTIVE STATISTICAL INTERPRETATION OF TEXTURE.....	73
5.4	EXAMPLE OF RELATIONSHIP BETWEEN TEXTURE AND FIELD DATA	74
5.5	DISCRIMINANT ANALYSIS RESULTS.....	79
5.5.1	<i>Results using the first AVI Layer</i>	<i>79</i>
5.5.2	<i>Results Using All AVI Layers.....</i>	<i>88</i>
5.6	CHAPTER SUMMARY	101
CHAPTER 6	SUMMARY AND CONCLUSIONS	103
6.1	SUMMARY.....	103
6.2	CONCLUSIONS AND CONTRIBUTIONS TO RESEARCH	106
6.3	RECOMMENDATIONS FOR FURTHER RESEARCH	107
REFERENCES	109
APPENDIX A:	EXAMPLES OF ORIGINAL PLOT DATA COLLECTED IN THE FIELD	119
APPENDIX B:	PER SPECIES CONTRIBUTIONS TO CROWN CLOSURE AND PER SPECIES BASAL AREA USING THE FIRST AND OTHER LAYERS (DATA AND BIVARIATE LINEAR REGRESSIONS)	120
APPENDIX C:	PER PLOT PERCENT OF SHADOW PIXELS AND STAND COMPLEXITY INDEX (DATA AND BIVARIATE LINEAR REGRESSION).....	122
APPENDIX D:	SUBSET WINDOW TEXTURE VISUAL INTERPRETATION FIGURES.....	124

APPENDIX E: RADIANCE FOR ASPEN (SHOWING RANGE OF DEFOLIATION) AND CONIFER STANDS USING 60 CM <i>CASI</i> IMAGERY	136
---	------------

LIST OF TABLES

Table 2.1 AVI classification: moisture regime	12
Table 2.2 AVI classification: crown closure.....	12
Table 2.3 AVI species abbreviations	13
Table 2.4 AVI classification: tree age adjustment factor.....	14
Table 2.5 AVI Classification: timber productivity rating (TPR)	14
Table 2.6 Technical specifications of <i>casi</i>	18
Table 3.1 Crown closures for the 45 study plots.....	35
Table 3.2 <i>casi</i> Bands for the three image resolutions	38
Table 4.1 AVI labels for the 45 study plots	43
Table 4.1 Correlation Matrix for the Seven Spectral Bands at 60 m pixel resolution	50
Table 4.2 Correlation between resolutions for the first principal component	52
Table 4.3 Preliminary DA results in % to determine the best texture window size	61
Table 5.2 Structural information based on the collected field data for the 3 field plots.....	76
Table 5.3 Summarized classification results and accuracies for six-class sample stratification.....	80
Table 5.4 a Classification results for the six-class sample stratification using only the spectral 60 cm data.....	83
Table 5.4 b Classification results for the six-class sample stratification using only the textural 60 cm data	83
Table 5.4 c Classification results for the six-class sample stratification using combination of spectral and textural 60 cm data.....	83
Table 5.5 a Classification results for the six-class sample stratification using only the spectral 1 m data.....	84
Table 5.5 b Classification results for the six-class sample stratification using only the textural 1 m data.....	84
Table 5.5 c Classification results for the six-class sample stratification using combination of spectral and textural 1 m data	84

Table 5.6 a Classification results for the six-class sample stratification using only the spectral 2 m data.....	85
Table 5.6 b Classification results for the six-class sample stratification using only the textural 2 m data.....	85
Table 5.6 c Classification results for the six-class sample stratification using combination of spectral and textural 2 m data	85
Table 5.7 Summarized Classification Results and Accuracies for Thirteen-class sample stratification.....	89
Table 5.8 a Classification results for the thirteen-class sample stratification using only the spectral 60 cm data.....	92
Table 5.8 b Classification results for the thirteen -class sample stratification using only the textural 60 cm data	93
Table 5.8 c Classification results for the thirteen -class sample stratification using combination of spectral and textural 60 cm data.....	94
Table 5.9 a Classification results for the thirteen-class sample stratification using only the spectral 1 m data.....	95
Table 5.9 b Classification results for the thirteen -class sample stratification using only the textural 1 m data.....	96
Table 5.9 c Classification results for the thirteen -class sample stratification using combination of spectral and textural 1 m data	97
Table 5.10 a Classification results for the thirteen-class sample stratification using only the spectral 2 m data.....	98
Table 5.10 b Classification results for the thirteen -class sample stratification using only the textural 2 m data.....	99
Table 5.10 c Classification results for the thirteen -class sample stratification using combination of spectral and textural 2 m data	100

TABLE OF FIGURES AND PLATES

Figure 2.1 An example of an AVI coverage produced from airphotographs and field surveys.....	16
Figure 2.2 Vegetation succession with increasing horizontal and vertical vegetation complexity.....	20
Figure 2.3 Grey level co-occurrence matrix and image texture.....	22
Figure 3.1 Location of the study area in Kananaskis Country on a true colour composite 2 m <i>casi</i> imagery.....	26
Plate 3.1. Photo of the study area showing the aspen and conifer stands	27
Plate 3.2 Close up of the damaged leaves in the aspen canopy	27
Plate 3.3 Photograph examples of plots measured in the field.....	33
Figure 4.1 Sample stratification showing the six and thirteen-classes	46
Figure 4.2 The first principal component three <i>casi</i> imagery resolutions	53
Figure 4.3 False colour composite showing subset window.....	59
Figure 5.1a Homogeneity texture for the subset window using 60 cm <i>casi</i> imagery and three window sizes	70
Figure 5.1b Homogeneity texture for the subset window using 1 m <i>casi</i> imagery and three window sizes	71
Figure 5.1c Homogeneity texture for the subset window using 2 m <i>casi</i> imagery and three window sizes	72
Figure 5.2 Statistical summary of change in the homogeneity texture measure for the aspen conifer imagery subset	75
Figure 5.3 Statistical Summary of Change in Homogeneity for Three Field Plots	78
Figure 5.4 Texture similarity between the heavily defoliated aspen and conifer plots	87

Chapter 1 Introduction and Research Objectives

1.1 Introduction

Nature created forests as a complex system experiment, complete with interrelated processes and flexibility. In the last few decades, humans have been able to apply new technologies, such as remote sensing, global positioning systems (GPS), and geographical information systems (GIS), in understanding these processes and the resulting forest dynamics. Since 1634 when the first (recorded) shipment of masts left for Britain, Canada's forests have been one of the world's most valuable renewable (if properly managed) resources, comprising close to a thousand million hectares of land (CCFM 1996). If properly managed the rewards include economic benefits (e.g. exports) and, more importantly, environmental benefits (e.g. reduction of greenhouse gases, protection from erosion, reduction of surface run-off). If managed correctly, these environmental benefits can contribute to a sustainable economy and environment, and therefore, society. Successful management of the forest involves knowledge and understanding of forest ecology, which can be based on description of forest composition and diversity. One basic source of information on Canada's forest composition is the modern forest inventory (Gills and Leckie 1993). With new technologies (refer to Aplin 1997; Stoney and Hughes 1998) the tools to facilitate the development and application of forest inventory databases are becoming more reliable, faster, and cost-effective. In the process, forest ecology will be easier to understand and management decisions may be easier to implement through improvements to the maintenance and use of digital forest inventories.

Most forest inventory data used for management decisions are extracted from the manual interpretation of aerial photographs, which are often verified in the field, and entered into a computer (Spies 1997). These techniques involve considerable labor and are potentially costly, although new technologies, in particular, GIS and GPS, allow for relatively smooth computer data integration. With respect to remote sensing, Franklin *et al.* (1998) have noted that it is generally acknowledged that digital remote sensing can provide information that is not currently part of an existing forest inventory. According to Leckie *et al.* (1995: p. 337)

the “*use of digital high resolution (<1 m) multispectral imagery as an alternative to aerial photography for forest inventory mapping is a possible revolutionary innovation*”, providing data-rich digital layers to be integrated with the other digital databases. The recent (September 1999) successful launch of the IKONOS satellite, which provides 4 m pixel resolution multiband imagery, and hopeful launches of several proposed satellites that will generate 1 m pixel data (Glackin 1998), will help make this alternative remote sensing method – based on high spatial detail imagery – more achievable. With such large amounts of spectral and spatial data available for analysis, a much greater amount of information can be extracted from this imagery than from the previous generation of satellite data, which typically had 10-100 m pixel resolution. The methodology of handling this type of data is still relatively new; high spectral and spatial resolution aerial imagery has been suggested as appropriate in developing analysis tools for dealing with future high resolution sensors (Strome *et al.* 1991). For example, in the case of the forest inventory, the desired class stratification should be more complex than provided by earlier generation low resolution satellite imagery, such as Landsat TM.

The new high spatial detail imagery may be able to replace, or at the very least, complement the use of aerial photography in forest inventory. However, numerous authors have noted that additional research is required on how best to incorporate such high spatial resolution imagery into operational forest inventory procedures.(Leckie *et al.* 1995; Ryher and Woodcock 1996; St.-Onge and Cavayas 1995; St.-Onge and Cavayas 1997; Wulder 1996; Lark 1996; Roach and Fung 1994). Most applications rely, to a certain extent, on advanced digital image processing to extract forest information from the digital imagery rather than analogue interpretation of photography. For example, one idea has been to use digital imagery rather than large-area mapping in sampling forest stands (Fish *et al.* 1995); a second possibility lies in providing aerial photo-interpreters with access to the spectral information that is not readily available from aerial photography (Leckie *et al.* 1995). A different strategy has been to incorporate a digital elevation model (DEM) with the mean spectral response measured by digital sensors in an automated classification of forest inventory conditions (Franklin 1994). The approach is similar to the low resolution classification

methods used in Landsat image analysis and relies on the existing software and methods established over the past two decades of digital remote sensing. An improvement in this classification approach is the idea that the spectral response can be augmented with texture derivatives in an attempt to capture the information contained in the high spatial detail imagery.

Image texture is the spatial variation in image tones (Haralick 1979), and has long been recognized by both air photo-interpreters and digital image analysts as a powerful source of information in forestry image analysis (Avery and Berlin 1992; Jensen 1996; Lillesand and Kiefer 1994). Texture is generated by the interplay of shadows and objects in the image. The use of image texture analysis has been recommended for classification of digital imagery in cases where the objects in the image (e.g. trees) are larger than the pixel size (Hay *et al.* 1996; Wulder *et al.* 1996). However, an understanding of where and under what conditions image texture can be most useful in forestry applications has not yet been established. In one study, using aerial multispectral imagery from a variety of sample forests in New Brunswick and Alberta, Franklin *et al.* (1998) found that image texture analysis could improve forest inventory classification results approximately 10% over results obtained using spectral response patterns alone. They noted that texture improved accuracy the most in the hardwood and mixedwood stands that appeared to contain complex structures or layers in the canopy.

Mixed and structurally complex forest stands with multistory canopies comprise a significant fraction of Canadian Boreal and Montane environments and may be of crucial importance in ecosystem functioning at the landscape and stand level (e.g. wildlife habitat). To understand fully the complex interactions in forest ecosystems, some knowledge of the structure of the stand is necessary. This information should include not only the species composition of the stand but other characteristics such as stand density and canopy complexity (layering). Forest stand parameters such as density, species composition and class structure, which comprise the forest inventory, allow us to begin to understand the complexity of interactions in a forest ecosystem.

Image texture analysis of multi-layer canopy stands is the focus of the research described in this thesis. A digital remote sensing application of image texture using the Alberta Vegetation Inventory (Nesby 1997) standard was designed to provide insight whether texture analysis can be used to improve the accuracy and usefulness of high spatial detail imagery in forestry. The present study will focus on the detection of class structure, which is essential in maintaining and using a digital forest inventory database. Specifically, this study will address the detection and the percentage species composition of stand overstory and middlestory, using high resolution aerial remote sensing imagery and texture derivatives. Inventory measures such as these composition estimates have been declared to be possible and desirable using aerial data (Wulder *et al.*, 1996), in applications ranging from classification (Franklin and McDermid 1993) to improved estimation of biophysical variables, such as forest stand leaf area index (Wulder 1996; Wulder *et al.* 1996b). Bruniquel-Pinel and Gastellu-Etchegorry (1998) have identified the significance of accurate relationships between forest canopy structure and image texture in automated classification processes. The focus in this study is first on classification, because an accurate stand classification, based on a successful classification of stand structure, (in this case an AVI label) is the foundation for the forest inventory. Subsequent digital remote sensing work could be aimed at deriving mensurational variables, such as stems/ha, or biophysical variables, such as leaf area, in the forest-mapping environment.

It is not the scope of this study to develop new algorithms for image texture and image classification, or new programs to achieve optimal texture window size, but to focus on optimizing a combination of existing methods to ensure that the highest image classification accuracy possible is achieved. Although the understory has been shown to contribute, sometimes significantly, to spectral signatures (Bruniquel-Pinel and Gastellu-Etchegorry 1998) the effects of understory on the classifications are considered beyond the scope of this study; only the overstory and middlestory structures are analyzed.

1.2 Research Objectives

The main hypothesis of this research is that:

Image texture derived from high spatial resolution multispectral imagery will significantly increase the classification accuracy of multistory forest stands identified according to the AVI system as part of a forest inventory.

To test this hypothesis, the following tasks will be accomplished:

- i) Establish a relationship between stand complexity and an image component;
- ii) Visually interpret image texture as an indicator of multistory stands;
- iii) Conduct a classification on spectral and textural data based on field samples in a wide range of AVI coded forest plots.

The digital images used in this study were obtained specifically for this analysis in the Kananaskis study site by the *casi* (Compact Airborne Spectrographic Imager), a relatively new instrument designed to provide high spatial detail imagery and hyperspectral imagery for terrestrial and aquatic applications (Anger *et al.* 1994). This work is one part of a larger set of projects (Maudie 1999; Franklin *et al.* 1998; Wulder *et al.* 1996b) with goals to determine the extent to which digital remote sensing instruments (such as the *casi*) and methods (such as image texture analysis and classification) can contribute to mapping and monitoring Canadian forests, with the objective of sustainable forest management (CCFM 1997).

1.3 Thesis Organization

The thesis is organized into six chapters, commencing with the presentation of the research hypothesis and goals in Chapter 1. Chapters 2, 3, 4 and 5 provide a review of remote sensing in forest inventory methods, a description of the study area and data collected, the methodology undertaken and the discussion of the results of the analysis, respectively. A summary of the research and the conclusions is given in Chapter 6.

The research is placed into the context of remote sensing in forest inventory in Chapter 2. A literature survey of pertinent background touches upon the *casi* instrumentation, the AVI, and the use of digital mapping in forestry.

The study area and data collected are discussed in Chapter 3. The field and *casi* data collected are explained; the relationship between the imagery and field measurements is also established.

Chapter 4 discusses the methodology undertaken in this research. Image preparation is explained along with Principal Component Analysis (PCA), the creation of texture channels and the relationship of texture to forest structure is explained. The method of statistical summaries for the field data and data extraction are discussed. The classification procedure and the application of Discriminant Analysis (DA) to the Alberta Vegetation Inventory (AVI) class structures are explained. Finally, the accuracy assessment methods including co-occurrence matrices, errors of commission and omission and Kappa statistic are discussed.

In Chapter 5 the results of the visual homogeneity texture interpretation leading to the discovery of inversion of the texture measure is discussed and supported with descriptive statistical interpretations. An example of the relationship between texture and the field data is established and supported by descriptive statistics. The DA based on both types of sample stratifications (six-class and thirteen-class) is given. The accuracy assessment is also reported.

A summary of the significant results and conclusions based on this research along with the contributions to present research and areas of further research are provided in Chapter 6.

Chapter 2 Remote Sensing of Forest Structure

2.1 Introduction

Forest structure includes the size, type, spatial arrangement and configuration of trees in a forest (Spies 1997). Foresters typically designate structure as a component of a forest stand; a stand, therefore, is a unit of trees that is homogeneous in age, structure, composition, and physical environment (Oliver and Larson 1996). Stands are delineated using aerial photographs and field data in a well-understood and accepted practice (Gills and Leckie 1993), however, some insights available through digital remote sensing have contributed to suggestions to improve the methods used in the practice of forest inventory.

In this chapter the background to understand the possibilities for digital remote sensing in forest inventory is presented; this includes a brief summary of the characteristics of the compact airborne spectrographic imager (*casi*), a high spatial resolution multispectral sensor developed by Itres Research Ltd., a Calgary-based remote sensing company. The *casi* was selected for this research because of availability, but also because this sensor has recently received a great deal of attention as a valuable tool in vegetation resource surveys in Alberta (e.g. Fish *et al.* 1995) and elsewhere (Wulder 1996). The Alberta Vegetation Inventory (AVI) is reviewed briefly in this chapter. The AVI is used by the Alberta Forest Service (and all commercial forest companies) as the standard forest inventory tool in the province, and will be applied in this study. This review is followed by a discussion of relevant remote sensing applications, with a particular focus on the use of image texture analysis in forestry remote sensing research.

2.2 Remote Sensing in Forest Inventory Methods

Forest inventory originates with a stand discrimination or classification strategy that is necessarily regional and narrow in scope (Leckie and Gillis 1995). In Canada, this scope is defined provincially, and then combined nationally to provide an annual prospective on the

status of forest resources in the entire country (CCFM 1997). Each province has established an inventory system that results in mapped areas represented by polygons in a GIS database. According to Franklin *et al.* (1998) it is *this 'inventory standard, or this definition of stand strata, that digital remote sensing must attempt to emulate in a wide range of forest conditions'*. It can be hypothesized that only when a more successful emulation of the existing inventory occurs will a more widespread adoption of the digital remote sensing method in forest inventory take place.

The use of remote sensing in forest inventory has been limited to aerial photointerpretation with occasional instances of airborne or satellite inventories at broader scales (J. Franklin *et al.* 1986; Bauer *et al.* 1994; Baulies and Pons 1995). Normally air photos are collected every 10-20 years, interpreted by skilled photo-interpreters, and digitized onto a provincial base-mapping template (Leckie and Gillis 1995). Much work has focused on the type of film and filter combinations that might be useful in different forest conditions; less attention has been paid to the actual reasoning process used by interpreters and the resulting error pattern or uncertainty in the final classifications (Ryerson 1989; Pitt *et al.* 1997). For example, Lowell and Edwards (1996) noted that up to 50% disagreement on the position of stand boundaries existed between different forest stand air photo-interpreters; other studies have noted that aerial photointerpretation is perhaps on the order of 75% correct in interpreting species composition (Leckie and Gillis 1995).

A prominent research theme in remote sensing for applications of forest inventory has been the use of satellite sensors such as Landsat and SPOT. Forest inventory can benefit from a larger view, a broader classification approach, and then individual areas could be examined in more detail by aerial photography, or a combination of aerial photography, digital remote sensing from airborne platforms, and field data collection. For example, Bobbe *et al.* (1994) found that digital multispectral video data could be acquired in an adaptable (multiresolution, multitemporal, multispectral) way to accommodate mapping concerns in riparian zones. A study by Atkinson and Curran (1997) has shown that higher spatial detail provided by high spatial resolution imagery is appropriate for vegetation studies by providing spectral and

spatial information for individual trees making up the forest. Pitt *et al.* (1997) in their review of remote sensing in even-aged vegetation management (clearcuts and regeneration surveys) noted that wider application of digital frame cameras is imminent because of the speed and flexibility in analysis that digital products provide compared to analogue aerial photography. King (1995) reviewed the literature on systems and designs for digital frame cameras and other digital sensors and suggested future increased applicability in forest management.

Two trends that may increase the likelihood of satellite and airborne remote sensing use in developing forest inventories are the needs for:

- a) Annual updates
- b) Specific details of stand conditions

To monitor sustainable forest management, foresters require information on a timelier basis than the current ten to twenty year cycles for the forest inventory based on aerial photointerpretation. Five-year intervals might be possible; but the cost and logistics of interpreting manually the entire provincial forestland areas suggest that such an approach is not feasible. Digital methods do take time and effort, but increases in efficiency and automation will likely match the increased information content of the new image sources (Heygi *et al.* 1992). More specific information on forest conditions over large areas can be extracted digitally than can be extracted manually (Eldridge and Edwards 1993; Baulies and Pons 1995). For example, leaf area index (LAI) is a critical structural variable in understanding forest dynamics such as photosynthesis, and forest conditions, such as forest health (Running *et al.* 1986; Wulder 1996). However, LAI, which is readily extracted from digital multispectral imagery, is not available from the interpretation of aerial photographs, and is not a part of most forest inventories. Yet, there are increasing demands for new, timely and reliable estimates of LAI for input to ecosystem models of productivity (for example Leckie *et al.* 1995; Wulder 1998).

These two trends, and the increasing pressure to generate sustainable forest management decisions based on the forest inventory, are likely to increase the need and development of digital remote sensing methods to improve and enhance the forest inventory databases.

Furthermore, the above mentioned trends have concentrated on using high resolution imagery to conduct forest inventory analysis. High resolution imagery allows the extraction of spatial measures such as texture, which are an additional source of information that can be utilized in classification procedures. Various studies have used high resolution imagery such as *casi* and *msv* (multispectral video) to delineate forest stands and their structural characteristics (refer to Fish *et al.*, 1994; Wulder, 1996; Gerylo *et al.* 1998; Franklin *et al.* 1998). In all of these studies, successful classification results were attributed to the higher spatial resolution imagery (25 cm to 4 m), which provided the more detailed information of the areas of interest. The *msv* study conducted by Gerylo *et al.* (1998) suggested that the three spectral bands of the *msv* instrument (green, red and near infrared) were not the most suitable for distinguishing between the conifer species pine and spruce. The authors encourage the application of a sensor with higher spectral resolution capabilities such as the *casi* instrument.

2.3 Characteristics of AVI

The Alberta Vegetation Inventory (AVI) is an operational, integrated field inventory system using aerial photo-interpretation and field surveys based on six parameters: moisture regime, crown closure, tree height, species composition, stand origin (age) and timber productivity rating. The forest polygon code also allows information on stand structure (e.g. single or multistory), disturbance, treatments and understory (Alberta Forestry, Lands and Wildlife 1991).

The first part of the AVI forest polygon code is the moisture regime. Table 2.1 describes the classification of moisture regime and its associated AVI code. Moisture regime is assigned based on plant indicators, soil properties, environmental factors, slope position, gradient, and soil texture. Dry sites are typically well drained whereas mesic sites are moderately well

drained. Wet sites are characterized by poor drainage, with possible shallow water where the water table is near or at the surface. Aquatic sites (non-forested) have permanent deep-water cover and hydrophilic vegetation (e.g. water lily).

Table 2.1 AVI classification: moisture regime

<i>Class</i>	<i>AVI code</i>
Dry	A
Mesic	B
Wet	C
Aquatic	D

Crown closure or the percentage of ground area covered by a vertical projection of tree crowns onto the ground can be determined using a spherical densiometer. The most common approach is to take an average of a few readings from each stand to determine the crown density, accounting for the variability within the stand. For AVI, crown closure is classified into one of the four classes in Table 2.1. It should also be noted that stands with crown closure of less than 6% are not considered forest stands.

Table 2.2 AVI classification: crown closure

<i>Crown closure %</i>	<i>AVI code</i>
6 - 30	A
31 - 50	B
51 - 70	C
71 - 100	D

Tree height is determined through field measurements, using such instruments as a cyclometer, and recorded to the nearest meter. Although this instrument is mostly used for measuring slopes, tree heights can also be obtained. The standard height of a plot is composed of the average heights of the most dominant specie(s). For a clearly differentiated multistory stand, the height of each story is recorded. In stands where multistory canopies are

not clearly differentiated use either average tree height for only one main canopy, or two average three heights to form two dominant canopies.

The species composition part of the code is designed to list a maximum of five species in decreasing order, based on percent crown closure. The code indicates the percentage of each species (in 10 % increments) with a subscript. Species which constitute less than 10 % of the stand content, are not included in the AVI code. For example, a species composition label: Aw₃ Sw₃ Pl₂ Pb₂ can be read as 30% trembling aspen, 30% white spruce, 20% lodgepole pine and 20% balsam poplar. It should be noted that if a single species comprises 90% a stand, such a stand can be considered pure and assigned a label of 10 (100%). In Table 2.3 other species abbreviations for the AVI code are given.

Table 2.3 AVI species abbreviations

<i>Species</i>	<i>Abbreviation</i>
Aspen, <i>Populus tremuloides</i> Michx.	Aw
Fir Subalpine, <i>Abies lasiocarpa</i> (L.) Mill.	Fa
Fir Douglas, <i>Pseudotsuga menziesii</i> (Mirb.) Franco	Fd
Lodgepole Pine, <i>Pinus contorta</i> Loudon	Pl
Balsam Poplar, <i>Populus balsamifera</i> L.	Pb
Spruce White, <i>Picea glauca</i> (Moench) Voss	Sw
Spruce Engelmann, <i>Picea engelmannii</i> Parry ex Engelm.	Se

The following part of the forest polygon code describes the stand origin by age. For example, if a stand was planted in 1944, the stand origin code will be "94", with the "9" referring to the century (e.g. 1900s) and the "4" referring to the fourth decade (e.g., the 40s). At this time there is no consistent way of dealing with the upcoming year 2000 origin scenarios (the "Y2K" problem). The stand origin is determined from the average tree age; the age can be extrapolated from the diameter at breast height (DBH). The age adjustment factor (Table 2.4) to account for the growth of the tree to reach breast height must be added to breast height age.

Table 2.4 AVI classification: tree age adjustment factor

<i>Species</i>	<i>Adjustment</i>
White Spruce	15 years
Pine	10 years
Deciduous	6 years

The last part of the forest polygon code is the timber productivity rating (TPR). The classification scheme for TPR is shown in Table 2.5, and is used to describe the potential productivity or potential growth rate of a stand. This rating is based on the height and age of the dominant and co-dominant species occurring in the stand. The TPR is assumed to be the same if the species in the overstory and the understory (second canopy layer) are the same. However, if the species composition differs between canopies, TPR is assigned to each story independently. TPR reflects factors affecting tree growth including soil, topography, climate, elevation, moisture, etc.

Table 2.5 AVI Classification: timber productivity rating (TPR)

<i>TPR class</i>	<i>AVI code</i>
Good	G
Medium	M
Fair	F
Unproductive	U

Single and multistory stand structure can be incorporated in an AVI code. Hence, a single story stand originating in 1954, in a rapidly (well) drained substratum, with 80% crown closure, pure aspen canopy of 21 m in average height, and good timber productivity would result in the AVI code shown:

$$\frac{dD21Aw_{10}}{95 - G} \quad [1]$$

When the aspens are not of the same height and the average height of the top layer differs from the average height of the lower layer by more than 3 m the stand should be classified as

a multistory stand. For example, if the two average heights were 21 m and 10 m and the lower layer stand origin was determined to be 1970, the AVI code would read:

$$\frac{dC21Aw_{10}}{95-G} \quad \frac{dA10Aw_{10}}{97-M} \quad [2]$$

The AVI is intended to be a continuous inventory requiring an average of 1/20 of the land to be re-inventoried annually (Alberta Forestry Lands and Wildlife 1991). Figure 2.1 shows the broad AVI polygons for the study area, produced from aerial photographs by the Canadian Forest Service in 1986. This type of inventory does not capture the complexity of the stand actually recorded on the ground.

2.4 Digital Methods Applied to Imagery in Forestry Applications

Remote sensing applications in forestry include defoliation assessment, disturbance regime monitoring, modeling productivity, and developing inventory maps, and many other applications (Avery and Berlin 1992). Many of these studies have required an automated or semi-automated classification of remote sensing data, which is a detailed description of the forest area based on the relatively coarse resolution satellite imagery (Running *et al.*, 1986; Hall and Crown 1987; Spanner *et al.*, 1990), or on the highly detailed, high spatial resolution aerial imagery (Franklin 1994). The range of possible (or available) image processing techniques and methods is wide, and their potential applications are not yet fully understood.

In aerial remote sensing studies, a number of authors have attempted to achieve detailed forest classifications from the spectral signatures inherent in the multispectral images (Marceau *et al.*, 1994a,b; Ghitter *et al.*, 1995; Gerylo *et al.*, 1997). However, spectral classes and forest stands are not necessarily closely correlated to each other (Hall and Crown, 1987), resulting in low classification accuracies based strictly on spectral reflectance. This may be a

634770 m E
5664204 m N

635777 m E 16
5664204 m N

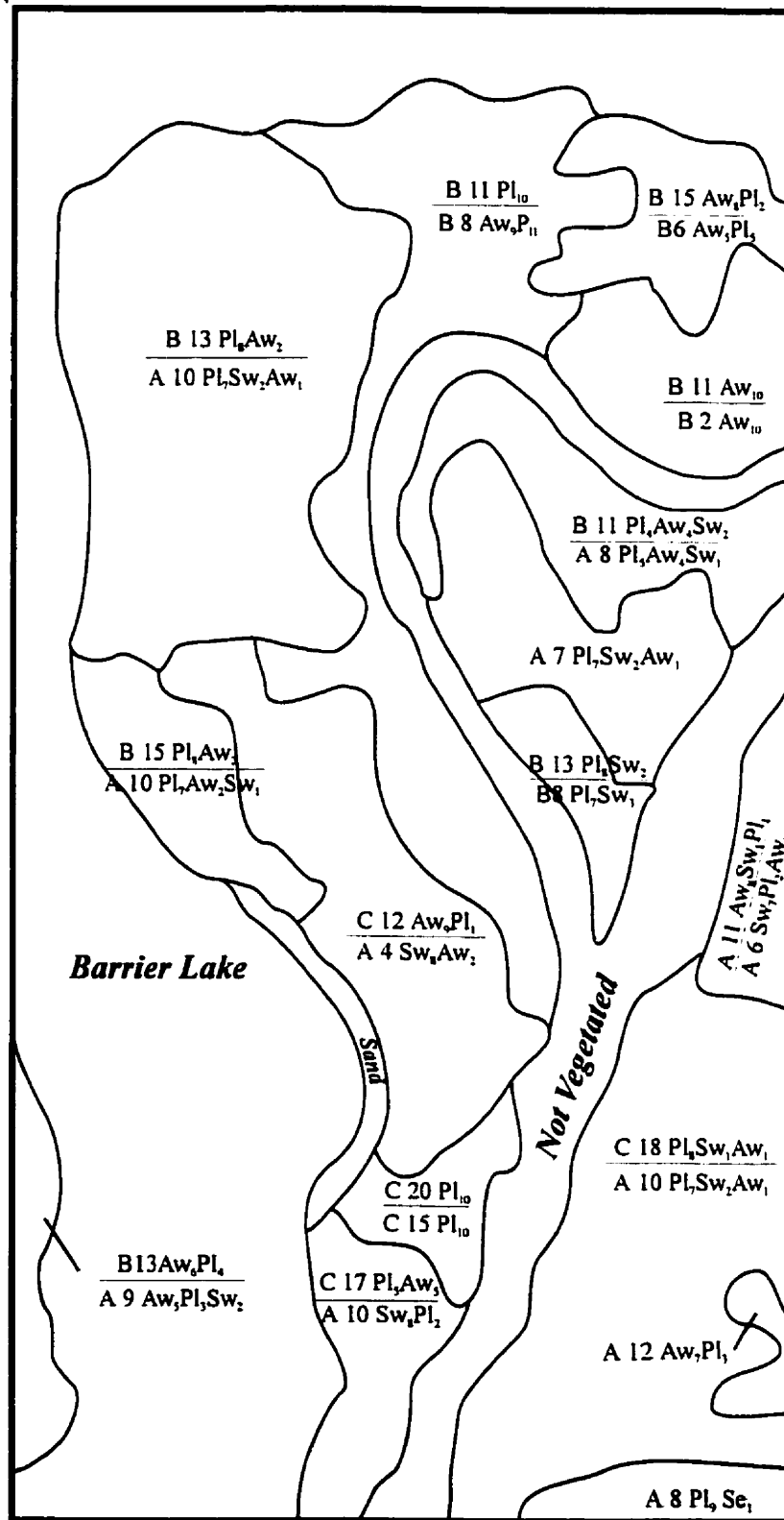


Figure 2.1 An example of an AVI coverage produced from air photographs and field surveys

result of the greater variability of spectral signatures in aerial applications (compared to satellite applications). Therefore, other image characteristics such as texture have been employed to improve aerial image classification accuracy. A recent example of this increased accuracy was documented by Franklin *et al.*, (1998). Their work showed that accuracies of approximately 40% could be achieved using spectral signatures alone in a classification, but that increases to approximately 60% were possible when spectral signatures were augmented with texture derivatives in certain forest conditions.

The present thesis was an outgrowth of those results, which indicate that texture worked best in areas of mixedwood stands and multistory conditions in the Kananaskis Study Area on high resolution (25cm/pixel) multispectral video imagery. This thesis further tests the increase in accuracy, using second-order texture derivatives, and specifically, shows the application of image classification using texture in multistory stand detection and mapping.

Since 1991 a series of experiments has been conducted to provide AVI mapping and classifications from aerial and satellite digital remote sensing in a variety of ecological systems using a wide range of image sensors and classification procedures (Franklin *et al.*, 1994; Butler *et al.* 1995; Fish *et al.*, 1995; Getty 1996). More recent work in the Kananaskis Study Area has dealt with object specific detection of inventory parameters on high resolution multispectral data (Gerylo *et al.*, 1997). Much of this work has indicated (some) promise for employing aerial remote sensing digital maps and methods in forest inventory and ecological assessment, based on the AVI standard.

Although AVI allows for multistory stand structure annotation in the AVI code, this is only done based on data collected in the field (Hall, 1998 personal communication). Aerial photographs used for AVI mapping have not been studied for feasibility of detecting the multistory stand structure. The problem of detecting multistory canopies through the application of texture to digital imagery also remains unanswered, but is the focus of the present thesis.

2.5 Characteristics of *casi*

The aerial sensor choice in this research is *casi*, designed in 1989 by Itres Research Ltd., Calgary, Alberta, to provide users with a high performance, low-cost and easy to install visible-near infrared push-broom instrument. The actual ground cover of the *casi* is dictated by the fore-optic field of view, aircraft altitude above ground level, aircraft speed, and integration time. The instrument operates over a spectral range of 400 nm to 1000 nm, with a sampling interval of 1.9 nm making it quite suitable for vegetation and forestry based applications (Wulder *et al.*, 1996). The wide array of options provided by the *casi* instrument and the technical specifications required to operate the sensor have been summarized (Wulder *et al.* 1996c) and listed in Table 2.6.

Table 2.6 Technical specifications of *casi*

<i>Parameters</i>	<i>Summary</i>
Spatial Coverage	512 pixels, 37.8° field of view across track (may be optimized to 44.7° with motorized aperture lens). Ground resolution governed by aircraft speed, altitude and sensor configuration time. Typical 1-10 m.
Spectral Coverage	545 nm spectral range with 400 nm to 1000 nm. Using 288 channels; 2.2 nm spectral resolution, with 1.9 nm sampling interval.
Spatial Mode	Full spatial resolution (512 pixels) resolution across 37.8° across track field of view for up to 19 user selected bands.
Spectral Mode	Full spectral (288 pixels) resolution for up to 39 look directions accrues the 37.8° field of view. Includes a single band, full spatial resolution scene recovery channel.
Enhanced Spectral Mode	Full spectral (288 bands) resolution for up to 101 look directions. Change summation increases spatial coverage if spectral resolution is reduced (511 look directions, 48 contiguous bands at spectral resolution of 11.4 nm).

2.6 Application of Texture in Image Classification

Texture can be defined as the variability of tone of neighboring pixels of a digital image. A comparative study of texture measures for terrain classification by Weszka *et al.*, (1976) confirmed the general usefulness of texture features, even in the absence of multispectral information. Texture tone analysis has been applied to automated land use mapping based on digitized aerial photography (Hsu 1978), improving classification results significantly, with a maximum classification accuracy of up to 85-90%. On low resolution imagery, (Landsat TM) texture-enhancements reduced the misclassification of 'forest' as 'orchard' from 75% of the 'forest' pixels to fewer than 7% (Gordon and Philipson 1986). Subsequent studies using a variety of digital imagery acquired from videographic sensors, frame cameras, spectrographic imagers and so on, have confirmed the critical role of texture in successful classification studies (refer to He *et al.*, 1988; Sali and Wolfson 1992; Wulder 1996). Continuing work is aimed at generating a more complete understanding of image texture and the conditions under which image texture can contribute to classification of forests (Franklin *et al.*, 1998).

Figure 2.2 shows how the texture of a stand can change during development. It is important to note that although the average spectral reflectance of the stand can be quite similar during the later stage of succession (Wulder 1996), the texture is always varied. Texture is possibly the only discriminating factor between the stands. During applications of texture, concern must be given to the actual texture measure or derivative, the window size and orientation for computation, the number of bands and the quantitative resolution (or quanta). In the initial stages of texture research, the simplest measures, which are readily available to end-users, should provide a reasonable starting point for tests.

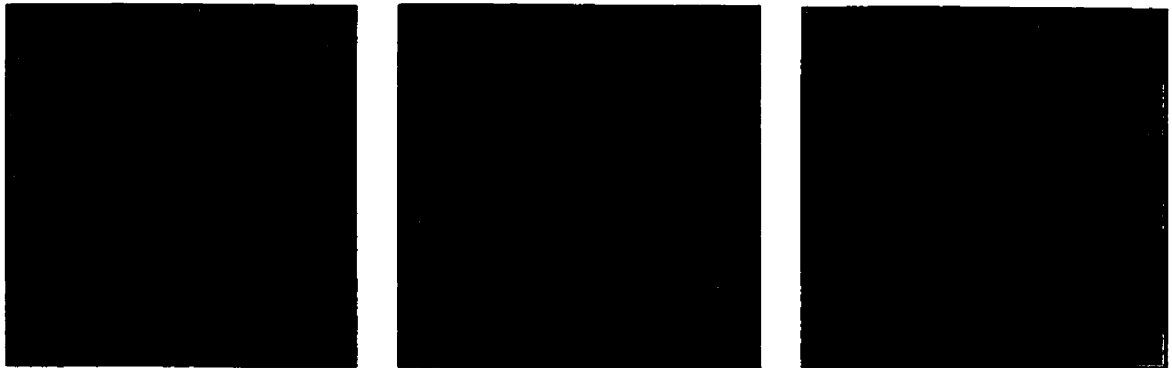
First order texture measurements include: the mean-average reflectance of pixels within a window; standard deviation-the standard deviation of reflectance within a window; minimum and maximum-minimum reflectance value within a window and range-the range of minimum and maximum values within a window. First order texture is derived



As a stand matures the horizontal and vertical complexity of the stand changes. The second stage shows two distinct vegetation layers in the stand. The complexity maximizes when the stand is mature with varied horizontal and vertical expression.



The birds eye view shows the spatial complexity increasing as the stand matures. The crowns of shade intolerant trees compete for the available light, and a shade tolerant lower layer develops. In the mature stand all gaps in the canopy are taken up by crowns.



These simulated high resolution images demonstrate the information captured by a sensor. A source of illumination was added to produce the shadows. The spectral variability of the tree crowns is captured by the sensor, so are other components of the stand such as the understory, and shadows. As the stand grows a young second layer develops. The sensor captures some of the non-shadow covered crowns of this layer. In a mature stand the tree crowns are recorded, with little understory and shadow. The not yet established third layer (less than 1 m in height) might not be detectable.

Figure 2.2 Vegetation succession with increasing horizontal and vertical vegetation complexity. The high resolution imagery is simulated and simplified.

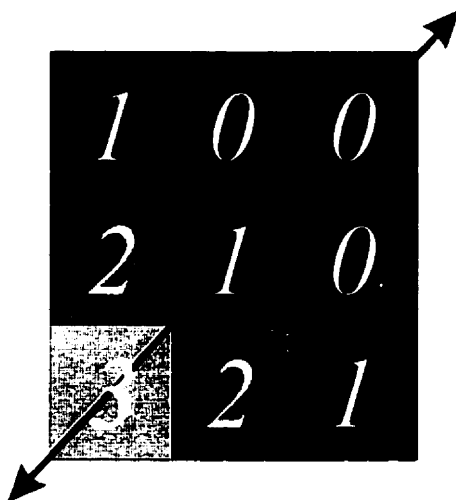
from custom filters (refer to Irons and Petersen, 1981 and Wulder *et al.*, 1997) and is commonly available in commercial image processing systems such as PCI. Second order texture using generalized co-occurrence matrices was shown to improve classification accuracies from 50-57% to 80+%, from the gray-level co-occurrence matrix (Davis *et al.*, 1979); the data set used in this study consisted of five different texture classes (pebbles, tree, bark, orchard, iron grating and scrap iron. The grey-level co-occurrence matrix can be defined as a metric of relative frequencies in which two neighboring pixels, separated by a distance and having an angular relationship, occur in the image, one with grey tone (i) and the other with grey tone (j). The term 'second-order' refers to the fact that the image texture is derived from this co-occurrence matrix, rather than from the original image data.

The example in Figure 2.3 shows how texture is derived from the grey-level co-occurrence matrix. Textural values are determined by computing, for a particular distance and angle, statistics in the matrix based upon spatial relationship of the pixel values in the imagery (Wulder *et al.*, 1997). Obviously, many possible texture derivatives can be derived and considered in this research (e.g. semivariance texture, 1st order texture including the minimum/maximum measures and so on), but the first-order and second-order measures are the most readily available and easily understood texture variables. In one study, Carr and Pellon de Miranda (1998) found that second-order texture variables outperformed all other texture measures tested, including the semivariance texture used by Wulder (1996) in his LAI texture analysis. No simple measure of texture optimality has been devised. It is likely that those interested in forest applications will continue to use the commercially available software for image processing. Therefore, the simpler more available texture measures will be more commonly used than others.

Texture has also been used in forestry related measurements applied to other (non-spectral) wavelength regions in remote sensing. For example, Wilson (1995) examined the relationship between the forest structure of two conifer species using various tone and texture measures derived from SAR data. He found that the simple texture measures were the most

Window of imagery

Low texture
- low variability in image tone



High texture
- high variability in image tone

Resulting co-occurrence matrix

		neighboring pixel value			
		0	1	2	3
reference pixel value	0	6	5	2	0
	1	5	4	4	1
	2	2	4	2	2
	3	0	1	1	0

Figure 2.3 Grey level co-occurrence matrix and image texture.

useful for that application, and that significant increases in accuracy could be achieved using such first-order and second-order texture derivatives in image classifications. A comparison assessment of performance of the first and second order of texture algorithms for the estimation of forest leaf area was given by Wulder *et al.*, (1997). They showed that measures other than first and second-order texture were best (specifically the semivariance measures), but this was an estimation test, not an image classification procedure. In earlier work, Bowers *et al.*, (1994) showed that semivariance measures were most sensitive to canopy-level changes associated with leaf area (defoliation by the balsam woolly aphid in pure balsam fir stands was estimated).

Texture windows or the square/rectangular pixel array, for which dimensions are fixed by the analyst, are applied to the larger image region during the texture analysis. Marceau *et al.*, (1990) has showed that window size accounts for 90% of the classification variability in a land cover mapping application. However, an adaptable window size might be required to optimize image characteristics such as image texture on high resolution images (Franklin and McDermitt 1993). A strategy has been developed by Franklin *et al.* (1996) to automate the derivation of texture window sizes through semivariance calculation. This work has shown that an increase of 5%, shown to be statistically significant, in classification accuracies can be achieved when the range of a semivariogram is used to predict geographic window size, as compared to fixed window sizes.

2.7 Chapter Summary

Forest inventories are a critical source of information for sustainable forest management in Canada. Forest managers require tools which are easily accessible, reliable, faster than manual methods and cost effective. New technologies are promising to provide these tools capable of facilitating timely updates to forest inventories, hence, allowing forest managers to monitor ecological processes such as forest succession, forest biodiversity and forest change in general. The produced results need to be easily interpretable and integratable with other digital databases. High resolution digital imagery such as airborne and *casi* sensor imagery have been shown to contain the above ground organization of the vegetative element

(forest canopies), or the vertical and horizontal forest structure. Forest managers utilizing high resolution digital imagery will most likely be working with commercially available image analysis packages, classification algorithms and textural derivatives inherent to these packages. Relatively simple techniques are required which can best extract this type of data from the imagery.

The AVI is a standard accepted method of collecting and describing forest inventories in Alberta. One of the major descriptive variables in AVI is the per species, canopy composition expressed in percents of dominant and co-dominant species. Delineation of canopy layers and the species composition of these layers can also be recorded. The focus of this study is to test the increase in classification accuracy (compared to using spectral information only) of multistory forest stands according to the AVI system by applying textural and spectral signatures of the investigated classes. The main variables to be implemented in the analysis will be the second-order texture derivatives of the high spatial resolution *casi* imagery, which have been shown to contain information pertaining to forest structure.

The relationship between the imagery and field data is extremely important and will be established in this thesis. Developing on this relationship the textural imagery will be visually interpreted and related to structural components of the stands.

Chapter 3 Study Area and Data Collected

3.1 Location and Description of the Study Area

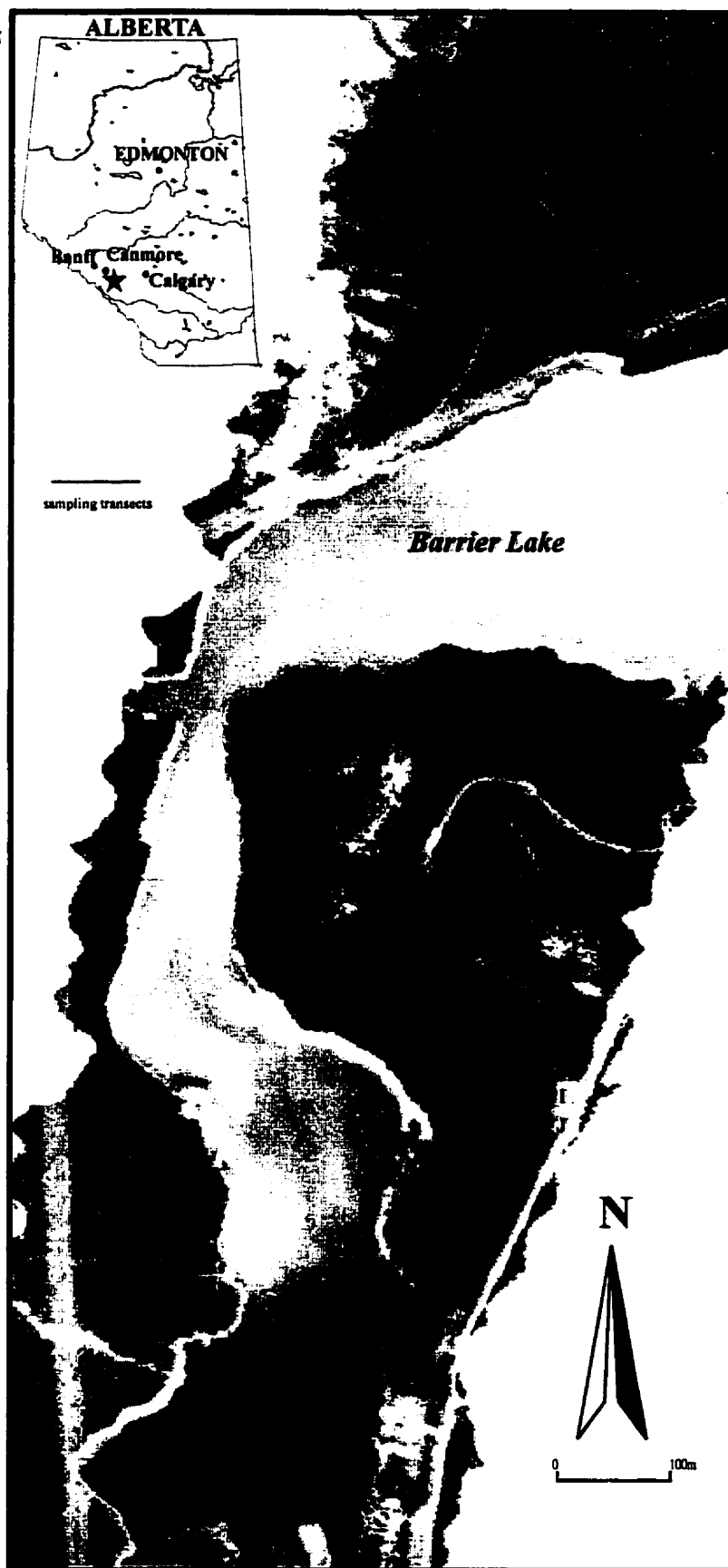
Located within the Kananaskis Valley on the eastern slopes of the Rocky Mountains of Alberta, the study area is positioned within a transition zone extending from a mountainous region to the foothills. Covering approximately seven by eleven kilometers (refer to Figure 3.1), the study area contains part of Barrier Lake, formed by Barrier Dam on the Kananaskis River, and is adjacent to the University of Calgary Kananaskis Field Station. Within the greater Montane Cordilleran ecozone, this area lies near the southern border of the Eastern Continental Ranges ecoregion, as defined by Archibald (1996).

Although the subalpine summers are generally cool and damp while the winters are cold with snow and Chinooks, there is considerable variation in temperature. Mean summer temperature is 12°C and the mean winter temperature is -7.5°C. However, throughout the year temperatures can range from 35°C to -45°C. Only 30% of the precipitation falls as snow, the mean annual precipitation ranges from 600-800 mm, which increases with elevation from east to west. The study area ranges in elevation from approximately 1400 m at Barrier Lake to 2000 m at the top of Prairie View located on the west side of Barrier Lake. Previous fieldwork conducted in this area during the summer of 1997 has shown that multistory stands are common in this hardwood and mixedwood forest.

The lower subalpine forests of the study area are predominantly composed of Lodgepole Pine (*Pinus contorta*), White Spruce (*Picea glauca*), Douglas Fir (*Pseudotsuga menziesii*), and Aspen Poplar (*Populus tremuloides*). Although not a true tree, beaked willow (*Salix bebbiana*), varying in height from 1 m to 10 m, exists in mixed woods and moist depressions. The beaked willow is a shrub which is not included in AVI. The understory is dominated by bear berry (*Arctostaphylos rubra*), creeping juniper (*Juniperus communis*), hairy wild rye grass

634300 m E
5655900 m N

635800 m E
5655900 m N



634300 m E
5652050 m N

635800 m E
5652050 m N

Figure 3.1 Location of the study area in Kananaskis Country on a true colour composite of 2 m *casi* imagery, sampling transects are shown in red.

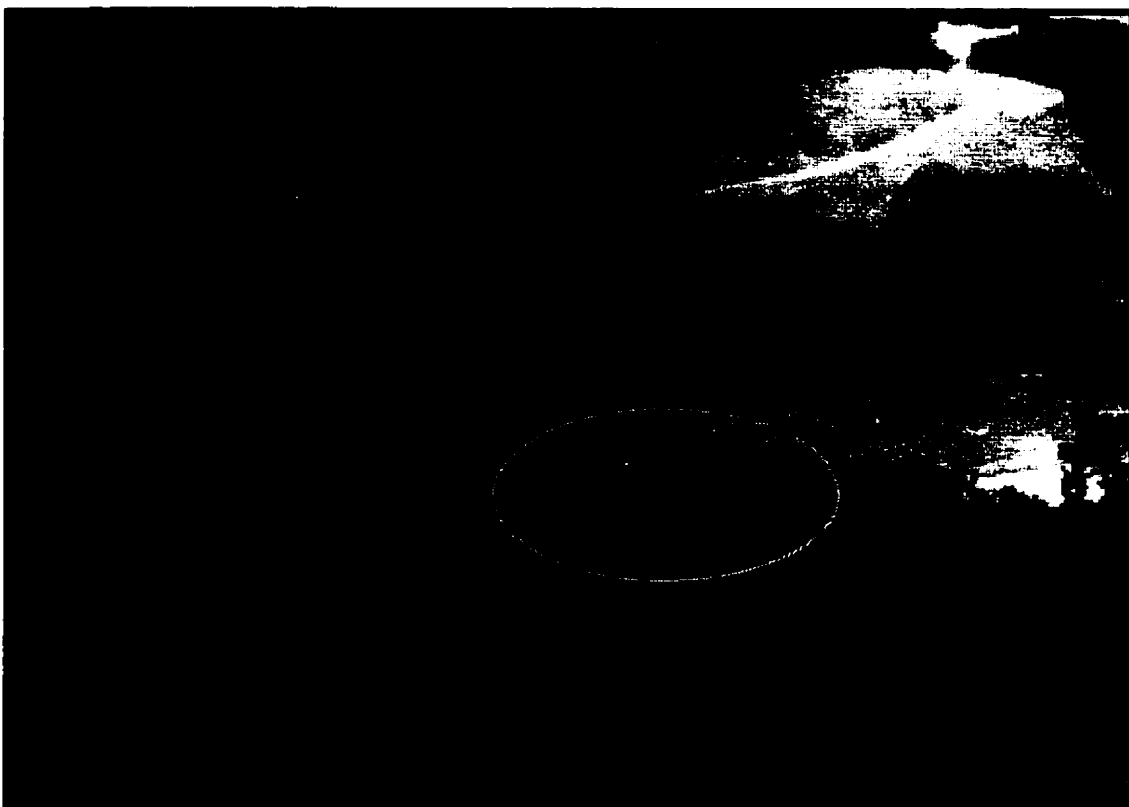


Plate 3.1. Photo of the study area showing the aspen and conifer stands (notice the defoliation of some of the aspen stands)

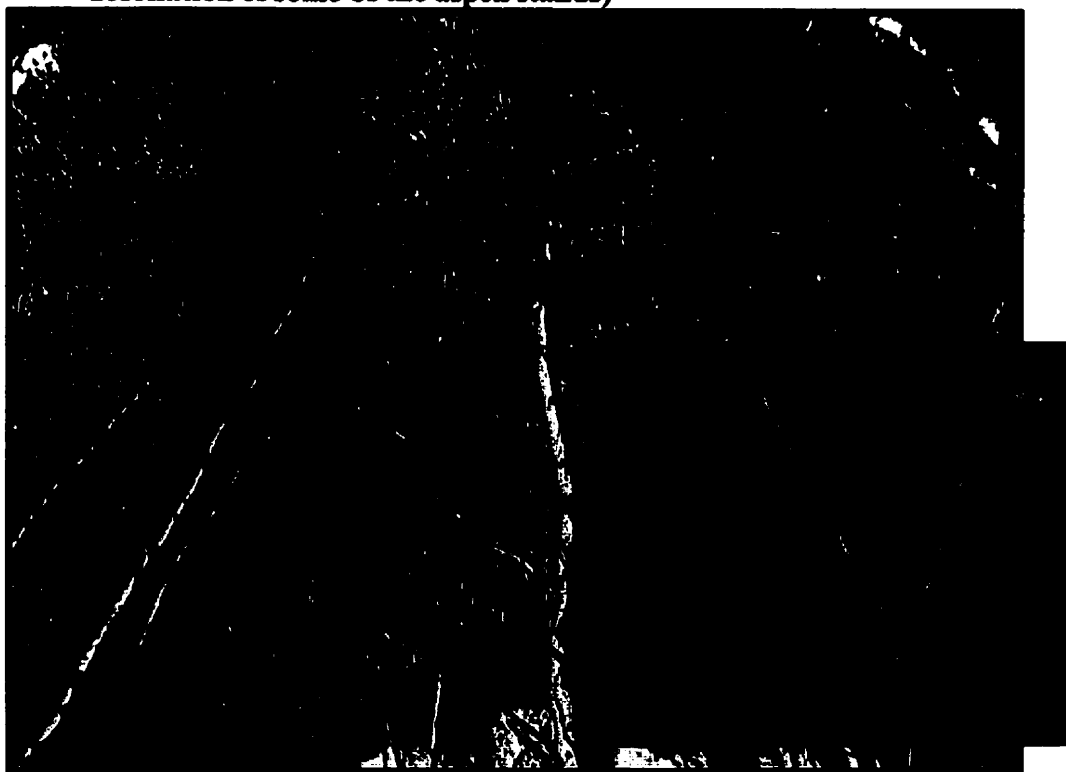


Plate 3.2 Close up of the damaged leaves in the aspen canopy

(*Elymus innovatus*) and litter. The slope in the area ranges from gentle to extreme (between 1300 m and 2350 m) exposing barren rock at the highest elevations. The heavily glaciated terrain is covered with soils originating from limestone, the predominant parent material (Kirby 1973).

During the summer of 1998, an outbreak of the Bruce spanworm (*Opherophtera bruceata*, Hulst, *Lepidoptera: Geometriadae*) damaged some of the aspen stands (refer to Plate 3.1), (Judy Buchanan-Mappin, 1998). The bright green, looping larva feeds on the developing aspen buds in the spring. The damage is initially inconspicuous, but when the leaves expand, the damage becomes visible as holes in the leaves (refer to Plate 3.1). The outbreaks of this insect are typically short-lived, and severe infestation seldom lasts more than two or three years (Peterson and Peterson 1992).

3.2 Data Acquisition

Two types of data were acquired during the summer of 1998, the field data including ground spectral reflectance and forest measurements, and the *casi* imagery. Both will be discussed in this section. Further chapters will establish empirical relationships between these two data types.

3.2.1 Field Data

During the 1998 Kananaskis Field season, a cooperative effort for data collection was formed between the Universities of Calgary, Lethbridge, and Regina, as well as the Canadian Forest Service from the Northern Forestry Center in Edmonton. Each institution had different research objectives; therefore, all decisions regarding which data were to be collected and the best method to do so were evaluated by the research teams to provide the best products for use by all members. All parties shared in the data collection responsibilities using agreed upon methods.

3.2.1.1 Spectroradiometer Data

Two spectroradiometers were used during the field season: a full range (FR) (350 - 2500nm) and a personal spectrometer II (PS2) (350 - 1050nm). Optically thick stack of the most dominant species in the study area were collected, the sample consisted of pure and mixed stacks at regular percent composition intervals to simulate the natural combination of species composition. Nadir looking measurements of each pure and mixed vegetation sample were collected to simulate the orientation of the *casi* airborne sensors, as well as limited bi-directional measurements. Each set of measurements began with the collection of white reference spectra using a Spectralon panel with the FR spectroradiometer and Kodak Grey Cards (KGC) with the PS2 spectroradiometer. The white reference spectra provided a means of converting raw data to reflectance. The vegetation samples collected and placed in optically thick stacks were located outside the forest canopy to reduce the amount of scattered and diffuse light contacting the sample. Two sets of spectral measurements were collected for each sample: first in raw digital number mode for conversion to absolute reflectance, and second in relative reflectance mode (compared to either the spectralon or KGC) to provide a field check of data quality.

3.2.1.2 Sampling Procedure

Accurate ground measurements are critical to performing this type of research. The fixed plot method of ground sampling (similar to methodology utilized by Franklin and McDermid, 1993 and Gerylo *et al.*, 1997) gathered the amount of detailed information necessary for comparison to imagery data. A regular placement sampling method was chosen over fully random sampling methods. One reason for this decision was that historical data had been collected in these plots. Second, not enough random samples could have been collected in the time allocated. Ten transects (labeled from A to J) on the East side of Barrier Lake were used (refer to Figure 3.1 of the study area). The transects were previously used by Gerylo *et al.* (1997), as well as by a "Remote Sensing in Ecology" field methods course taught at the Kananaskis Field station during the summer 1996 term. The sampling transects run diagonally on a 200° declination and are spaced 50 m apart. Each transect had four plots

sampled on it, spaced 50 m apart. Some additional transects (transects 1 and 2 in Figure 3.1), running directly north were placed on the north-west side of the Barrier Lake by the parking lot and on the north side of Barrier Lake dam; 4 plots were sampled along these additional transects in a similar fashion. The additional sampling transects were necessary to introduce more variability to the data set; they also fulfilled the research needs of the two other research teams. Of the 60 plots collected, data from 51 were suitable for the analysis addressed in this research.

Each 10 m by 10 m plot was aligned north-south through the center transect of the plot. The plot corners were labeled numerically clockwise so that corner one is always oriented towards the north-west. The plot center was labeled as five. This consistent scheme provided for easy comparison between plots. The orientation of the *casi* flight lines is north south or east west, therefore, the plots and image pixel orientation are aligned. This simplified the location of the plots on the imagery.

It is not the objective of this thesis to study the effects of terrain, topography and illumination on the classification of the high resolution imagery, as previously discussed by Pellikka (1996). In order to avoid these effect, plots with slopes greater than 3% were not included in the sample.

3.2.1.3 GPS Data Collection

All plots were located with a Trimble GPS field unit, using the four corners of the plot as well as the center to collect 30 consecutive readings. The Kananaskis Field Station GPS base station was used to differentially correct the plot field readings. The data were converted to 1983 North American Datum (NAD 83) in the Universal Transverse Mercator (UTM) Projection and exported as a GIS coverage using the Trimble software.

3.2.1.4 Forest Measurements

To establish the AVI label for a sample plot a wide range of tree attributes was collected (an example of field data collected is shown in Appendix A), including:

- a) Tree species
- b) Tree height and height to canopy
- c) DBH (diameter at breast height)
- d) Crown diameter (2 directions, wide and narrow)

Structural information for the plot was also necessary, especially the crown closure and percentage species composition which could be calculated from the empirical measurements.

Once the plot was located and the dimensions of the plot were established, each tree was marked with flagging tape and numbered. This procedure facilitated in making a plot map, where each tree was marked on a 1 m by 1 m grid. These data were collected to ease the location of the plots on the imagery and to provide a graphic representation used in interpreting the results of the analysis. An older *casi* image of the study area was also used to locate the plots on the imagery. All trees were identified to species. Because of the low diversity of these stands, the species identification procedure was simple and did not require field species identification guides.

Height and height to canopy (the live crown of the tree) were estimated using a Suunto clinometer. A 20 m distance from the tree was measured in an equal slope direction. The clinometer converts the angle recorded through a viewing slot into a height for this preset distance; refer to Luckai (1997).

Diameter at breast height was collected for all trees using a fixed height of 1.3 m. A tape converting the circumference to diameter in cm was used in this measurement. If split trees were encountered, the height of the split was measured. Trees splitting above breast height were counted as one stem and trees splitting below breast height were counted as two stems.

Crown diameters of the trees were measured in the widest and narrowest directions; see Cole (1995).

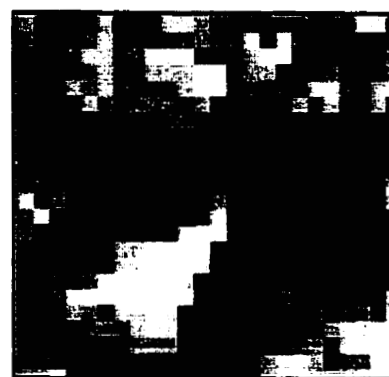
Other measurements taken were the slope and aspect of all plots. To eliminate topographic effects, plots with extreme slopes (greater than 3%) were not used in the analysis.

Field Photograph



casi 60 cm imagery

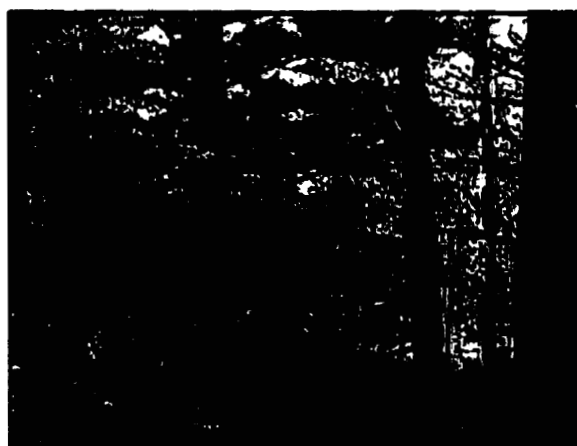
33



Plot ID	Plot AVI Code		
	Layer 1	Layer 2	Layer 3
93	Se ₁₀	Aw ₅ Se ₅	Aw ₁₀



Plot ID	Plot AVI Code		
	Layer 1	Layer 2	Layer 3
f3	Aw ₉ Pb ₁	Aw ₁₀	



Plot ID	Plot AVI Code		
	Layer 1	Layer 2	Layer 3
500gg	Pl ₅ Sw ₅	Sw ₆ Pl ₂ Aw ₂	Sw ₁₀

Plate 3.3 Photograph examples of plots measured in the field. The AVI information gathered and the 60 cm *casi* imagery of the plots are also shown.

Two methods and instruments (concave mirror densiometer and Geographic Resource Solutions (GRS) brand densiometer) were employed to measure the canopy closure in the plots sampled. The mirror densiometer was used at five locations in the plot; 2.5m towards the plot center from each corner (equals four estimates) and one estimate at the plot center. The mirror densiometer is divided into twenty-four squares, each square was subdivided into four quadrants and an imaginary dot can represent the center of the quadrant. The dot counting technique involves counting dots that are covered by vegetation and ignoring dots that are not. All together 96 dots were estimated (24 squares, 4 dots each) and a converting factor of 1.04 was used to convert the estimate to crown closure percentage for the location. The five readings at the plot were averaged and the average reading reported for the plot (Table 3.1). The GRS densiometer works like a periscope looking up at the canopy through an inverted mirror. A dot in the viewing scope of the instrument is used as the sampling point. A transect needs to be walked through the plot (a crisscross was used); at every second step a reading is taken. Special care needs to be taken to make sure that the instrument is leveled (determined by looking at the level bubble). Sixty readings were recorded using this procedure. The benefit of using the GRS densiometer is that information such as species type and the canopy layer of the tree being recorded can be seen and therefore taken at the same time. This allows reports on crown closure per species and crown closure per canopy layer (Table 3.1) for each plot. Plots with a crown closure of 30% or less were not sampled.

A 8% difference in the crown closure readings was noted between the two instruments, especially in the deciduous stands. This discrepancy was observed by all three research teams. The differences in the crown closure readings can be attributed to the fact that the GRS densiometer has a magnifying lens on it. The defoliation caused by the Bruce spanworm larva did not destroy the whole leaf, but only perforated the leaf surface. Therefore, the leaf might be difficult to detect in the mirror of the concave densiometer (only the general 'greenness' of the canopy is used to record the crown closure), but the magnification of the GRS densiometer allowed the condition of the leaf to be captured. Due to the type of defoliation that occurred in the summer of 1997, the GRS densiometer was more successful at capturing the actual crown closure of the plot. Furthermore, this type of

Table 3.1 Crown closure readings for the 45 study plots

Plot ID	Crown Closure		Difference between Instruments	Layer Contribution to Crown Closure based on the GRS densiometer	
	Spherical Densiometer	GRS Densiometer		Layer I	Other Layers
94	48%	45%	3%	100%	-
500c	55%	50%	5%	100%	-
e2	46%	40%	6%	100%	-
g3	51%	43%	8%	100%	-
i2	50%	52%	2%	100%	-
i3	40%	33%	7%	100%	-
500d	53%	50%	3%	91%	9%
500e	50%	42%	8%	92%	8%
500hh	51%	46%	5%	88%	12%
g4	41%	30%	11%	86%	16%
h3	40%	31%	9%	93%	7%
98	54%	47%	7%	60%	40%
500b	55%	50%	5%	82%	18%
i4	56%	42%	14%	94%	6%
500i	38%	30%	8%	82%	18%
95	45%	30%	15%	97%	3%
d3	50%	35%	15%	100%	-
j1	54%	47%	7%	84%	16%
500h	39%	33%	6%	72%	28%
f3	41%	37%	4%	91%	9%
97	40%	30%	10%	93%	7%
96	59%	45%	14%	81%	19%
500ii	52%	47%	5%	79%	21%
500f	63%	50%	13%	59%	41%
500gg	60%	51%	9%	81%	19%
500k	50%	42%	8%	92%	8%
g1	42%	40%	2%	71%	29%
500jj	46%	39%	7%	62%	38%
99	35%	30%	5%	79%	21%
f1	54%	50%	4%	73%	27%
1000cc	45%	41%	4%	86%	14%
h1	59%	51%	8%	66%	34%
j2	60%	50%	10%	69%	31%
e1	39%	33%	6%	70%	30%
g2	39%	31%	8%	96%	4%
i1	62%	33%	29%	65%	35%
h2	60%	57%	3%	49%	51%
1000bb	53%	51%	2%	44%	56%
9	59%	53%	6%	77%	23%
500ff	65%	61%	4%	78%	22%
19	56%	58%	2%	79%	21%
f2	62%	52%	10%	85%	15%
500bbb	40%	50%	10%	87%	13%
18	60%	49%	11%	90%	10%
h4	42%	36%	6%	46%	54%

Average Difference between crown Closure readings
using the spherical and GRS densiometers

8%

defoliation has significant implications in the high resolution imagery. The spectral signature of the aspen stands is contaminated as the reflectance from the hard tissue of the tree, and possibly the understory, penetrated the canopy and were recorded by the *casi* sensor.

In Plate 3.1, the faded (grayer in tone) aspen stands are visible, the canopy photograph shows the condition of the defoliated leaves. However, the close up in Plate 3.2 shows that the leaves are partially damaged.

The second benefit of the GRS densiometer is that although both instruments capture the canopy of the plot, which can be comprised of more than one layer, only the GRS allows for the measurements of the contribution of each layer to the total crown closure. Hence, the data illustrates that the second layer can contribute between 9% and 58% to the crown closure of the stand.

3.2.2 *casi* Imagery

The Compact Airborne Spectrographic Imager was flown over the study area on July 18th, 1998 between eleven AM and two PM. The month of the imagery was chosen to coincide with the most “leaf on” in the forest; it is also the season least likely to experience rain or drought conditions. This timing coincided with clear atmospheric conditions for the flight and ensured that no stress was affecting the vegetation. The time of day was chosen close to solar noon for this season, allowing for the maximum sun-lit canopies necessary for the spectral information being collected. The contrast between sun-lit and shadowed canopies is lowest during solar noon (Fournier *et al.*, 1995); hence, the spectral information content of the imagery can be maximized. Three spatial resolutions of imagery were collected: 60 cm/pixel resolution, 1 m/pixel resolution and 2 m/pixel resolution. At the 1 m pixel resolution, five flight lines were flown to cover the full study area. Only two flight lines were flown at the subsequent (1 m and 2 m) resolutions (refer to Figure 3.1 of the study area).

The *casi* instrument can collect a large amount of spectral information as already discussed in Chapter 2, (refer to Table 2.1 Technical specifications of *casi*). When possible, mission planners must carefully select central wavelengths and spectral bandwidths according to key features in the canopy signature (Fournier *et al.* 1995). Therefore, spectroradiometric data collected for the dominant and co-dominant species in the study area, was the primary consideration for *casi* band selection. Central wavelengths and bandwidths most successful at spectrally distinguishing between tree species, especially the two major conifer species in the study area, were selected. Previous work in the area with multispectral video imagery (Gerylo *et al.* 1997) showed that only three spectral bands (green, red and near-infrared) were not successful at distinguishing between white spruce and lodgepole pine. The second consideration was the ability to combine the bands to simulate bandwidths of satellite imagery, specifically Landsat TM and SPOT. The most suitable bands, which were chosen, are presented in Table 3.2. In total seven bands were collected at the 60 cm pixel resolution and eighteen bands were collected at the lower 1 m and 2 m pixel resolutions. The 60 cm pixel resolution band set was limited to only seven bands. Two major reasons contributed to this, first the time that it takes the *casi* instrumentation to collect information of such high spatial detail is lengthy, and second, the conflict between the slowest speed that an aircraft can maintain and digital data recording in order to collect this information (this limitation is discussed further by Mah *et al.* 1995, and Wulder *et al.* 1996c).

The *casi* imagery was acquired on a non-cloudy day, July 18th 1998. The 2 m data were collected first, then the aircraft lowered in altitude to collect the 1 m data, and subsequently the 60 cm data. The mission was flown close to solar noon to reduce the shadows in the imagery and allow for the best crown illumination conditions. The solar zenith angle at the time of the flight was calculated at 59.78° (Peddle *et al.* 1995). Works by Guyot *et al.* (1989) and Bruniquel-Pinel and Gastellu-Etchegorry (1998) have shown that image acquisition parameters play an important role in the type of texture that the imagery can provide. For example, larger shadows can provide texturally coarser imagery, which can be suitable for some studies. However, operationally the imagery had to suit at least three types of research projects. In two of these projects, maximum spectral response from the canopy was crucial

to the studies. In this thesis the shadows in the *casi* imagery played a major role in deriving texture from the imagery, nevertheless, optimal spectral data were also required for distinction between species.

Table 3.2 *casi* Bands for the three image resolutions

<i>18 Band set (1 m & 2 m pixel resolution)</i>	<i>Wavelength (nm)</i>	<i>7 Band set (60 cm pixel resolution)</i>	<i>Wavelength (nm)</i>
1	415 - 450		
2	450 - 500		
3	500 - 520		
4	520 - 540		
5	540 - 560	1	540 - 560
6	560 - 590		
7	610 - 640	2	610 - 640
8	640 - 680	3	640 - 680
9	690 - 715	4	690 - 715
10	715 - 730		
11	730 - 755	5	730 - 755
12	755 - 790		
13	790 - 810	6	790 - 810
14	810 - 830		
15	830 - 850		
16	850 - 875	7	850 - 875
17	875 - 890		
18	900 - 960		

Coincident with image acquisition, down welling irradiance was measured at the top of the aircraft with an Incident Light Sensor (ILS).

3.3 Chapter Summary

The field data and *casi* imagery collected for this research are described in this chapter. A sampling procedure that captured the wide variety of attributes necessary for AVI, with plots representing the variability of the stands encountered in the study area, was discussed. Central wavelengths and bandwidths collected by *casi* enabled the isolation of spectral information and the extraction of textural derivatives. The constraints of the high resolution *casi* imagery are introduced and discussed. Other factors affecting the imagery, such as defoliation of the aspen stands during the field season are also presented.

Chapter 4 Methodology

4.1 Introduction

This chapter contains a description of the methods used to test the hypothesis that image texture analysis can be used to improve the accuracy of an AVI-based forest classification in the Kananaskis study area using high spatial resolution *casi* imagery. A standard supervised classification approach commonly used to determine the accuracy of input classification variables was used (Jensen 1996; Lillesand and Kiefer 1994). This approach requires that the analyst identify the classes based on field data, the variables, based on image data, a decision-rule based on a training sample, and an accuracy assessment procedure, based on a testing sample. The power of this approach has been shown in numerous satellite and airborne remote sensing studies (e.g. Skidmore 1989; Foody *et al.* 1992; Franklin and McDermid 1993). Here, the focus is on testing the improvement in classification accuracy that can be achieved with the texture variables compared to a classification accuracy that can be achieved without the texture variables, relying only on the spectral information.

First, the method used to develop the AVI label for each ground plot is described. Sample stratification based on different canopy layers was carried out to create different groups of classes. Second, the image data set was prepared by applying a Principal Components Analysis (PCA) to create a 'brightness' image from which texture derivatives could be extracted. This step was necessary to reduce the sheer volume of data that could be analyzed in the classification and texture extraction procedures. For example, presently a standard commercial remote sensing package can include as many as 12 second-order texture measures, and new measures are regularly being developed and added. The texture can be produced on various window sizes, view directions, input bands and image resolutions, leaving the user with an opportunity to potentially calculate a nearly infinite number of textural images. A preliminary analysis of the relationships between the *casi* image, the stand structure and the stand shadow components was conducted in support of the texture extraction. Third, the plots were compiled into the classification structure with a training

sample and a testing sample. Discriminant Analysis (DA) was applied to determine the level of accuracy that could be achieved with and without the texture variables. The last step was to determine the classification accuracy and compute statistical tests to support the accuracy assessment.

4.2 Basal Area and AVI Plot Labels

The AVI labels for each plot were constructed using basal area (BA) measured in the field. This is the standard technique of the Alberta Forest Service, has also been used by other remote sensing scientists (Franklin and McDermid 1993; Gerylo *et al.* 1998; Maudie 1999). The basal area of a tree has been determined to be positively correlated with the crown diameter of the tree (personal correspondence Hall 1998; also refer to Maudie 1999). It is due to this relationship between crown diameter and basal area, that this method was chosen. In forest applications of high resolution remotely sensed imagery, the most valuable image component is the sun-lit crown of the tree that is detected by the sensor. Hence, if the plot species composition is stratified according to a variable such as crown closure that can be measured or estimated by the remote sensor, a stronger relationship can be developed between the field data and the imagery. The basal area can be defined as the area in square units of the cross section at breast height of a single tree or per species in a stand (as defined by Avery 1967)

$$BA = \frac{\pi dbh^2}{4} \quad [3]$$

The basal area was calculated for each tree species in each plot. The different canopy layers were identified by examining the tree heights for an average canopy height difference of 3 m or greater (as discussed in Chapter 2). Species composition per canopy (Table 4.1) was determined using the basal area per species percentage values. Hence, an AVI label of AW₈Pl₂ indicates that 80% of the plot basal area can be attributed to aspen and 20% of the plot basal area can be attributed to lodgepole pine.

A bivariate regression of per species crown closure using the 45 sample plots (determined with the GRS densiometer method described in Chapter 3) and per species basal area was performed for the first and other canopy layers. This resulted in an adjusted R^2 of 0.613, and a standard error of the estimate of 0.1256, for the coniferous species and an adjusted R^2 of 0.804 and a standard error of the estimate of 0.1583 for the deciduous species. Both of these results were calculated for the first canopy layer and were significant at the 95% confidence interval. The other canopy layers produced results of an adjusted R^2 of 0.574 (standard error of the estimate of 0.05494) for the deciduous species and an adjusted R^2 of 0.814 (standard error of the estimate of 0.06262) for the coniferous species (refer to data and graphs in Appendix B). Both were significant at the 95% confidence interval. The higher goodness of fit for the aspen trees, at the first canopy layer, can be partially attributed to the same age of the stand. Aspens have less age variability between individual trees within a stand compared to conifer species, therefore, their crowns (crown closures) and basal areas are less likely to vary. The results for the other canopy layers show that the basal areas of shade intolerant species (deciduous) are less likely to correlate with crown closures, when these species are competing with an above layer for sunlight. Also, the conifer species in the second layer contribute to as much as 55% of the crown closure for the stand, compared to only 30% for the shade intolerant deciduous species. The shade tolerant conifers, such as white spruce, are more successful at competing for the residual sunlight left after the first canopy intersection. These symbiotic relationships (protection from insects and frost) are discussed in more detail by Peterson and Peterson (1992). All these characteristics are consistent with observations made in the field during data collection. These analyses confirm the relationship between tree crown and basal area, which can be further interpreted as a relationship between dbh and crown diameter discussed above is useful as the basis of the AVI species label (Table 4.1) in this study.

Table 4.1 AVI Labels based on basal area for the 45 study plots

Plot ID	Plot AVI Code			Basal Area (m ²)		
	Layer 1	Layer 2	Layer 3	Layer 1	Layer 2	Layer 3
94	Aw ₁₀			59.6		
500c	Aw ₁₀			54.2		
e2	Aw ₁₀			31.5		
g3	Aw ₁₀			52.9		
i2	Aw ₁₀			37.7		
i3	Aw ₁₀			44.0		
500d	Aw ₁₀	Aw ₁₀		65.3	1.8	
500e	Aw ₁₀	Aw ₁₀		42.7	4.3	
500hh	Aw ₁₀	Aw ₁₀		50.2	6.3	
g4	Aw ₁₀	Aw ₁₀		37.0	4.3	
h3	Aw ₁₀	Aw ₁₀		40.7	2.0	
98	Aw ₁₀	Aw ₆ Pl ₄		17.8	11.9	
500b	Aw ₁₀	Aw ₇ Sw ₃		33.8	7.4	
i4	Aw ₁₀	Pb ₁₀		47.4	3.2	
500ii	Aw ₁₀	Pl ₉ Pb ₁		36.8	7.9	
95	Aw ₁₀	Sw ₇ Aw ₃		59.1	2.1	
d3	Aw ₇ Pl ₂ Sw ₁			36.8		
j1	Aw ₈ Pl ₂	Aw ₁₀	Aw ₇ Pb ₂ Sw ₁	41.5	6.6	1.3
500h	Aw ₁₀	Aw ₁₀		18.2	7.0	
f3	Aw ₉ Pb ₁	Aw ₁₀		36.5	3.8	
97	Pb ₁₀	Pb ₁₀		37.1	1.8	
96	Pb ₁₀	Pb ₇ Aw ₃		53.1	12.6	
500i	Pl ₁₀	Sw ₁₀		50.5	9.6	
500f	Pl ₄ Sw ₃ Aw ₃	Pl ₆ Sw ₂ Pb ₁ Aw ₁	Sw ₅ Pl ₅	47.1	20.0	3.3
500gg	Pl ₅ Sw ₅	Sw ₆ Pl ₂ Aw ₂	Sw ₁₀	34.2	7.4	0.4
500k	Pl ₅ Sw ₅	Sw ₁₀		61.0	0.9	
g1	Pl ₇ Aw ₃	Aw ₇ Sw ₃		51.1	12.2	
500jj	Pl ₇ Pb ₃	Sw ₁₀	Aw ₁₀	11.8	1.5	5.9
99	Pl ₈ Aw ₂	Aw ₁₀		18.5	4.9	
f1	Pl ₈ Aw ₂	Pl ₆ Aw ₄		35.4	4.1	
1000cc	Pl ₈ Sw ₂	Pl ₇ Sw ₃	Sw ₁₀	46.6	6.6	0.7
h1	Pl ₉ Aw ₁	Aw ₆ Sw ₄		32.0	16.7	
j2	Pl ₉ Aw ₁	Aw ₉ Pl ₁		21.0	9.3	
e1	Pl ₉ Aw ₁	Pb ₈ Pl ₂		21.1	8.9	
g2	Pl ₈ Sw ₂	Pl ₅ Sw ₅		159.9	7.4	
i1	Pl ₁₀	Pl ₁₀	Pl ₇ Aw ₃	43.2	20.8	3.1
h2	Pl ₁₀	Pl ₅ Sw ₃ Aw ₂		31.2	32.1	
1000bb	Pl ₁₀	Pl ₈ Sw ₂	Pl ₆ Sw ₄	23.0	28.3	3.1
9	Sw ₃ Se ₃ Fd ₂ Pl ₂	Sw ₁₀	Sw ₁₀	35.3	8.2	2.2
500ff	Sw ₄ Aw ₃ Pl ₃	Pl ₇ Aw ₂ Pb ₁	Pb ₇ Sw ₃	30.6	7.6	0.5
19	Sw ₈ Pl ₂	Se ₁₀		35.1	10.0	
f2	Sw ₈ Pl ₂	Sw ₁₀	Aw ₁₀	30.7	5.0	0.2
500bbb	Sw ₁₀	Sw ₇ Pb ₃		27.4	3.7	
18	Sw ₁₀	Se ₈ Aw ₁ Fa ₁		47.5	4.7	
h4	Sw ₁₀	Sw ₅ Pb ₃ Sw ₂	Pb ₈ Aw ₂	18.0	19.8	0.9

4.2.1.1 Sample Stratification Based on AVI First Canopy Layer

Previous remote sensing classification research has typically ignored the existence of multi canopy stands. Usually, samples were stratified using all plot information to produce a single (one layer) AVI label (e.g. Franklin *et al.* 1998). In one study, a multilayer AVI label was produced but the second layer was not considered in the analysis because of the complexity of the resulting classifications (Gerylo *et al.* 1998). However, it is exactly this complexity, which is the focus of the present study. Therefore, an AVI label was produced based on the single layer interpretation and a multilayer interpretation as described below.

Stratifying the sample by the first canopy layer information produced six initial classes. Note that all information about the second or third layers has been ignored in the initial grouping of the sample. The stratification and classes, shown in Figure 4.1 included:

1. Aspen
2. Aspen mixed
3. Pine
4. Pine mixed
5. Spruce
6. Spruce mixed

4.2.1.2 Sample Stratification Based on All AVI Canopy Layers

The second level of stratifying the sample (also shown in Figure 4.1) applied all of the AVI canopy layer information to produce thirteen-classes. These classes showed a dominant layer and a second layer, which was sometimes comprised of the second and third layer in the AVI label. The third layer sample stratification was not approached because attributes such as small basal area (on average 2% of the plot area), would not be possible to detect with the presented methods. The classes produced at this level were:

1. Aspen
2. Aspen with a second pure aspen canopy
3. Aspen with a second aspen conifer mixed canopy
4. Aspen with a second conifer canopy
5. Aspen mixed with a second aspen canopy
6. Poplar with a second poplar canopy
7. Pine and spruce mixed with a second conifer canopy
8. Pine and aspen mixed with a second aspen canopy
9. Pine and aspen mixed with a second pine canopy
10. Pine with a second pine canopy
11. Conifer mixed with a second conifer canopy
12. Spruce with a second spruce canopy
13. Spruce with a second conifer canopy

In three cases the same plots that were combined into a class in the six-class sample stratification were also combined in the thirteen-class sample stratification. As shown in Figure 4.1, Class 2 (six-class sample stratification) was composed of the same plots as Class 5 (thirteen-class sample stratification); Class 3 (six-class sample stratification) was composed of the same plots as Class 7 (thirteen-class sample stratification); and Class 6 (six-class sample stratification) was composed of the same plots as Class 13 (thirteen-class sample stratification).

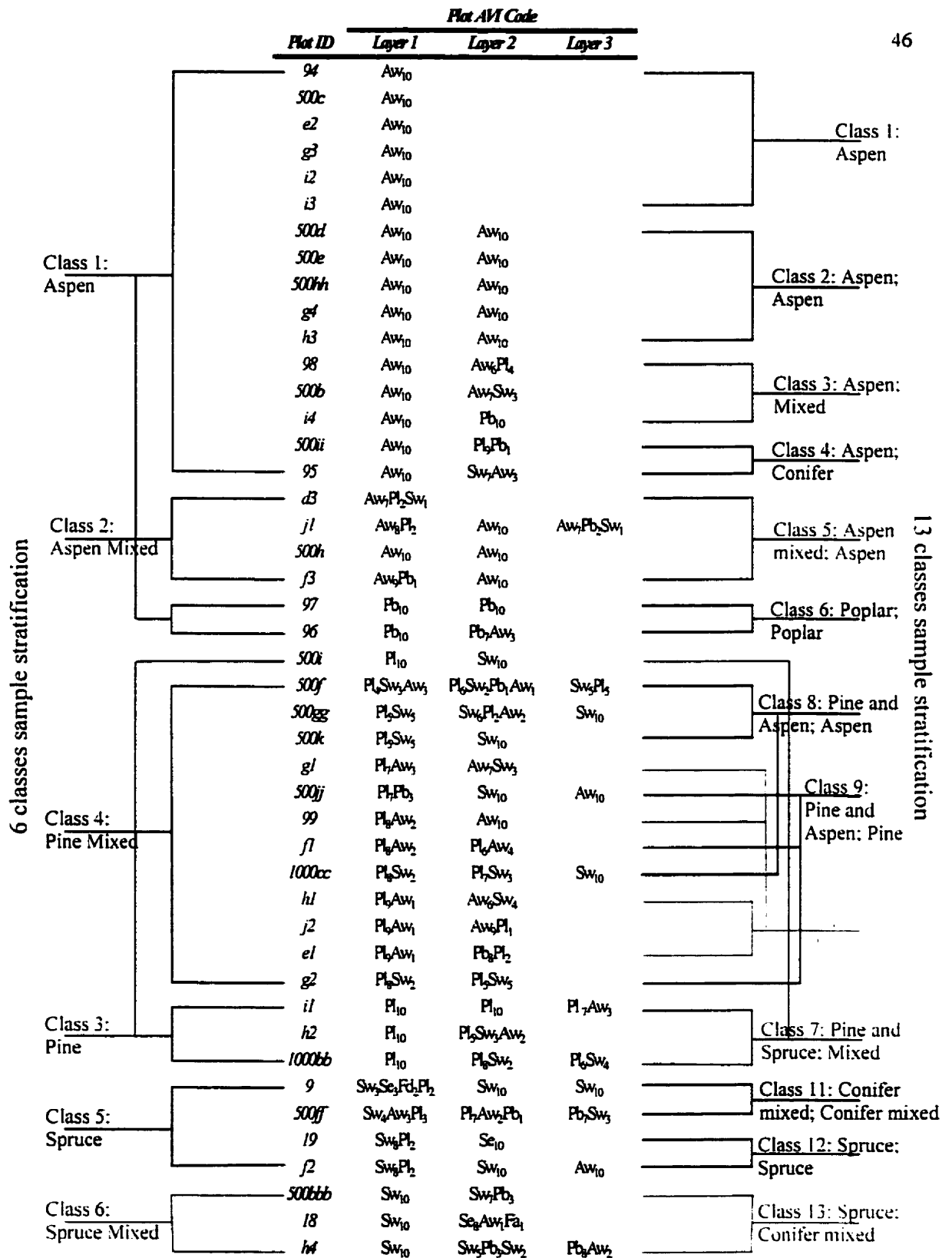


Figure 4.1 Sample stratification showing the six and the thirteen classes. The six-class stratification does not use the second and third canopy information, the thirteen-class stratification uses the full AVI information of the second layer in the class name (listed after the semicolon).

4.3 Image Preparation and Statistical Data Extraction

Subsets of the study area were extracted from the 12 km *casi* flight lines, this greatly reduced the size of the image database. The GPS data, field maps and plot maps were used to locate the plots on the imagery. This procedure was simplified by the constant geographical alignment/orientation to North of all plots (described below). Graphic masks, representing the exact location and area of each of the plots, were created. This procedure was repeated for all three resolutions of the *casi* imagery.

Before any aerial digital image analysis can take place some additional image preparation needs to be undertaken. The use of image corrections to improve radiometry and consequent classification accuracies is well documented (e.g. Robinove 1981; Franklin and Giles 1995).

Once the radiance of the study area was collected by the *casi* instrument, the data were corrected using a pre-flight sensor calibration in-house (Itres Research Ltd., also refer to Grey *et al.* 1997 who describe this procedure extensively). These data are in a raw form supplied to the user on digital tapes with a quantization of 16-bit. Two rectifications, also done in-house by Itres Research Ltd. (Mah *et al.* 1995) are:

- a) The geocorrection for aircraft roll, pitch and yaw; and
- b) Fitting the imagery to a geographical space, also known as georectification.

A 10 m horizontal and 4m vertical resolution Digital Elevation Model (DEM), derived from 1:25000 National Topographic Series (NTS) map sheets, was used in the corrections of all three resolutions of data; the DEM was resampled to each resolution (60 cm, 1 m and 2 m). During the flight mission a GPS unit in the aircraft was used to collect the exact location of the flight lines. These readings were differentially corrected using data from the Kananaskis Research Field Station base station located less than a kilometer away from the actual study area. The imagery was georectified (using the nearest neighbor resampling method) to

Universal Transverse Mercator (UTM) projection using the 1983 North American Datum (NAD 83). A study by Dikshit and Roy (1996) has shown that effects of image resampling (such as geocorrection or orthorectification) upon the spectral and textural supervised classification of high spatial resolution multispectral imagery are minimal.

Atmospheric correction is known to improve analysis based on spectral response and is recommended for studies where different imagery will be compared (e.g. different resolutions, different sensors); (Jensen 1996). Although down welling irradiance was measured at the top of the aircraft with an Incident Light Sensor (ILS) during the flight mission, and spectral reflectance target readings were collected on the ground, an atmospheric correction was not performed on the imagery. Atmospheric correction was not considered crucial to performing the classification study in this thesis. There are four major reasons for this decision:

- a) The high resolution imagery requires the aircraft to fly at low altitudes (between 1000 feet and 2000 feet); hence, the amount of atmosphere between the *casi* sensor and the canopy targets was minimal.
- b) There was no cloud coverage prior to and during the *casi* imagery collection. Clouds did not appear until at least an hour after the commencement of the flight mission. Therefore, the effects of the atmosphere were judged minimal.
- c) The radiance imagery was not available for analysis until the Fall of 1999.
- d) Furthermore, since texture analysis measures the spatial component of the shadow/sun-lit crowns within the imagery, the absolute radiometric differences would not be required in order to capture adequately the differences in very bright and very dark objects. Although spectral bands were used in the classification, the objective was not to determine how well the classification would perform but how much information the textural component adds to the classification.

4.4 Principal Component Analysis

Multispectral digital imagery can produce large amounts of data, but because of the spectral characteristics of the data, many bands are highly correlated (Table 4.1). Although ample information for an observation is necessary for a successful classification, highly correlated information and too much information can overwhelm the statistical classifier producing a large null or unclassified class (Lillesand and Kiefer 1994). One approach is to simply select a few bands based on visual analysis, or statistical tests such as the Bhattacharya-distance separability measure on a band with high contrast – usually the near-infrared band (e.g. Marceau *et al.* 1990). However, these methods are subjective and can be extremely sensitive to statistical assumptions (such as the assumption of a normal distribution) or to the increased number of bands in the sample, and may result in the loss of information and a non-optimal data set for classification (or statistical) purposes.

Another approach is to apply a Principal Component Analysis (PCA) to reduce the redundancy in the spectral data and create fewer dimensions in a predictable linear model. Although this method can also be sensitive to statistical properties of the data set, this approach was adopted in this study because of the large number of texture bands that can be produced from a single image dataset. PCA was applied to the seven spectral bands to produce seven Principal Components (PC). The results of the Principal Component Analysis are:

- a) Reduction in the number of bands needed for effective classification, while retaining the information content of all bands and discarding noise .
- b) One band, now called 'brightness', on which texture analysis was performed.

Even on the 60 cm imagery, where the resolution was the highest, the spectral bands show correlation ranging from adjusted R^2 of 0.59 to adjusted R^2 of 0.99 (Table 4.1). This is related to the information content of the imagery, in this case vegetation and shadows. For example, the lowest correlation occurs between band three (the red band where chlorophyll

absorption by vegetation can be measured) and band seven (the near infrared band where high scattering caused by the vegetation cell structure is significant). The relationship between the third band (red) and the subsequent bands all located at longer wavelengths, e.g. band four (adjusted R^2 of 0.89), band five (adjusted R^2 of 0.64), band six (adjusted R^2 of 0.62) and band seven (adjusted R^2 of 0.59) documents the increase in the spectral reflectance of the vegetation at longer wavelengths. The highest correlation occurs between bands closely neighboring on the electromagnetic spectrum, where similar vegetation characteristics are measured, at an adjusted R^2 of 0.99 between bands five and six.

The data in the seven 60 cm *casi* imagery bands is significantly correlated (at 95% confidence interval), therefore, the amount of information stored in these bands can be modeled through a regression line (line of best fit) equation. The first principal component is an axis along the regression line in the direction of most variance. The digital numbers in this principal component image indicate how far out along the new line the values fall, or how much spectral variability for a specific pixel is represented by that component.

Table 4.2 Correlation Matrix for the Seven Spectral Bands at 60 m pixel resolution

	<i>Band 1</i>	<i>Band 2</i>	<i>Band 3</i>	<i>Band 4</i>	<i>Band 5</i>	<i>Band 6</i>	<i>Band 7</i>
<i>Band 1</i>		0.93	0.85	0.97	0.89	0.88	0.86
<i>Band 2</i>			0.98	0.93	0.74	0.71	0.69
<i>Band 3</i>				0.86	0.64	0.62	0.59
<i>Band 4</i>					0.92	0.89	0.85
<i>Band 5</i>						0.99	0.95
<i>Band 6</i>							0.98
<i>Band 7</i>							

When the data are this highly correlated, most variability occurs along this new component, but if the data are less perfectly correlated, there is still some variability along another new axis orthogonal to the first principal component. This is the second principal component, which accounts for the maximum amount of the variance remaining after variance along the first principal component has been accounted for. Because there were seven original spectral

bands, seven principal components were calculated. The procedure was repeated for the other resolution (1 m and 2 m) *casi* imagery, but only the seven spectral (as opposed to PC) bands that overlap in all imagery were used in the analysis.

The percentage of variance accounted for by each component is expressed by that component's eigenvalue. The variance expressed by the first principal component of the 60 cm imagery was high at 89.77% for the whole image, meaning that 89.77 % of the variability contained in the seven spectral bands is mostly represented by the first principal component. The second principal component contains a small amount of the remaining information of only 8.96%. The results follow a similar pattern for the 1 m imagery, the first principal component explains 83.62% of the variance and the second principal component 14.73% of the variance. The 2 m PCA and resulting eigenvalues determined that the first principal component explained 80.93% variability and the second contributed to 17.88% variability. A trend was observed, as the resolution decreased and the number of objects contributing to a spectral response of a pixel increased, the variability explained by the first principal component (brightness) decreased and the second principal component became more important.

When performing PCA on a multiresolution image data set, such as the one used in this thesis, it is critical to the analysis to be working with the same elements in all imagery. When various resolutions of imagery are collected, the area covered by these images is not always identical on the ground or on the image. In this study, special care was taken to assure that only areas of image overlap were used to calculate the principal component. Given that the goal of this research is forestry-oriented, only the vegetated areas were included in the PCA. To investigate the success of the procedure the first principal component was tested for correlation between all resolutions resulting in relationships between 82% and 87%.

Table 4.3 Correlation between resolutions for the first principal component

	<i>60 cm pixel resolution</i>	<i>1 cm pixel resolution</i>	<i>2 cm pixel resolution</i>
60 cm pixel resolution	■	0.85	0.82
1 cm pixel resolution		■	0.87
2 cm pixel resolution			■

Figure 4.2 shows the first principal component imagery for all three resolutions, where the lightest pixels represent pixels undergoing high tonal variability captured by the bandset of *casi* imagery, their location on the axis of variability is far from the origin and therefore, the values are high. The dark pixels represent the pixels of low change through the seven spectral bands, their location on the variability axis is very close to the origin and therefore, the values are low. Spectral signatures, the way in which different ground components reflect or absorb different wavelengths of light, are used in remote sensing to distinguish between scene components or classes. They are the most important pieces of information driving a supervised image classification (Price 1994).

Two signatures, composed of sun-lit crown pixels and shadowed pixels are graphed in the Figure 4.2. The shadow pixels show exceptionally little variability in the different bandwidths, as compared to the vegetated pixels, and are represented as dark tone pixels in the first principal component imagery. Hence, the first principal component captures the one most important element necessary to identify multistory stands, the shadow. It also captures the different types of vegetation covers. The first principal component represents a brightness variable because it captures the tonal variability in the imagery. It was this variable which was used to perform texture analysis discussed later in this chapter. The figure also documents the increase in spectral values as the resolution decreases for the shadowed pixels, and the decrease in spectral values as the resolution decreases for the vegetation pixels. This inverse relationship can be explained by the merging of pixel components (vegetation and shadows) as the resolution decreases. It also explains the trend (demonstrated above) of reduction in variability expressed by the first principal component and increase of variability expressed by the second principal component as resolution decreases. Hence, with the loss of spatial detail pixel components merge.



1st Principal Component 'brightness' image based on the spectral bands of *casi*

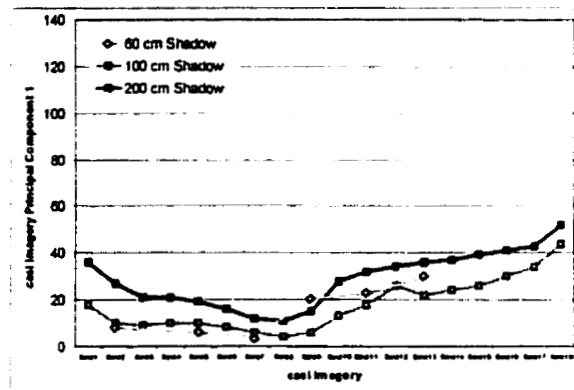
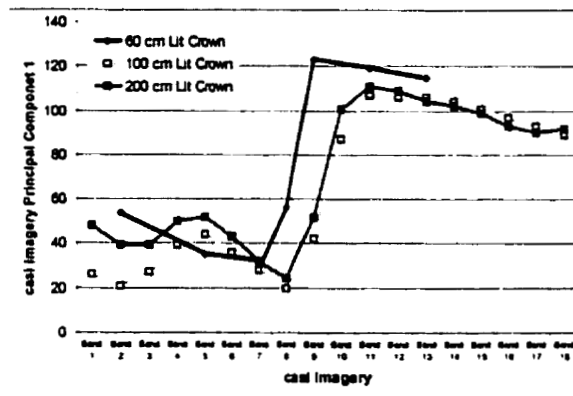


sun-lit crown



shadow

The thumbnail images above show the 'brightness' channel which was extracted from the *casi* imagery by using principal component analysis. The shadowed area in all *casi* image bands are represented by the dark areas in this imagery. The sun-lit crowns are the brighter areas. As image resolution increases the number of pixels representing each feature decreases. The edge (boundary) pixels of the features no longer represent the spectral characteristics of that individual feature but are a combination of spectral signatures of other components (adjacent features).



The above graphs summarize the mean pixel values for the sun-lit crown pixels and the shadowed pixels outlined in the 1st principal component imagery. All three resolutions are represented, the information for all spectral bands is shown, although only the seven overlapping spectral bands (see 60 cm) were used to calculate the 1st principal component. As the imagery resolution increases the mixing of various components can be interpreted in these graphs by the higher 'brightness' values of the targets. For example the shadowed pixels become lighter as they begin to mix with adjacent sun-lit vegetation pixels, this is well demonstrated in the second graph. Also, the spectral signature of the sun-lit crown changes as the resolution of the imagery decreases and adjacent objects contribute to the signal.

Figure 4.2 The first principal component for three *casi* imagery resolutions (60 cm, 1 m and 2 m) and graphs showing the spectral characteristics of a shadowed pixel and a lit-canopy pixel.

4.5 Structure and *casi* Imagery Shadow

To establish the relationship between the field data and the *casi* imagery a simple unsupervised classification (density slicing) of the first principal component was performed to isolate the shadow class captured by the low grey level values in this type of imagery. The percentage of shadow per plot was calculated. A structural complexity index was developed by averaging the standard deviation for physical characteristics of the plot (tree height, dbh and crown diameter); note that species composition was not explored by this index. This method is a simplified version of a Structural Complexity Index (SCI) used and described by Cohen and Spies (1992) and Cohen *et al.* (1995). The SCI used by Cohen produced a Principal Component based on the means and standard deviations of structural field data (dbh, crown diameter, basal area, height and tree density). In this thesis only the standard deviations were used because the variability within the plot was measured and not the variability among the plots. Hence, plots that had a lot of variability in tree size suggesting that more than one canopy is present had a higher average standard deviation than plots where the tree size was uniform (such as the same age aspen plots). The plots were sorted from highest to lowest, based on the structural complexity index, highest representing most structurally complex plots and lowest representing the least structurally complex plots. The per plot percentage of shadow pixels and stand complexity data are available in Appendix C. This procedure was repeated for all resolutions of the imagery.

Linear regressions based on data in Appendix C (graphs), showed the relationship between the structural complexity and the shadow percentage captured by the first principal component of the *casi* imagery, for all three resolutions. The R^2 of 0.60 at the highest resolution (60 cm) imagery, R^2 of 0.56 at the 1 m resolution imagery and R^2 of 0.55 at the (2 m) lowest resolution were calculated. In general, the aspen stands had a lower stand complexity index value than the coniferous stands, which can be related to the same age of these trees and low variability in tree characteristics (dbh, height, crown diameter) within the stand. The regressions confirmed that, as expected, a relationship exists between stand structure and the *casi* imagery (Appendix C). This is interpreted to mean that the shadow

component in the stand represents structural complexity of canopy elements, and is captured by the image data. This relationship can be the basis upon which the texture analysis and classification of multilayer stands can be conducted.

4.6 Creation of Texture Channels

The grey level co-occurrence matrix (GLCM) is constructed from the image by estimating the pair wise statistics of pixel intensity. Each element (i, j) of the matrix represents an estimate of the probability that two pixels with a specific spatial separation have grey levels i and j. The textural derivatives used in this thesis were based on the GLCM and not directly from the imagery, hence the name; second order texture measures. Second order texture has been shown to be effective in classification methodology (as outlined in Chapter 2); in one study, second-order texture outperformed newer texture measures based on semivariance for optical imagery similar to those employed in this thesis (Carr and Miranda 1998). Many second-order texture measures are readily available in commercial remote sensing packages, and were therefore selected for use in this study.

To perform texture analysis of an image five control variables need to be identified by the user. They include:

- a) The image channel to measure the image texture;
- b) The texture algorithm;
- c) Window size;
- d) Quantization level (8-bit, 16-bit or 32-bit);
- e) and the spatial component (relation between pixels)

The first principal component image was chosen to perform the texture analysis on the rationale that the first component represented the brightness feature in the image data set; in essence, one band represented the combined variability of all the image bands in a single dimension that is more easily handled than the original multispectral imagery.

The available commercial software program provides twelve texture measures; one of the original texture developers (Haralick 1986) presented fourteen different measures based on the co-occurrence matrix or second-order approach. Many of these measures are redundant and capture similar concepts (Wilson 1995). Therefore, from these available measures, five statistically different measures were chosen for this thesis research, including:

$$AngularSecondMoment = \sum_{j=1}^n \sum_{i=1}^m P(i, j)^2 \quad [4]$$

$$Correlation = \sum_{j=1}^n \sum_{i=1}^m \frac{P(i, j)R(i) - MeanR(i)(C(j) - MeanC(j))}{\sqrt{(VarianceR(i)(VarianceC(j))}} \quad [5]$$

$$Dissimilarity = \sum_{j=1}^n \sum_{i=1}^m P(i, j)(R(i) - C(j))^2 \quad [6]$$

$$Entropy = \sum_{j=1}^n \sum_{i=1}^m (-P(i, j) \ln(P(i, j)), \quad \text{assuming that } 0(\ln(0))=0 \quad [7]$$

$$Homogeneity = \sum_{j=1}^n \sum_{i=1}^m \frac{P(i, j)}{(1 + [R(i) - C(j)]^2)} \quad [8]$$

where:

- $P(i, j)$ = the spatial co-occurrence matrix element
- $R(i)$ = the grey level value for a row and
- $C(j)$ = the grey level value for a column (PCI, 1997).

Interpretation of these different measures can be considered conceptually. For example, the angular second moment employs probability of a pixel occurring based on the surrounding values. The higher the probability, the brighter the corresponding pixel value is in the texture channel. Therefore, in imagery which is homogenous, the angular second moment texture value will be high and in imagery which is heterogeneous the value will be low. The

algorithms apply an exponential approach; hence, the growth in probability changes rapidly. The correlation algorithm measures the linear dependency of the grey levels of neighborhood pixels; the more often like value pixels occur in a give area, the more likely it is that a pixel will be of the same value.

The dissimilarity texture algorithm is similar to the contrast texture algorithm. It measures the variability of the grey level values in the image, but the relationship between grey level values is linear. This measure is less sensitive to slight changes in image texture. Entropy measures the probability of the rate of change of a pixel grey-level value. Because of this logarithmic function, this measure is quite sensitive to slight changes in grey level value. Entropy is almost the opposite of the angular second moment measure. Homogeneity measures the likelihood of a pixel being similar (this has previously been demonstrated in Chapter 2, Figure 2.3) to the surrounding pixels, or the local similarity of the grey level values in an image. The homogeneity measure functions in almost an opposite manner to the dissimilarity measure. Low values relate that the image tone is variable and high values suggest high similarity in image tone.

Using coarse satellite data in an urban area, Marceau *et al.* (1990) concluded that on average the selection of the second-order texture algorithms used accounted for only 7% of the variability in classification results in their analysis. This was attributed to the fact that all of these algorithms are using the same co-occurrence matrix to calculate the texture and therefore, they are highly correlated. The same study concluded that choosing the window size of the texture measure is most important and can account for as much as 90% of the variation in classification accuracies (refer to also Hodgson 1998). In this thesis, six window sizes (3x3, 5x5, 9x9, 11x11, 17x17, 21x21) were used in the texture analysis. The smaller windows were chosen to capture textural characteristics of the individual objects in the analysis (trees), and as the window size increases the textural characteristics of the forest stands are measured. The methodology for choosing the window size is presented in the section on discriminant analysis.

Marceau *et al.* (1990) also showed that the quantization level of the data only accounted for 3% of the variability in classification results; therefore, it is the least important parameter. In this thesis, all textural measures were produced at the 32-bit quantization level based on *casi* imagery of 16-bit quantization level.

The distance (separation) parameter used to construct a grey level co-occurrence matrix specifies the scale at which the texture is analyzed; therefore, the optimal choice of this distance as well as the direction (angle), is dependent on the inherent scale of the texture being analyzed. In high resolution imagery, more than one pixel can represent an object on the ground. Furthermore, the pixel values can change rapidly across a few pixels. To best capture the characteristics of high resolution imagery the invariant spatial component (the mean of all four main inter-pixel angles) with an inter-pixel value of one was used. This is in agreement with the findings of Marceau *et al.* (1990) and agrees with the later studies by Franklin and McDermid (1993) and Maudie (1999). Hence, on 60 cm imagery the scale of the texture measure using a 3 x 3 window was 60 cm, on 1 m imagery the scale of the texture measure using a 3x3 window was 1 m and on the 2 m imagery the scale of the texture measure using a 3x3 window was 2 m.

4.7 Texture and *casi* Imagery Shadow

To illustrate the relationship between texture and image shadows (created by different forest stand structures) a sample subset multispectral image was chosen, shown in Figure 4.4. The subset was extracted from the imagery at all resolutions from a known location centered on an edge between a pure aspen and pure conifer stand, so that half of the image subset is an aspen stand and half is a mixed conifer spruce and pine stand. The size of the area is approximately 40 m by 20 m. The subset extraction was performed to facilitate the visual analysis of the relationships between image texture and shadow, and is interpreted in Chapter 5, section 5.2.

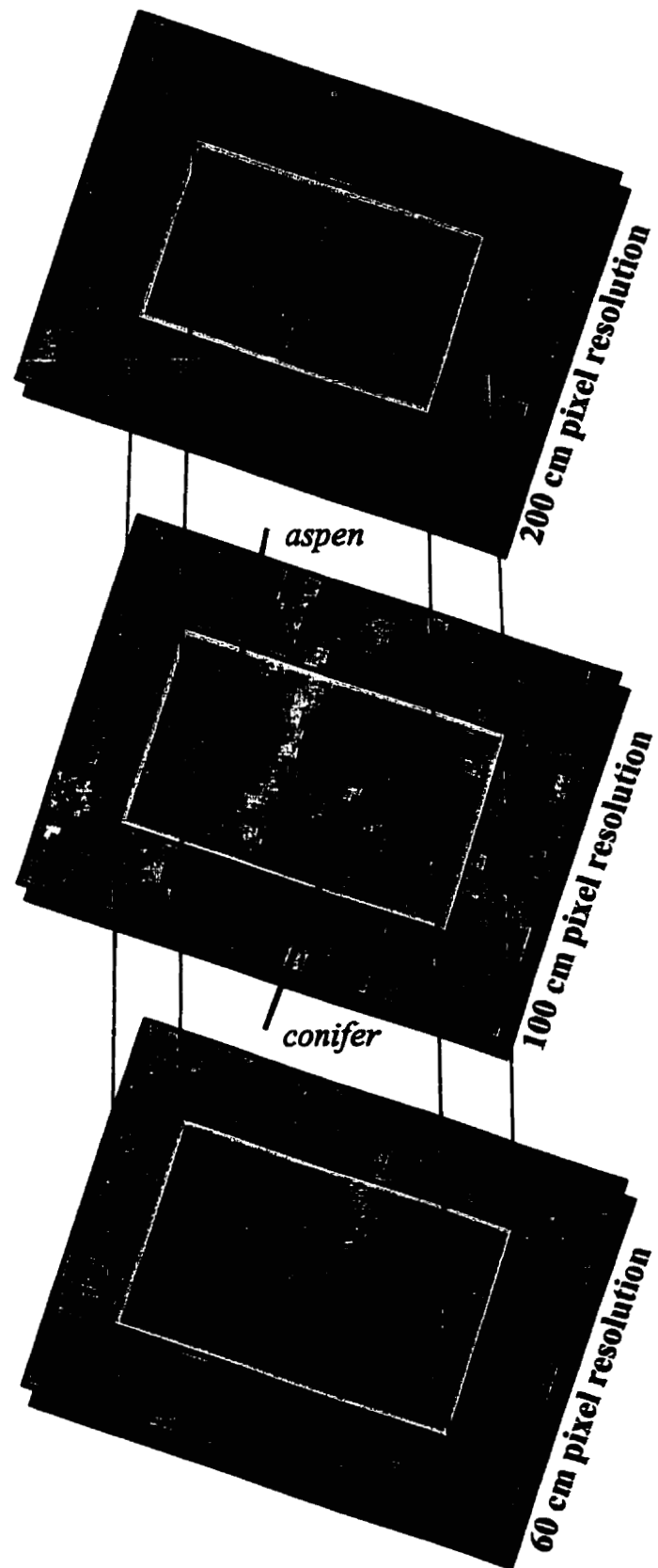


Figure 4.3 False colour composite showing the subset window

4.8 Statistical Data Extraction from *casi* Imagery

Per pixel data were extracted for all bands at all resolutions from underneath the graphic mask of the plots. The data were imported to the SPSS (SPSS 1997) statistical package. In classification analysis, statistical summaries of the data are used as the signatures, which separate the classes. To reduce the amount of data, and decrease the processing time, the plot spectral and textural information was summarized with the plot mean. This approach is feasible in higher resolution imagery where the plot comprises many objects including tree canopy, shadows and to some extent (depending on the crown closure) the understory. The plot standard deviation was also extracted and tested, but it did not prove to contribute significantly to the analysis.

4.9 Classification Procedure

The classification decision rule selected for this study was the discriminant analysis (DA) function (Klecka 1982; Tabachnick and Fidell 1996). Discriminant analysis is useful for situations where one needs to develop a predictive model of group membership based on observed characteristics of each case. The procedure generates a discriminant function (or, for more than two groups, a set of discriminant functions) based on linear combinations of the predictor variables that provide the best discrimination between the groups. The functions are generated from a sample of cases for which group membership is known; the functions can then be applied to new cases with measurements for the predictor variables but with unknown group membership (SPSS 1997). In this thesis, the group is the AVI class (based on field data) and the set of predictors are the spectral bands and the textural bands derived from the first principal component of the *casi* imagery.

A preliminary DA had to be performed to determine the best window size of the texture measure (already identified in the previous section as the most important factor in texture analysis). In this exploratory analysis, the six-class sample stratification based on the first AVI canopy layer was used. The results are reported in Table 4.3. Since, this analysis was

only part of the paramilitary data exploration, this DA was not assessed for accuracy. Therefore, all cases were used to develop the DA function.

Table 4.4 Preliminary DA results in % to determine the best texture window size

<i>Data combinations</i>	<i>60 cm pixel</i>	<i>100 cm pixel</i>	<i>200 cm pixel</i>
<i>7 Spectral Bands</i>	64.7	51	60.8
<i>7 Spectral Bands, 5 Textures (3x3 window)</i>	74.5	72.5	80.4
<i>7 Spectral Band, 5 Textures (5x5 window)</i>	62.7	80.4	80.4
<i>7 Spectral Bands, 5 Textures (9x9 window)</i>	64.7	68.6	76.5
<i>7 Spectral Bands, 5 Textures (11x11 window)</i>	66.7	68.6	74.5
<i>7 Spectral Bands, 5 Textures (17x17 window)</i>	64.7	66.7	70.6
<i>7 Spectral Bands, 5 Textures (21x21 window)</i>	60.8	82.4	82.4
<i>5 Textures* (3x3 window)</i>	51	54.9	56.9
<i>5 Textures (5x5 window)</i>	43.1	58.8	54.9
<i>5 Textures (9x9 window)</i>	49	35.3	51
<i>5 Textures (11x11 window)</i>	49	39.2	47.1
<i>5 Textures (17x17 window)</i>	41	47.1	52.9
<i>5 Textures (21x21 window)</i>	45.1	52.9	52.9

**The five texture measures include: homogeneity, dissimilarity, correlation, entropy and angular second moment*

The best classification results of 82.4 % occurred on the largest window size 21x21 confirming results by Marceau *et al.* (1990); Hodgson, (1998) and Maudie (1999). Hence, texture measure of the stand (large window size) was a better discriminating factor than texture of individual tree crowns (smaller window size). It is important to notice that on the high resolution imagery the best results 74.5% occurred at the smallest 3x3 window size. The second best result (80.4 %) also occurred on the lower resolution imagery at a smaller window size (3x3 and 5x5 window size on the 2 m and 5 window size on the 1 m).

The results of this initial test established that the classification should proceed based on the seven spectral bands as predictors in conjunction with the five textural measurements at 21x21 window size. In the final analysis three different discriminant analyses were run:

- a) Seven spectral bands as the only set of predictors;
- b) Five textural bands as the only set of predictors;
- c) Seven spectral and five textural bands as the set of predictors.

The procedure was repeated for all three resolutions of imagery and two different levels of classes. It is important to note that this classification procedure is designed to test the study hypothesis at the field plot locations, and is not the same approach that would produce a classification map. In that type of analysis, much more attention would need to be focused on developing training signatures and testing statistical assumptions of the resulting training data. As Franklin (1994, p 1238) pointed out in an earlier forest inventory classification study using 2.5 m *casi* data, '*while the casi data Discriminant well the required inventory stands, this does not necessarily mean that the stands can be mapped well*'. Operational problems in mapping based on the image data represent an entirely new set of problems and issues that are beyond the scope of this thesis.

4.10 Accuracy Assessment

Accuracy assessment is an essential final step in any classification study to determine the validity of the classification approach and the utility of the final products (Congalton and Green 1998). The DA in SPSS allows for accuracy testing of the model by using some observations to develop the DA function and using the rest of the observations to test the function. Hence, a random 25 % of the class sample was used to test the DA accuracies, except for classes where only two samples existed; here one randomly chosen observation was used to develop the model and one to test it. Co-occurrence matrices were calculated for the two DA scenarios, and for both of the model developing observations and the model testing observations. The final, overall accuracies, for the developing and testing of the model are not the average accuracies on the diagonal but are normalized taking into consideration the size of the sample.

Producer's and user's accuracies as suggested by Felix and Binney (1989) are also reported for each co-occurrence matrix. The bottom row of each matrix shows the errors of omission also known as the producer's accuracy. The values summarize the percentage of plots correctly classified. The extreme right column of the co-occurrence matrices shows the errors of commission also known as the user's accuracy. Errors of commission indicate the probability that a plot classified as a given class actually represents that class on the ground.

The Kappa coefficient of agreement represented by the KHAT statistic defined by Cohen (1960) was used to score the actual agreement minus the chance agreement of a co-occurrence matrix. This has been defined both in Lillesand and Kiefer (1994) and Jensen (1996):

$$KHAT = \frac{oa - ca}{1 - ca} \quad [9]$$

where:

oa = observed accuracy

ca = chance agreement

The Kappa Statistic (KHAT) is an index value ranging between 0 and 1 which expresses the proportionate reduction in error achieved by a classifier as compared with the error of a completely random classifier. Thus, a value of 0.75 would indicate that the classifier was avoiding 75 percent of the errors that a totally random process would have produced (PCI, 1997).

The KHAT statistics formula used in this analysis was taken from Jensen (1996):

$$KHAT = \frac{N \sum_{i=1}^r x_{ii} - \sum_{i=1}^r x_{i+} x_{+i}}{N^2 - \sum_{i=1}^r x_{i+} x_{+i}} \quad [10]$$

where:

r	=	number of rows in the error matrix
X_{ii}	=	number of observations in row i and column i (on the major diagonal)
X_{i+}	=	marginal total of row i
X_{+i}	=	marginal total of column i
N	=	total number of observations included in matrix

4.11 Chapter Summary

In this chapter, the processing of the field data (basal area extraction) to produce AVI labels and the two methods of sample stratification were discussed. The second layer in the canopy needed to be well established, therefore, trees less than 2 m in height but more than 1 m in height were combined in the second layer. It is part of the AVI field protocol to exclude any trees less than 1 m in height from the AVI label (Alberta Forestry, Lands and Wildlife 1991). The *casi* image preparation including the geometrical correction to remove aircraft roll, pitch, yaw and position have been presented. The methodology used to extract the 'brightness' variable carrying most information about stand shadow was discussed. The relationship between the stand structure and *casi* image shadow for an all three resolutions (60 cm, 1 m, and 2 m) was established. The chapter included a description of how the texture channels were generated and what variables were used in their construction. The statistical data extractions (signature creation) were summarized. The classification procedures using Discriminant Analysis for three types of classifications (spectral alone, textural alone and combination of the two) were discussed. Finally, the methods of accuracy assessment using errors of omission and commission as well as the Kappa statistic were outlined.

Chapter 5 Results and Analysis

5.1 Introduction

Spectral characteristics of a stand can be useful in studying forest structure. For example the near-infrared reflectance increases with the number of layers of leaves in the canopy (Lillesand and Kiefer 1994). Structural information derived from spectral data can be complemented by textural derivatives from the imagery, which are also sensitive to structural components of the canopy (Wulder 1996). The main hypothesis of this thesis is that image texture derived from high spatial resolution multispectral (*casi*) imagery will increase the classification accuracy of multistory forest stands identified according to the AVI system as part of a forest inventory. A classification approach is suitable to investigate this idea. In this study, three combinations of data were used as input to a classifier. These three combinations included spectral data alone, textural data alone, and the combined spectral and textural data classification (Table 5.1). The data were classified using the first layer class stratification and subsequently the same procedure was performed on the full information AVI label class stratification, as introduced and discussed in Chapter 4. Even this level of detail is not the full AVI field-label but is a summary of the characteristics of each plot that may be more suitable for a remote sensing classification. All classifications were repeated for the three spatial resolutions (60 cm, 1 m and 2 m) of *casi* imagery data available for the study area.

However, prior to testing this hypothesis, a greater understanding of the behavior of the individual texture measures and their relationship to field data was sought. The first section of this chapter will discuss the results of a visual and a descriptive interpretation of one texture measure as an example of the relationship between image characteristics and field characteristics. Although all of the texture measures used in the classification were visually interpreted, it is only practical to present the interpretation of one measure. In addition, because the textural measures are all based on the grey level co-occurrence matrix, they are

all highly correlated. The texture measure homogeneity was selected because this measure is the most readily understood of all the available measures. Descriptive statistics included the means and standard deviations of the texture measure computed at different window sizes on the different image resolutions. One final interpretation exercise was conducted on three individual plots (Plate 3.3 in Chapter 3) selected to relate the texture measures to the physical characteristics of the stands.

Table 5.1 Listing of information used in the classification of all three resolutions of data

<i>Data Combination</i>	<i>Data Used</i>
Spectral alone	7 bands, (540–560 nm, 610–640 nm, 640–680 nm, 690–715 nm, 730–755 nm, 790–810 nm and 850–875 nm)
Textural alone	5 textures, (angular second moment, correlation, dissimilarity, entropy and homogeneity)
Combination of spectral and textural	7 bands and 5 textures

5.2 Visual Interpretation of Image Texture

A set of visual analyses was conducted to determine the complexity of the second order texture measures in different types of forest stands; as mentioned, only the homogeneity measure is interpreted in detail here. Note that homogeneity is conceptually simple – it refers to the high probability of the similarity of adjacent pixel values. In the following figures of texture, high homogeneity values are expressed by a lighter tone in the imagery and the low homogeneity values are darker.

A subset area showing the intersection of aspen and conifer stands was used to produce the textural graphics which are the focus of this discussion (as shown in the Methods Chapter 4, Figure 4.3). This area shows that aspen appears as the “smooth” bright red stand on the false colour near-infrared imagery, and the conifer stand appears “coarse” and dark green.

Appendix D shows all of the textural measures, which are enhanced using an equalization stretch. The 3D graphic is used to show the same measure on a surface using the same vertical scaling for all window sizes (3x3, 5x4, 9x9, 11x11, 17x17 and 21x21) of texture imagery produced. All images were produced for the three resolutions of *casi* data (60 cm, 1 m and 2 m). The graphics in this section show abbreviated figures of the imagery for the homogeneity measure in Appendix D.

Figures 5.1 a, b and c show the homogeneity texture image of the subset area of aspen and conifer. A progression of change in the homogeneity texture measure is apparent in the images at the three different resolutions and the different three window sizes (3x3, 9x9 and 21x21) shown.

The window size defines the area that is incorporated in the texture measure. Hence, there is a relationship between the window extent and the objects being captured by the texture measure. For example, a 3x3 window covers an area of 1.8 m^2 on the 60 cm imagery, which is smaller than an average tree crown in the study area. This is interpreted to mean that the window includes the texture of the individual tree crown architecture in a stand comprised of the sun-lit and shadowed portion of the tree crowns separately. This is in agreement with other works, which discuss texture as a scale-specific phenomenon (refer to Hay and Niemann 1994). The larger 21x21 window covers an area of 12.6 m^2 on the ground at the same 60 cm pixel resolution. The individual tree crowns are no longer the main contributor to texture in this size of window, which may now be dominated by the stand structure comprised of clusters or groups of individual tree crowns and gaps (the shadows and the sun-lit crowns).

In Figure 5.1a, which shows the 60 cm 3x3 homogeneity texture window, the homogeneity appears high for the conifer stand. The standard deviation, best expressed by the surface image, is also quite high except for the areas of similarity. These are the groups of light tone pixels or groups of dark tone pixels on the imagery representing the sun-lit and shadowed parts of the conifer canopy. The aspen stand is dark in tone in the homogeneity texture

image, and there is less variability (expressed by the lower standard deviation). These observations are the exact opposite of the visual analysis of the texture of conifer and aspen stands in the original colour composite image (refer to Figure 4.4 in Chapter 4). This difference may be related to the ability of the texture measure to capture the texture of the tree crown itself and not the texture of the stand. The latter is what the human interpreter would focus on in the colour composite.

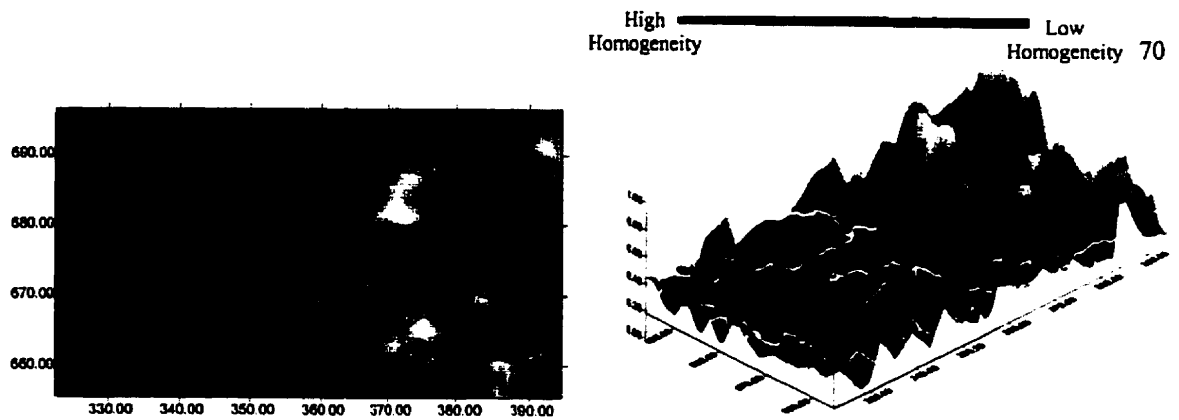
In the 9x9 texture window, the homogeneity of the conifer sun-lit and shadowed portions of the crowns is again expressed in the high homogeneity of the stand. The standard deviation is again quite high. Likewise, the aspen stand shows the low homogeneity typical of the aspen crown (no apex, variability in leaf position and direction). In the 21x21 texture window, the characteristics of the tree crowns are summarized by the homogeneity texture measure; here, the conifer stand appears light (high homogeneity) with low standard deviation. The aspen crowns are also summarized by the homogeneity texture measure; lower homogeneity and lower standard deviation than that of the conifer stand.

On the 1 m homogeneity imagery (Figure 5.1b) in the 3x3 texture window the two stands appear texturally similar, except for the two large or exceptionally large conifer crowns, which can be detected individually. A small difference is measured in the standard deviations of the two stands. In the 9x9 window the texture of the two stands is even more similar (an even smaller difference in tone and texture) and the two conifer crowns are still visible. This is mostly due to the architecture of the conifer crown but it should be noted that the conifer crown diameters in this location are larger than the aspen crown diameters). In the 21x21 window, the two stands are difficult to distinguish texturally, and they have a similar standard deviation.

Figure 5.1c shows the same location on the 2 m homogeneity texture measure. The 3x3 texture window now covering an area of about 6m² shows that the two stands are alike, but the boundary between the stands is visible. Notice that both individual conifer and aspen crowns are distinguishable in the imagery. In the 9x9 window, the aspen stand shows a much

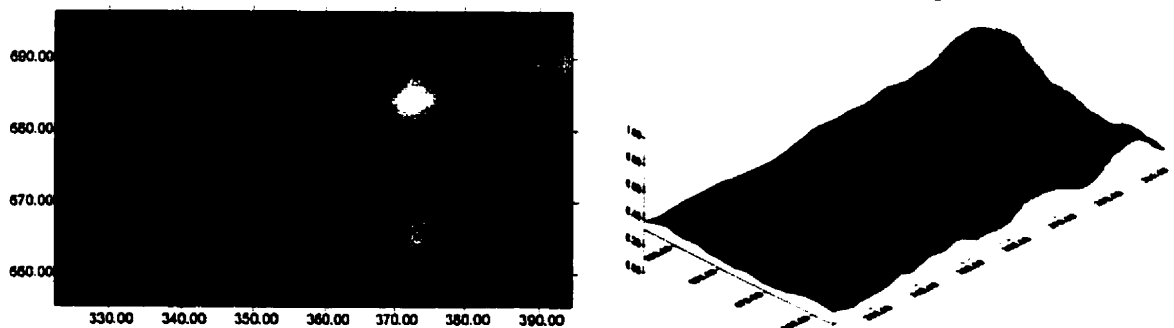
lighter tone than the conifer stand. This trend continues to intensify as the window size increases, and is even more dominant in the 21x21 window where the aspen stand has a high homogeneity (the aspen stands comprised of same age trees which are relatively similar in size and shape). The conifer stand appears as a low homogeneity stand. The shadow and sun-lit canopies of all trees as well as the more complex stand structure are captured by the texture measure.

This same type of texture inversion with window size and pixel resolution was observed when interpreting the entropy, dissimilarity and angular second moment textural images (refer to figure in Appendix D). The entropy measure captures the inversion of the texture measure but on average, the stands appear similar. The standard deviation also did not vary as much between the stands. The dissimilarity measure also captured this type of inversion; the stands did not appear visually different until the 9x9 window size on the 60 cm resolution imagery. On all of the 1 m resolution imagery and up to the 11x11 window size on the 2 m resolution imagery the most dominant feature on the imagery was the boundary of the two stands, with the stands still appearing similar texturally. Only at the 17x17 window size on the 2 m imagery did the two stands appear different. This suggests that dissimilarity texture measure can be utilized to detect boundaries and edges between vegetation classes. The correlation texture measure was least sensitive to the textural inversion between the two stands; it also brought out the boundary between the stands and in general behaved similarly to the dissimilarity measure. The angular second moment, the statistical opposite of the entropy measure, and was not shown graphically in Appendix D.



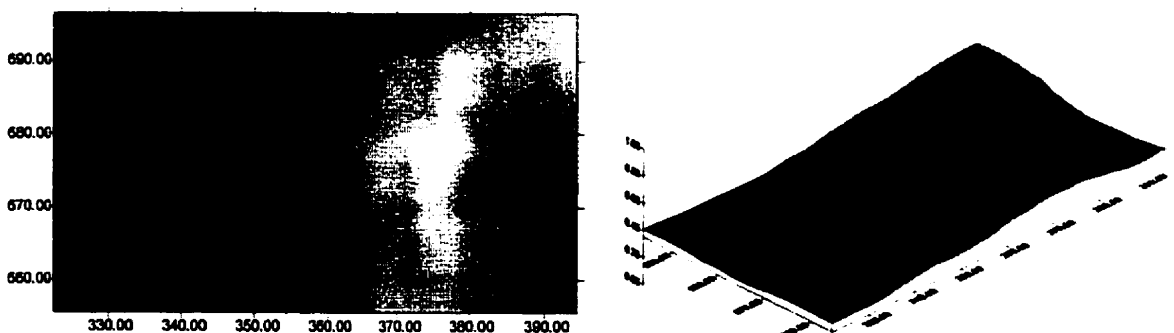
3 x 3 window

The aspen stand, on the left, appears dark in tone and has very low homogeneity texture values. The opposite is true for the conifer stand, on the right, which appears lighter in tone and the homogeneity values are higher. There is a wider range in the standard deviation of the conifer stand, but a few areas of concentrated, high homogeneity are visible. The texture captures the variability of reflectance and shadows within the aspen and conifer crowns.



9 x 9 window

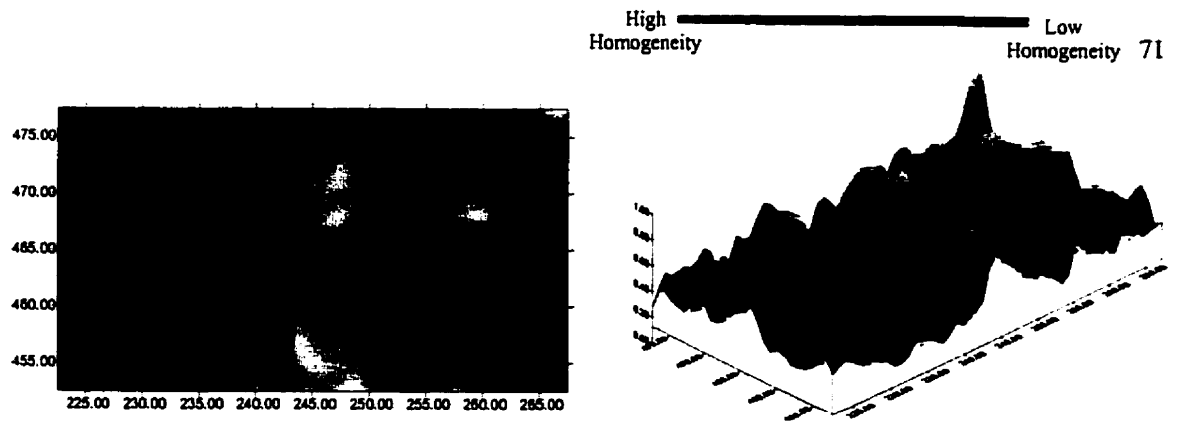
The aspen stand homogeneity texture using a 9 x 9 window appears very low, the opposite is true for the conifer stand, where the texture is higher and there are visible areas of concentration (sun-lit crowns and shadows of the conifer trees). The standard deviation is reduced at this window size, however, the conifer stand still shows a greater difference.



21 x 21 window

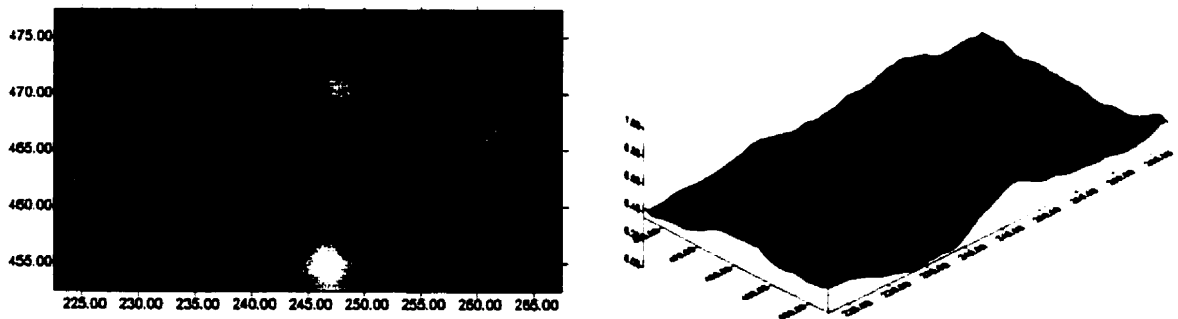
The variability of the tree crowns is expressed as the texture measure for the whole stand. The aspen stands show very low homogeneity for the whole stand (a function of the low homogeneity of the aspen tree crowns), the conifer stand shows high homogeneity for the whole stand (a function of the sun-lit and shadowed components of the conifer crowns).

Figure 5.1 a Homogeneity texture for the subset window using 60 cm *casi* imagery and three window sizes.



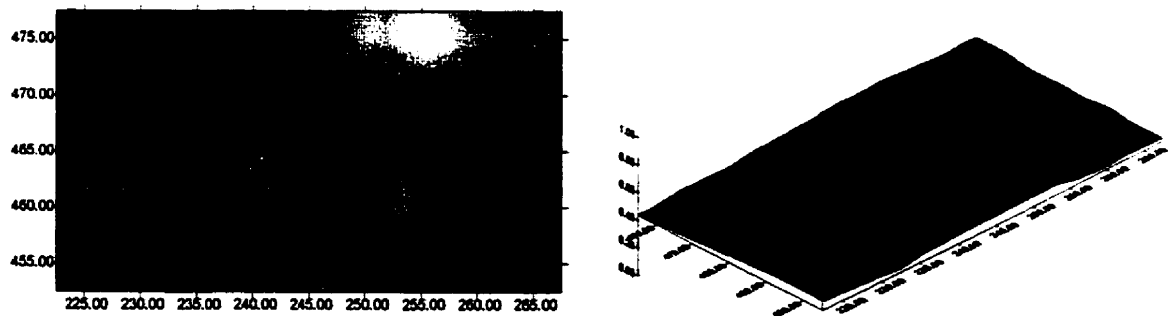
3 x 3 window

Using the 1 m *casi* imagery and a small window (3x3) it is difficult to distinguish between the aspen (left) and conifer (right) stands. The textural characteristics of the two stands are difficult to separate. However, the conifer stands still shows areas of localized high homogeneity which are inherent to the conifer sun-lit crowns and shadows. Some variability within these crown and shadows is still represented.



9 x 9 window

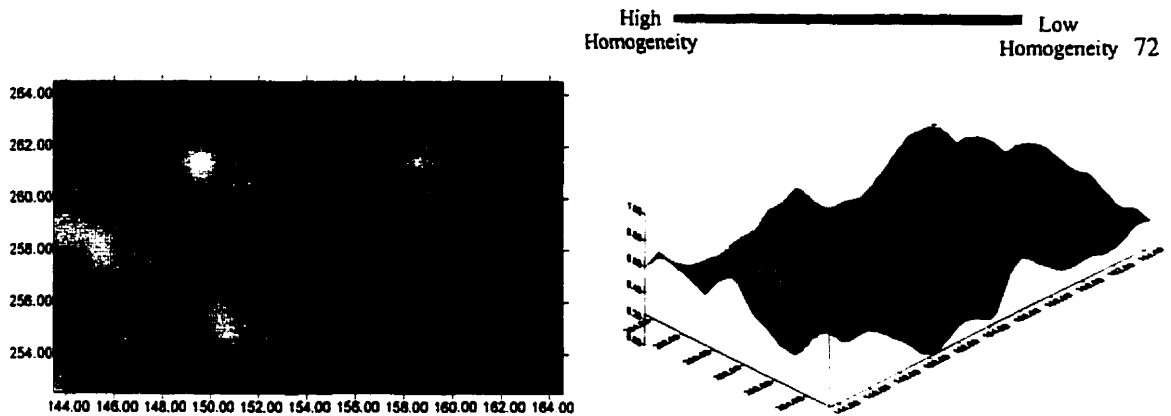
As the window size increases to 9x9, the variability within the localized high homogeneity areas diminishes. The conifer stand shows higher standard deviations (higher peaks, lower lows) than the aspen stands, but on average these are virtually undetectable as seen in Figure 5.2.



21 x 21 window

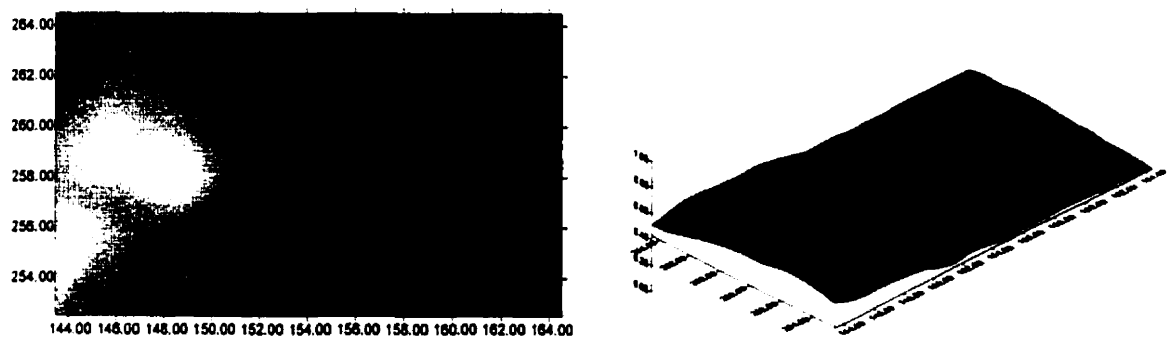
At the largest window size of 21x21 all within tree crown textural characteristics are minimized. The textural characteristics of the stand are increased. The conifer stands shows (on average) a slighter higher homogeneity texture compared to the aspen stand.

Figure 5.1 b Homogeneity texture for the subset window using 1m *casi* imagery and three window sizes.



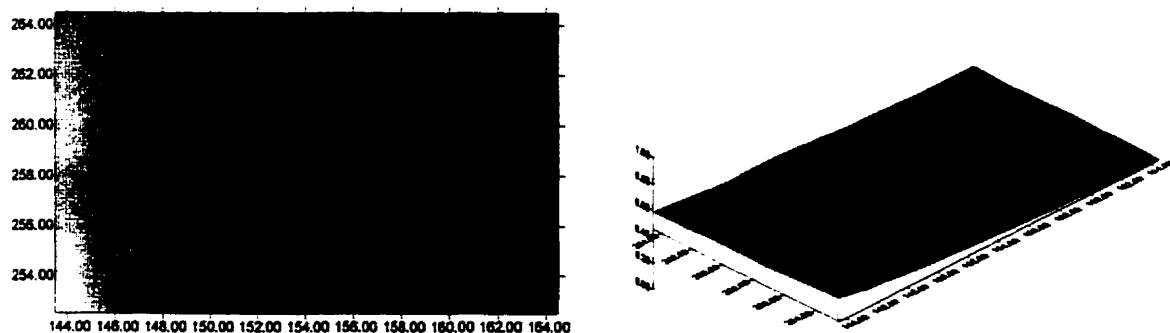
3 x 3 window

Using the 2m *casi* imagery and a small (3x3) window size homogeneity texture the aspen (left) and conifer (right) stands are not distinguishable. Within crown characteristics are not captured by this texture measure combination, however, areas of high and low concentrations of homogeneity are accentuated. The boundary between the two stands is also enhanced.



9 x 9 window

As the window size increases the differences between the aspen and conifer stands become visible. The aspen stands shows areas of high homogeneity, and has on average higher in homogeneity values than the conifer stand. Small variabilities within the stand are represented.



21 x 21 window

Using the largest window size 21x21, the two stands are very different in homogeneity measurements. The aspen is represented by high homogeneity, and the conifer stands is homogeneously low in values (inverse of what the higher resolution imagery shows). No within stand variabilities are captured by the texture.

Figure 5.1c Homogeneity texture for the subset window using 2m *casi* imagery and three window sizes.

In summary, based on a visual analysis of the homogeneity texture measure in different window sizes and different pixel resolutions, the texture of high resolution imagery (60 cm pixel resolution) appears to contain a great deal of information on the crown architecture of individual trees. The texture is comprised of differences within crown shadows or sun-lit and shaded crowns. The texture also can be interpreted to contain information on stand structure such as tree distribution, species and shadows. Texture of high resolution imagery (1 m and 2 m pixel resolution) reduces the ability to detect individual tree crown architecture and is more related to stand structure characteristics.

5.3 Descriptive Statistical Interpretation of Texture

The means and standard deviations of homogeneity texture extracted from the imagery in the subarea shown in Figure 4.3 (Chapter4) are summarized by graphs in Figure 5.2. These graphs show the simple descriptive statistics that confirm the visual interpretation in the preceding section. Essentially, there is an inversion of the homogeneity texture measure with window size; this is repeated at each of the available pixel resolutions. The visual analysis hinted at this trend but the statistics shown in these graphs provide a more definitive interpretation.

In particular, notice the aspen stand shown in red. Homogeneity always increases with decreasing pixel resolution, and this increase is more pronounced at the smaller window size. The inverse of this effect can be noted in the conifer stand shown in green. Here, the decrease of conifer stand homogeneity is related to the decrease in pixel resolution. In other words, a low homogeneity aspen stand at high spatial resolution becomes a high homogeneity aspen stand at low spatial resolution. A high homogeneity conifer stand at high spatial resolution becomes a low homogeneity conifer stand at low spatial resolution.

As described in the visual analysis of texture measures, this inversion occurs because of the change in the object that the texture is measuring from within tree crown architecture to the structural component of the stand itself. The largest difference between the means and

standard deviations of the two stands occurs at the 3x3 window of the 60 cm image, the most spatially detailed imagery. This could have significant implication in a classification where these types of statistical summary – e.g. the means and standard deviations - are used to distinguish between many classes. The 1 m textural imagery demonstrates that the aspen and conifer stands are texturally similar; this imagery has already lost the detail of the crown architecture (capable of distinguishing stands) but has not yet captured the structural complexity of the stand (also capable of distinguishing the stands). This is also captured by the shift in the standard deviation of the two stands, from lowest at 2 m to highest at 60 cm (as the window size increases).

- All these trends suggest that a small window size (3x3) at a high resolution (60 cm) should yield best class distinction results in a classification.

5.4 Example of Relationship between Texture and Field Data

The next step was to investigate visually the relationships between the interpretation of texture (represented by the homogeneity measure and its statistical characteristics) and the structural field information of the plots. Selected for this analysis were three plots (shown in Plate 3.3 in Chapter 3); one aspen, and two conifer stands. The idea was to show the relationships in these areas, which represent typical examples of the kinds of forest structures that must be classified or interpreted as part of a forest inventory. The plot structural information based on the collected field data is shown in Table 5.2. There are two conifer species stands, which vary in species composition and tree sizes. The two conifer stands have an established second canopy layer, the Douglas fir stand has an aspen second canopy layer and the mixed conifer stand has a mixed conifer second canopy layer. The aspen/poplar stand, with an aspen second canopy layer is pure and was not defoliated during the summer of 1998.

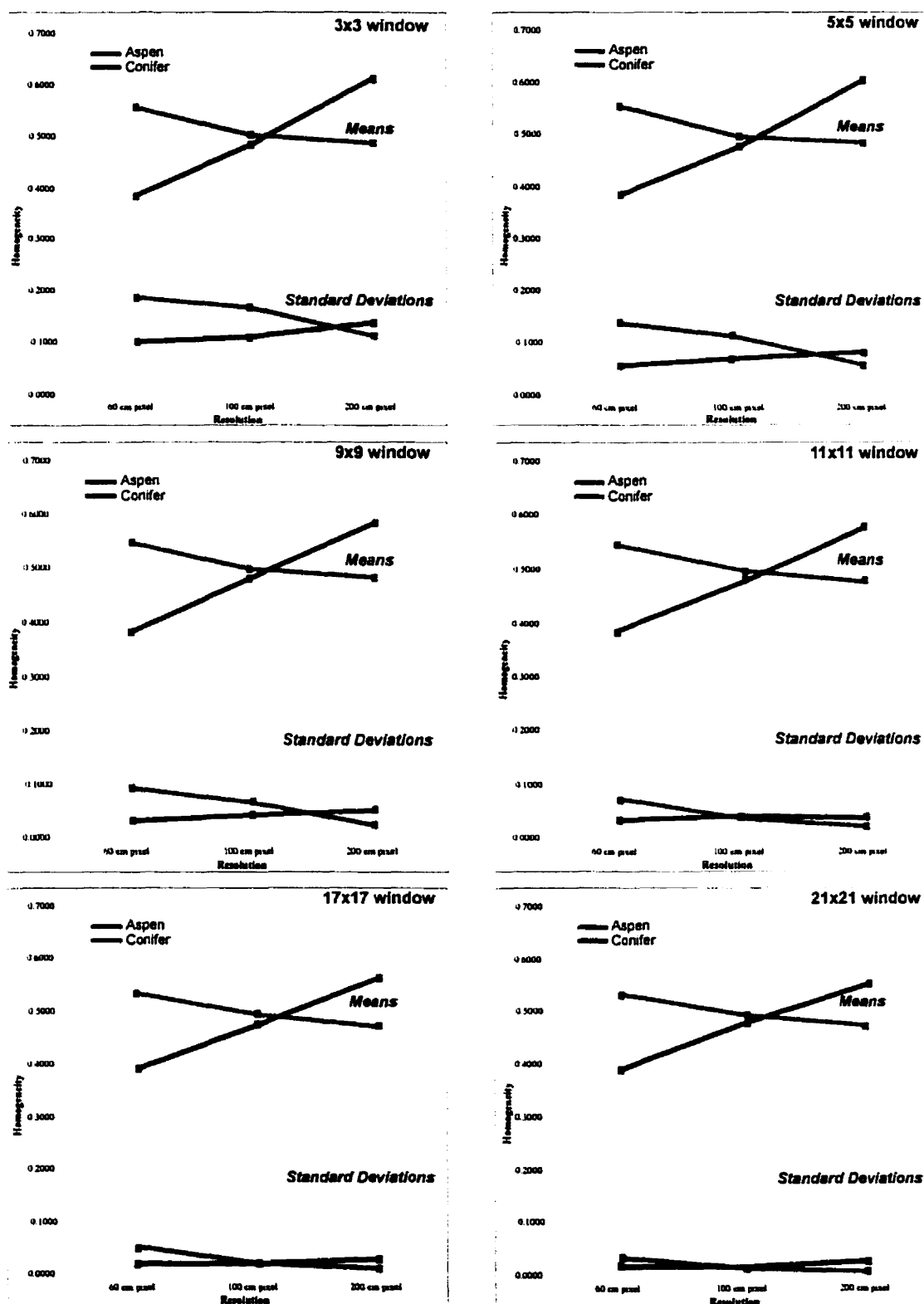


Figure 5.2 Statistical summary of change in the homogeneity texture measure for the aspen and conifer imagery subset. Six window sizes (3x3, 5x5, 9x9, 11x11, 17x17 and 21x21) and the three *cas* imagery resolutions are represented.

Table 5.2 Structural information based on the collected field data for the 3 field plots

<i>Plot AVI Code</i>				<i>Average Plot Structure</i>			
<i>Plot ID</i>	<i>Layer 1</i>	<i>Layer 2</i>	<i>Layer 3</i>	<i>GRS Crown Closure</i>	<i>Height</i>	<i>Crown Diameter</i>	<i>dbh</i>
<i>500gg</i>	Pl ₅ Sw ₅	Sw ₆ Pl ₂ Aw ₂	Sw ₁₀	60%	14.6m	2.8m	18cm
<i>93</i>	Se ₁₀	Aw ₁₀		60%	18m	5.2m	20cm
<i>f3</i>	Aw ₉ Pb ₁	Aw ₁₀		41%	10.9m	2.4m	13cm

The statistical trends for the plots are summarized by a graph showing the homogeneity texture in a 3x3 window and a second graph showing the texture based on a 21x21 window. All three resolutions are demonstrated. Due to the similarity between the graphs only the smallest and largest window sizes are needed to demonstrate the trends.

Figure 5.3 shows statistical trends, which appear to be exceptionally similar to the ones recorded for the subset imagery in the earlier visual and descriptive statistical analysis. There is a noticeable inversion of the texture measure as the spatial component being measured becomes less detailed. The largest difference in statistical summaries for the aspen and conifer stands occurs at the 2 m data. However, the two conifers are most statistically distinct at the 60 cm data. In the 3x3 window the large crown diameters (5.2 m) of the Douglas Fir stand contribute to the high homogeneity measure within the crown. The smaller crown diameters (2.75 m) of the mixed conifer stand are expressed as lower homogeneity. This is in agreement with Bruniquel-Pinel and Gastellu-Etchegorry (1998) who established in their work that the tree crown diameter is the most influential biophysical parameter on texture measures.

Based on this information it has been interpreted that crown sun-lit and crown shadowed parts of the canopy in such large trees are large areas of similarity to which the smaller window size texture homogeneity measure is sensitive. On the 21x21 window at the 60 cm resolution, the same inversion was observed as in the subset where the large trees of the

Douglas Fir stand contribute to the complexity of the structure of the stand resulting in lower homogeneity. The smaller conifers in the mixed conifer stand are more homogeneous in the 21x21 60 cm imagery. The aspen trend also shows the lower homogeneity values at higher resolution (60 cm) and high homogeneity values at the correct resolution (2 m).

Finally, texture is not as successful at showing differences between the aspen and conifer stands at high resolution (60 cm). For example, at the 2 m resolution the means of the two species are most different. The 1 m data also shows the least ability at distinguishing between the different species, or within species difference.

These results are significant when thinking about the classification scheme. Although texture is not as successful in distinguishing between the species, it can distinguish within species differences better at higher resolutions and smaller window sizes. This is interpreted to mean that because spectral bands are exceptionally adequate in species distinction, both the spectral and textural information at the highest spatial component (60 cm and 3x3 window size) should produce the best classification results where within species stratification is desirable.

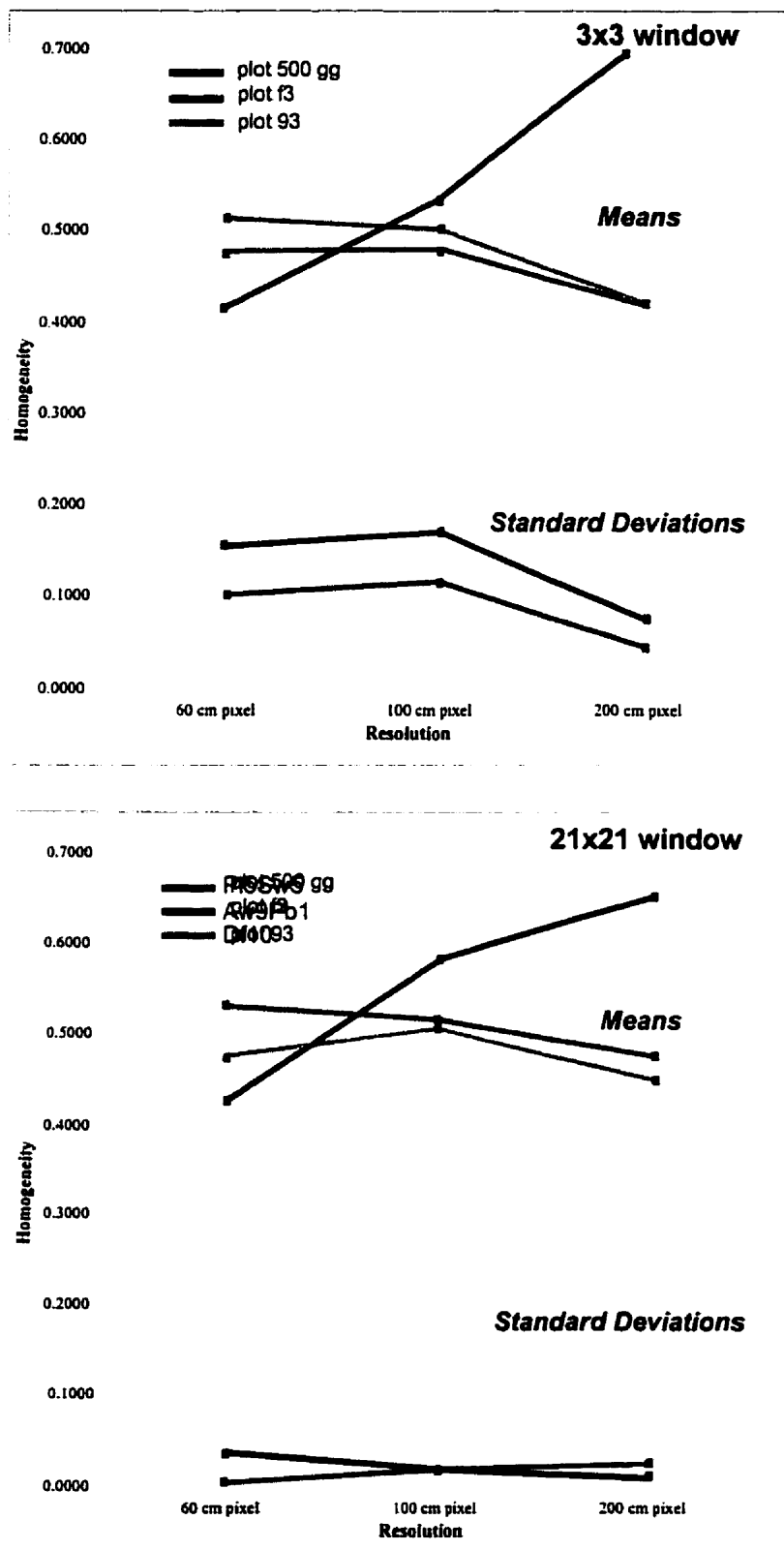


Figure 5.3 Statistical summary of change in homogeneity for three field plots. Two window sizes and the three *casi* imagery resolutions were used.

5.5 Discriminant Analysis Results

The DA classification methodology discussed in Chapter 4 was applied to two classification schemes based on the AVI labeling using the collected field data:

- a) Six-class sample stratification
- b) Thirteen-class sample stratification

The procedure was repeated for all three resolutions of the data (60 cm, 1 m and 2 m). All DA was performed on the spectral bands alone, textural bands alone and the combination of the spectral and textural bands. Only the 21x21 window size results are reported here because this window size, on average, provided the most separability among the classes at each resolution. At the six-class sample stratification, the DA function was developed with thirty-four plots and tested on eleven plots. At the thirteen-class sample stratification, the DA function was built on thirty plots and tested on fifteen plots.

The section presents and discusses the results in the form of omission/commission errors and statistical significance based on the KHAT statistic. Omission errors are computed by considering the rows in the contingency or classification tables; e.g. if a plot is omitted from the class in which it was originally placed based on the field data, then it would appear as a member of another class along the row. Commission errors are computed by considering the columns; e.g. that same plot then becomes a commission error of the class into which it has been wrongly placed by the image data.

5.5.1 Results using the first AVI Layer

In this section, the discriminant classifier was run on the same field/image samples, but the classification scheme is less detailed considering only the first layer or components of the canopy in the labeling of the stand. This level of classification is comparable to those that have been previously attempted (e.g. Franklin and McDermid 1993; Maudie 1999) and

represents a possible application of image texture similar to that which can be accomplished through traditional forest inventory procedures using aerial photointerpretation. Again, as noted by Wilson (1995) it is important to remember that this AVI classification is not the full AVI as implemented in the field, but is a grouping of the plot data to represent homogenous stands that are suitable for remote sensing classifications.

Table 5.3 Summarized classification results and accuracies for six-class sample stratification

<i>DA using six-classes</i>				
	<i>KHAT (confidence level</i>			<i>KHAT (confidence level</i>
	<i>Developing</i>	<i>95%)</i>	<i>Testing</i>	<i>95%)</i>
<u>60 cm data</u>		<i>34 plots</i>		<i>11 plots</i>
7 Spectral & 5 Textural	79.4	0.73 (+/- 0.0065)	63.6	0.57 (+/- 0.0103)
7 Spectral	61.8	0.51 (+/- 0.0118)	54.5	0.43 (+/- 0.0137)
5 Textural	50.0	0.37 (+/- 0.0151)	45.5	0.39 (+/- 0.0146)
<u>100 cm data</u>				
7 Spectral & 5 Textural	76.5	0.69 (+/- 0.0074)	63.6	0.57 (+/- 0.0103)
7 Spectral	55.9	0.47 (+/- 0.0127)	54.5	0.43 (+/- 0.0137)
5 Textural	44.1	0.33 (+/- 0.0161)	36.4	0.28 (+/- 0.0173)
<u>200 cm data</u>				
7 Spectral & 5 Textural	73.5	0.65 (+/- 0.0084)	72.7	0.66 (+/- 0.0082)
7 Spectral	58.8	0.53 (+/- 0.0113)	54.5	0.39 (+/- 0.0146)
5 Textural	44.1	0.33 (+/- 0.0161)	36.4	0.28 (+/- 0.0173)

For the 60 cm data set, the spectral bands produced a classification accuracy of 61.8 % when the model was developed, while testing of the model produced a 54.5% classification accuracy (refer to Table 5.3). Based on the literature (e.g. Franklin and McDermid 1993; refer to Chapter 3) this is a reasonable level of accuracy to expect at this spatial resolution with this type of classifier and this level of class stratification.

Most of the misclassification of plots occurred within similar classes. For example, Class 1 (aspen) was only 71 % accurate when developing the model and 50 % accurate when testing the model (refer to Table 5.4a). An error of omission occurred for the aspen class; 50% of the class was actually assigned to Class 2 (aspen mix). The conifer classes also displayed some confusion among them, especially Class 4 (pine mix) to which Class 5 (spruce) and Class 6 (spruce mix) were committed.

The DA using only textural derivatives showed an accuracy of 50% when developing the model and 45.5% when testing the model (refer to Table 5.3). Unlike the spectral band classification, the classes when separated using texture alone were misclassified not only into other similar classes but also into different species categories. For example, some plots from Class Four (pine mix) were committed to Class Two (mixed aspen class), and Class Six (mixed spruce class) (refer to Table 5.4b).

The combination of the two data types (spectral and textural) in DA produced accuracies of 79.4 % to develop the model and 63.3% to test the model. The aspen class (1) was still problematic, showing an accuracy of only 25% and committing some of the plots to the aspen mix class (2) and the pine class (3) (refer to Table 5.4c). This compares favorably to earlier reports of accuracies on the order of 75% using spectral and texture measures and similar classes (e.g. Franklin and McDermid 1993; Franklin *et al.* 1988, Gerylo *et al.* 1997).

For the 1 m DA, the spectral bands did not perform as well as for the higher resolution data (60 cm), yielding an accuracy of 55.9 % to develop the model and 54.5 % to test the model (Table 5.3). However, the same or similar errors of omission and commission occurred here as in the 60 cm data, with Class 1 (aspen) and Class 4 (pine mix) showing developing accuracies as low as 25 % and 33.3 % (refer to Table 5.5a). The textual derivative DA results were also lower for the 1 m data than for the 60 cm data results at 44.1% to develop the model and 36.4 % to test the model. Classes Four (pine mix) and Five (spruce) appeared to be the most problematic classes, both having plots being committed to Class Two (aspen

mix). In addition the aspen class (1) was committed to Class Two (mixed aspen), producing a DA model testing result of only 25% (refer to Table 5.5b).

The combination of the spectral and textural data produced a model developing result of 76.5 % and a model testing accuracy of 63.5 % (Table 5.3). Once more, the Fourth Class (pine mix) was the weakest in the classification at only 33%, committing its members to the Second Class (aspen mix) and Third Class (pine). The two aspen classes were also confused, where the First Class (aspen) was committed to the Second Class (aspen mix), 25 % of the First Class was also committed to the spruce mixed class (6). (refer to Table 5.5c).

Finally, the 2 m data set results produced the lowest accuracies in the six-class sample stratification scheme for the three spatial resolutions tested. For the DA using spectral bands only, model developing accuracy was 58.8 % and model testing accuracy was reported as 54.5% (refer to Table 5.3). The confusion occurred mostly in the first (aspen) class to which the second (aspen mix) and third (pine) classes were committed (refer to Table 5.6a). The textural bands produced DA results of 44.1 % and 36.4 %, for developing and testing accuracies respectively. Similar trends as observed in the 60 cm and 1 m data were observed, where the classes not only were confused with adjacent but even with exceptionally different classes. For example, Class 4 (pine mix) and Class 5 (spruce) plots were both committed to Class 2 (aspen mix) (refer to Table 5.6b). The spectral and textural DA produced results of 73.5% and 72.7% for developing and testing of the classification respectively. Class 1 (aspen) and Class 4 (pine mix) were once more the problematic classes producing results of 75% and 33.3 %, respectively (refer to Table 5.6c).

Table 5.5a Classification results for the 6 class sample stratification using only the spectral 1m data

Results from Building of the Discriminant Function
Plot Class Assignment

Class	Field Survey Data						Total
	1	2	3	4	5	6	
1	14	4	1	-	1	2	14
2	1	3	-	-	-	-	3
3	-	-	3	1	-	-	3
4	-	2	-	2	2	1	9
5	-	1	-	-	3	-	3
6	-	-	-	-	-	2	2
Total	7	9	4	4	5	5	
Errors of Omission	86%	22%	75%	100%	40%	40%	

Classification Accuracies in %

Class	Field Survey Data						Total
	1	2	3	4	5	6	
1	29	7	-	7	14	-	57
2	33	-	-	-	-	-	33
3	-	-	33	-	-	-	33
4	-	22	-	22	11	-	55
5	-	33	-	-	-	-	33
6	-	-	-	-	-	22	22

55.90% of selected original grouped cases correctly classified

Results from Testing of the Discriminant Function
Plot Class Assignment

Class	Field Survey Data						Total
	1	2	3	4	5	6	
1	4	1	-	-	-	-	4
2	-	3	-	-	-	-	3
3	-	-	3	-	-	-	3
4	-	-	-	2	2	-	3
5	-	-	-	-	3	-	3
6	-	-	-	-	-	1	1
Total	1	3	2	1	3	1	
Errors of Omission	100%	33%	50%	100%	33%	100%	

Classification Accuracies in %

Class	Field Survey Data						Total
	1	2	3	4	5	6	
1	50	25	-	-	-	-	75
2	-	33	-	-	-	-	33
3	-	-	33	-	-	-	33
4	-	-	-	67	-	-	67
5	-	-	-	-	33	-	33
6	-	-	-	-	-	100	100

54.50% of unselected original grouped cases correctly classified

Table 5.5b Classification results for the 6 class sample stratification using only the textural 1m data

Results from Building of the Discriminant Function
Plot Class Assignment

Class	Field Survey Data						Total
	1	2	3	4	5	6	
1	14	4	-	1	3	-	14
2	-	3	-	-	-	-	3
3	-	-	3	1	-	-	3
4	-	2	4	1	1	-	9
5	-	1	-	1	3	-	3
6	-	1	-	-	-	2	2
Total	6	11	6	4	3	4	
Errors of Omission	100%	27%	33%	50%	33%	25%	

Classification Accuracies in %

Class	Field Survey Data						Total
	1	2	3	4	5	6	
1	29	-	-	7	21	-	57
2	-	33	-	-	-	-	33
3	-	-	33	-	-	-	33
4	-	22	44	11	-	-	55
5	-	33	-	33	-	-	33
6	-	50	-	-	-	22	72

44.10% of selected original grouped cases correctly classified

Results from Testing of the Discriminant Function
Plot Class Assignment

Class	Field Survey Data						Total
	1	2	3	4	5	6	
1	4	1	-	-	-	-	4
2	-	3	-	-	-	-	3
3	-	-	3	-	-	-	3
4	-	2	-	1	1	-	3
5	-	1	-	-	3	-	3
6	-	-	-	-	-	1	1
Total	1	7	1	0	0	2	
Errors of Omission	100%	14%	100%	0%	0%	50%	

Classification Accuracies in %

Class	Field Survey Data						Total
	1	2	3	4	5	6	
1	75	-	-	-	-	-	75
2	-	33	-	-	-	-	33
3	-	-	33	-	-	-	33
4	-	67	-	33	-	-	100
5	-	100	-	-	33	-	133
6	-	-	-	-	-	100	100

36.40% of unselected original grouped cases correctly classified

Table 5.5c Classification results for the 6 class sample stratification using combination of spectral and textural 1m data

Results from Building of the Discriminant Function
Plot Class Assignment

Class	Field Survey Data						Total
	1	2	3	4	5	6	
1	14	3	-	-	-	-	14
2	-	3	-	-	-	-	3
3	-	-	3	1	-	-	3
4	-	1	-	2	2	-	9
5	-	-	-	1	3	-	3
6	-	-	-	-	-	2	2
Total	11	7	2	8	4	2	
Errors of Omission	100%	43%	100%	75%	50%	100%	

Classification Accuracies in %

Class	Field Survey Data						Total
	1	2	3	4	5	6	
1	21	-	-	-	-	-	21
2	-	33	-	-	-	-	33
3	-	-	33	-	-	-	33
4	-	11	-	22	-	-	33
5	-	-	-	33	-	-	33
6	-	-	-	-	-	22	22

76.50% of selected original grouped cases correctly classified

Results from Testing of the Discriminant Function
Plot Class Assignment

Class	Field Survey Data						Total
	1	2	3	4	5	6	
1	4	1	-	-	-	-	4
2	-	3	-	-	-	-	3
3	-	-	3	-	-	-	3
4	-	1	1	2	-	-	3
5	-	-	-	-	3	-	3
6	-	-	-	-	-	1	1
Total	2	3	2	1	1	2	
Errors of Omission	100%	33%	50%	100%	100%	50%	

Classification Accuracies in %

Class	Field Survey Data						Total
	1	2	3	4	5	6	
1	25	-	-	-	-	-	25
2	-	33	-	-	-	-	33
3	-	-	33	-	-	-	33
4	-	33	33	-	-	-	66
5	-	-	-	-	33	-	33
6	-	-	-	-	-	22	22

63.60% of unselected original grouped cases correctly classified

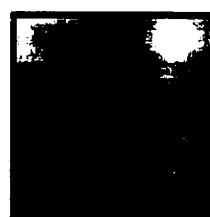
In summary, the six-class sample stratification was best classified using the combination of the spectral and textural information. The spectral data alone produced results where similar species were confused. For example aspen and mixed aspen were confused with each other and spruce and mixed spruce also caused errors. The inclusion of textural data in the DA confused classes with similar spatial component, or plots that appeared to be similar in tonal change. For example, two aspen plots were confused as spruce and spruce mixed plots. Figure 5.4 best explains the reasons for this misclassification, based on texture alone. The figure shows aspen plots with a range of defoliation, the false colour composite 60 cm *casi* imagery and textural representations of the plots are also shown. The heavily defoliated aspen plot has similar homogeneity texture characteristics (high homogeneity) to the coniferous plot. In some cases, an aspen plot was misclassified based on the spectral characteristics, resulting in commission to a coniferous class. Appendix E shows a summary of radiance characteristics (similar to reflectance curves) for aspen (ranging in defoliation) and conifer plots. The non-defoliated aspen plots have a much higher radiance values, in the near-infrared bands, than the heavily defoliated aspen plots. In fact, the heavily defoliated aspen plot shows a pattern of radiance similar to the one of the conifer plot. This conifer reflectance pattern is well known (Lillisand and Keifer 1994), where radiance is lower in the conifer species in the near-infrared wavelengths, compared to deciduous species. This explains why an aspen plot was confused with a conifer plot. Furthermore, the rates of change (the average digital number change from spectral band to spectral band) in the radiance curves for the non-defoliated aspen plots are higher (167, 158 respectively) than the rates of change for the defoliated aspen and conifer plots (127, 130 respectively); (also in Appendix E). This relates to the similarity of texture for the defoliated aspen and for the conifer plots. Both have a slower rate of change, which was captured by the 'brightness' image from which the texture was derived, hence, the higher homogeneity texture values for these plots.

Aspen non defoliated

casi false colour
composite



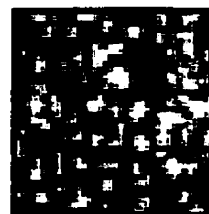
homogeneity texture
3 x 3 window



homogeneity texture
21 x 21 window

Aspen moderately defoliated

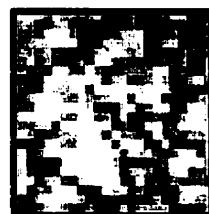
casi false colour
composite



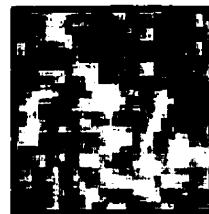
homogeneity texture
3 x 3 window



homogeneity texture
21 x 21 window

Aspen heavily defoliated

casi false colour
composite

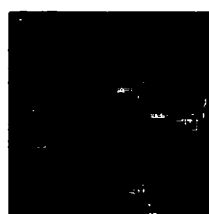


homogeneity texture
3 x 3 window



homogeneity texture
21 x 21 window

The Bruce spanworm defoliation in the aspen stands has been captured by the *casi* imagery. The defoliation resulted in reduction in the absorption in the red band and a reduction in the radiance being reflected by the trees in the near infrared bands. Therefore, stands which were very similar structurally (because of their clonal reproduction) appeared very differently to the *casi* sensor. The defoliation also reduced the structural complexity of the tree crowns, which is represented by the higher homogeneity in both the 3x3 and 21x21 window sizes.

Conifer

casi false colour
composite



homogeneity texture
3 x 3 window



homogeneity texture
21 x 21 window

The conifer plot showed a large amount of shadow in the *casi* imagery. The texture captures the low change in pixel values in the shadowed areas of the imagery, and produced an overall high homogeneity value using 21x21 window for the plot similar to that of the moderately and highly defoliated aspen stands.

Figure 5.4 Texture similarity between the heavily defoliated aspen and conifer plots

In this first DA, the classification was acceptable, but similar classes tended to be misclassified with each other. Grouping of plots with such a wide range of AVI species components in the first and other layers caused the signatures for these classes to be exceptionally broad and overlap each other, resulting in some misclassifications.

At all image resolutions, the plots that were near the edge of a class (their standard deviation was largest and their means were the farthest from the average class mean) caused the most errors of omission and commission. For example, some plots labeled as aspen plots in the six-class sample stratification scheme would often be classified as aspen mixed plots and were fully omitted from the aspen class. Examples are plots 98, 95 and 500ii. In all cases the plots were misclassified as aspen mixed, and in all plots the second layer had some conifer species contributing to the plot signature and causing this type of misclassification. The contribution of the second layer to the plots' signatures was significant. For example, at plot 98 as much as 11.9 m² in basal area belonged to the second layer. Also, the field data showed that 32% of the crown closure of the plot was contributed by this layer. This same error occurred with plots labeled pine and spruce; many of these plots would be misclassified as mixed conifer plots. In further investigation, most of these plots had a second canopy layer, which was not used in the six-class sample stratification scheme. Although the basal area in this layer is much smaller than the basal area of the first layer (refer to Table 4.1 in Chapter 4), the results show that this layer did contribute to the signature of the plots. This stratification scheme operates ineffectively near class boundaries. The results suggest that a better stratification scheme such as the thirteen-class sample stratification scheme, which takes into consideration the existence of the other layer, could be more appropriate.

5.5.2 Results Using All AVI Layers

In this section, the discriminant classifier was run on the same field/image samples, but the classification scheme was more detailed, considering all the components of the canopy (or layers) in the labeling of the stand. This level of classification is much more detailed than

has been previously attempted (e.g. Franklin *et al.* 1998), but was suggested by that earlier study as a possible application of image texture beyond that which can be accomplished through traditional forest inventory procedures. Only the 21x21 window size results are reported here because this window size, on average, provided the most separability among the classes at each resolution.

Again, as noted by Wilson (1995) it is important to remember that this AVI classification is not the full AVI as implemented in the field but is a grouping of the plot data to represent homogenous stands that are suitable for remote sensing classifications.

Table 5.7 Summarized Classification Results and Accuracies for Thirteen-class sample stratification

<i>DA using thirteen-classes</i>				
	<i>Developing</i>	<i>KHAT (confidence level 95%)</i>	<i>Testing</i>	<i>KHAT (confidence level 95%)</i>
<u>60 cm data</u>		30 plots		14 plots
7 Spectral & 5 Textural	86.7	0.85 (+/- 0.0036)	86.7	0.86 (+/- 0.0034)
7 Spectral	66.7	0.63 (+/- 0.0089)	66.7	0.64 (+/- 0.0086)
5 Textural	53.3	0.49 (+/- 0.0122)	53.3	0.5 (+/- 0.0120)
<u>100 cm data</u>				
7 Spectral & 5 Textural	83.3	0.82 (+/- 0.0043)	80.0	0.78 (+/- 0.0053)
7 Spectral	63.3	0.6 (+/- 0.0096)	60.0	0.57 (+/- 0.0103)
5 Textural	53.3	0.4 (+/- 0.0144)	46.7	0.5 (+/- 0.0120)
<u>200 cm data</u>				
7 Spectral & 5 Textural	70.0	0.67 (+/- 0.0079)	73.3	0.71 (+/- 0.0070)
7 Spectral	63.3	0.6 (+/- 0.0096)	60.0	0.57 (+/- 0.0103)
5 Textural	50.0	0.45 (+/- 0.0132)	40.0	0.33 (+/- 0.0161)

The thirteen-class sample stratification scheme classification was applied first to the 60 cm data. The classification accuracies for the spectral bands only DA were 66.7 % for both the developing and the testing of the model (refer to Table 5.7). The confusion occurred among the various aspen Classes 1 through 5, (refer to Table 5.8a). The texture data only DA produced results of 53.3% for both the developing and testing of the function. It can be

observed in Table 5.8b that the confusion between classes occurs throughout the matrix, where deciduous type classes can be confused with conifer type classes. An explanation for this was already discussed in the previous section, (also refer to Figure 5.4). The combination of the spectral and textural data produced the highest results; 86.7% occurred for both developing and testing of the model. The second class (aspen type class) was committed to the wrong classes (refer to Table 5.8c). It is possible that the defoliation in the aspen stands in the summer of 1998 is making these classes more problematic (refer to Figure 5.4). Regardless, this final result is 7.3% higher than the six-class sample stratification.

At the 1 m data, accuracies for the DA are less than the higher resolution (60 cm) data, but are still higher than the six-class sample stratification results. The spectral DA showed a result of 63 % for developing the model and 60 % for testing the model. On average, these results are about 5% higher than the six-class sample stratification results (refer to Tables 5.3 and 5.7). In Table 5.9a it can be observed that, once again, it is more the aspen type stands that are contributing to the errors in the classification. The textural data only DA shows that many of the stands are textually similar (Table 5.9b), the developing accuracy of the model is only 53.3 % and the testing is 46.7 % (refer to Table 5.7). The combined spectral and textural DA performed much better than the six-class sample stratification method (refer to Table 5.7) resulting in the accuracies of 83.3% for developing of the function and 80 % for testing of the function (refer to table 5.7). The aspen stands show a misclassification and the pure aspen stand with no second canopy layer (Class One) shows the lowest classification accuracies of 50% (refer to Table 5.9c). It should be mentioned that these were estimated to be of the same age, resulting in one layer aspen stands. These types of stands are most susceptible to and suffered from defoliation (Peterson and Peterson 1992). Hence, the spectral signature of these stands differs from non-defoliated stands (Appendix E). This is due to the contamination of the signature with other factors such as tree trunks and branches, understory or standing litter, (refer to vanLeeuwen and Huete 1996; or Guyot *et al.* 1989). Finally, KHAT results show higher accuracies than the six-class sample stratification results (refer to Table 5.7).

The lowest results in the DA occurred using the 2 m data. These were exceptionally similar to the results achieved in the six-class sample stratification (refer to Table 5.7). The DA using spectral data alone produced classification accuracies of 63.3% when developing the model and 60 % when testing the model (refer to Table 5.7). The textural data only DA also had low results of 50% and 40%, for developing and testing respectively. The aspen classes were once again the most problematic, not only in the spectral bands only DA, but also in the textural bands only classification (refer to Tables 5.10 a and b). The combination of the spectral and textural information produced results that were lower than the results using the six-class sample stratification. These results were at 70 % for developing the model and 73.3% when testing the model, with some of the aspen classes not being classified at all (refer to Table 5.10c). The KHAT statistic showed little difference between this classification scheme and the six-class sample stratification scheme (refer to Tables 5.3 and 5.7).

In summary for this section the classification accuracies:

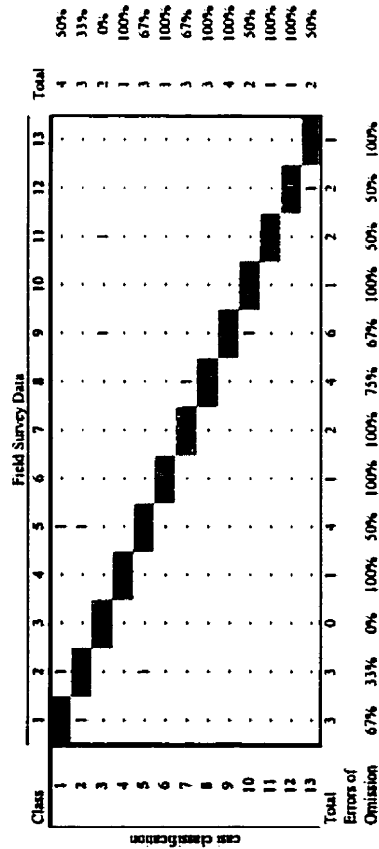
- c) Are higher or equal to the six-class sample stratification results
- d) The thirteen-class sample stratification produces smaller errors of omission and commission
- e) KHAT is higher for the thirteen-class sample stratification

However, as suggested in the visual analysis of the texture data, a quick DA of the 60 cm data with a 3x3 window size provided 92% accuracies developing and 73% testing results, which are quite comparable to those reported here with the larger window size. This suggests that the internal tree crown patterns captured with the higher resolution imagery (60 cm) and smallest window size (3x3) aid in the classifications of the multistory stands. Similar results, where internal tree crown patterns captured by fine textural component improved image classification, have been shown by Brandtberg (1997).

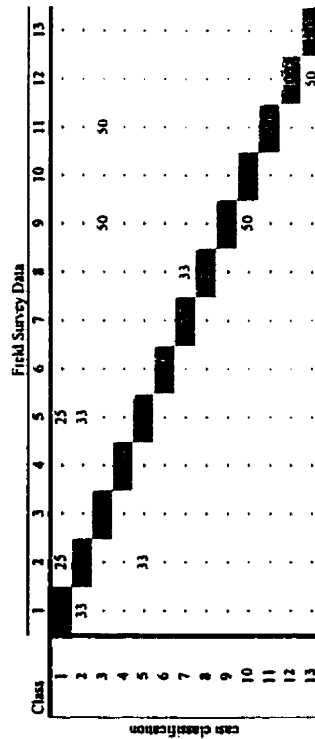
Table 5.8a Classification results for the 13 class sample stratification using only the spectral 60 cm data

Results from Building of the Discriminant Function

Plot Class Assignment



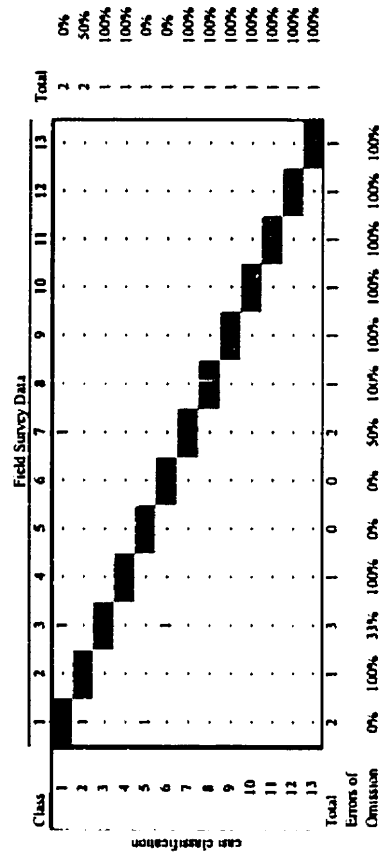
Classification Accuracies in %



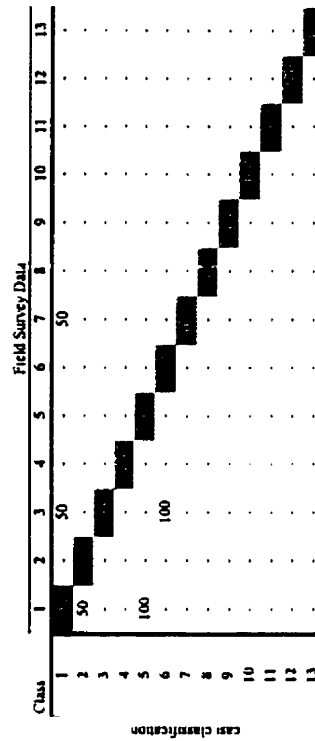
65 70% of selected original grouped cases correctly classified

Results from Testing of the Discriminant Function

Plot Class Assignment

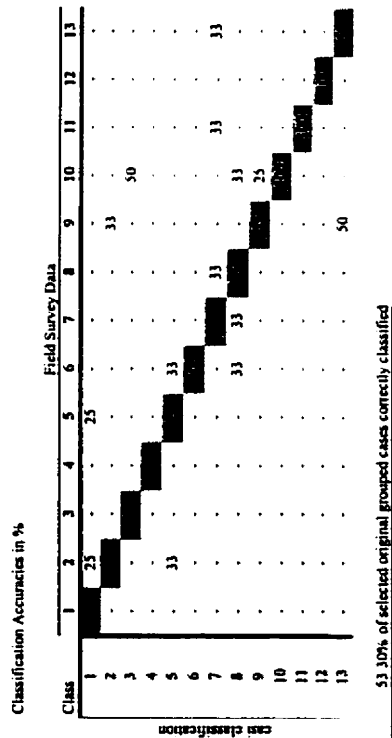
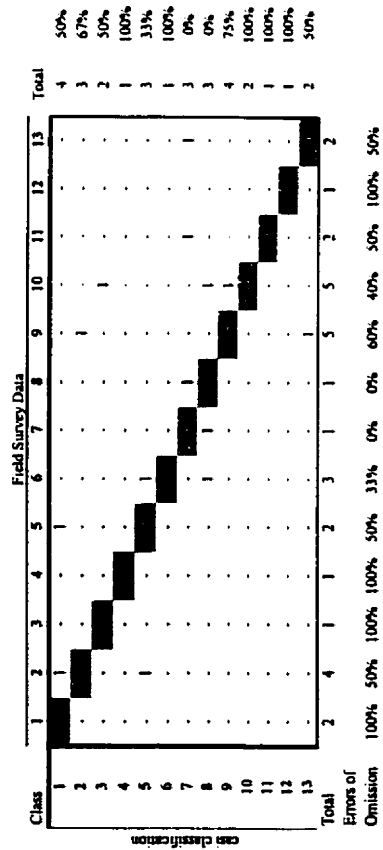


Classification Accuracies in %



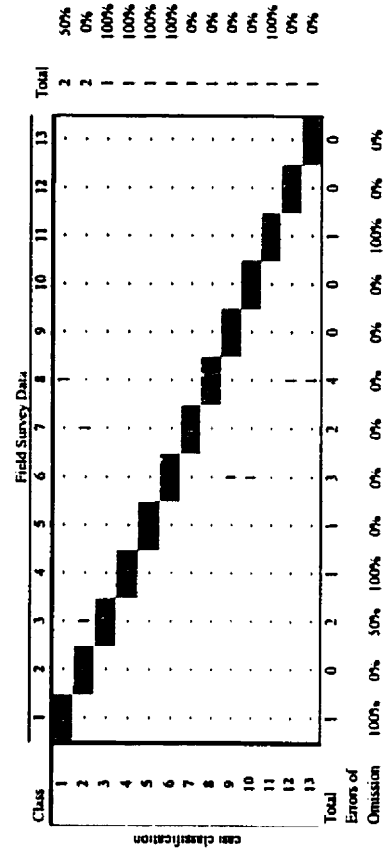
65 70% of selected original grouped cases correctly classified

Table 5.4b. Classification results for the 13 class sample stratification using only the natural 60 cm data
Results from Building of the Discriminant Function
Plot Class Assignment

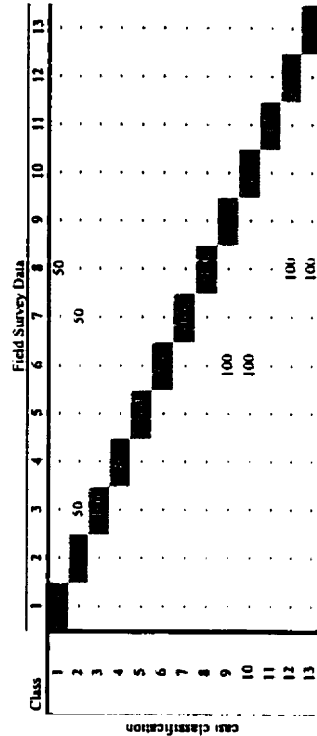


53 10% of selected original grouped cases correctly classified

Results from Testing of the Discriminant Function
Plot Class Assignment

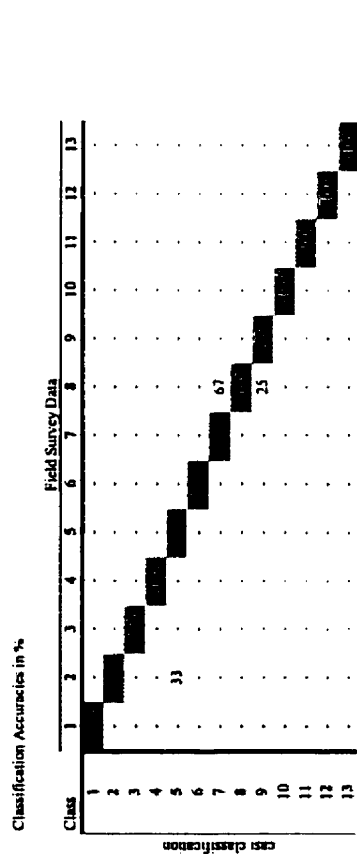
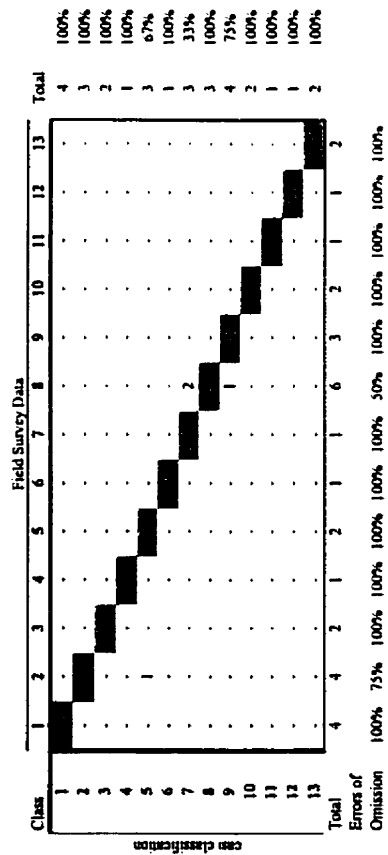


Classification Accuracies in %



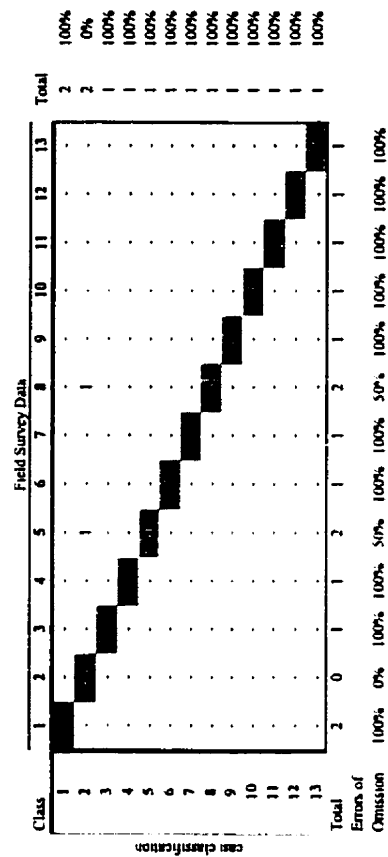
53 10% of selected original grouped cases correctly classified

Table 5.8c: Classification results for the 13 class sample stratification using the combination of spectral and textural 60 cm data
Results from Building of the Discriminant Function
Plot Class Assignment

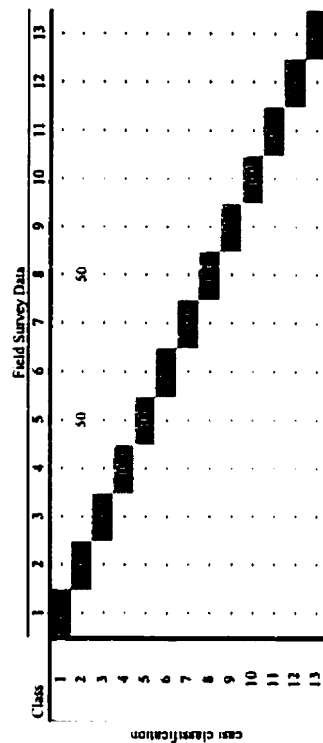


80.77% of selected original grouped cases correctly classified

Results from Testing of the Discriminant Function
Plot Class Assignment



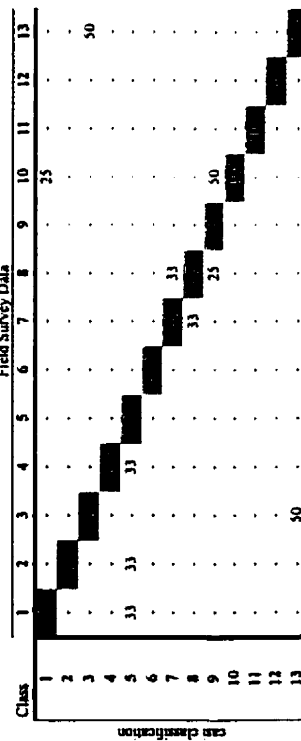
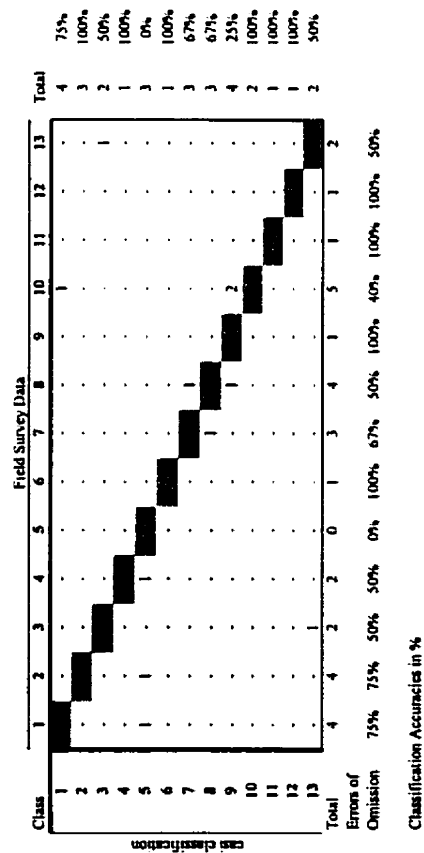
Classification Accuracies in %



80.77% of selected original grouped cases correctly classified

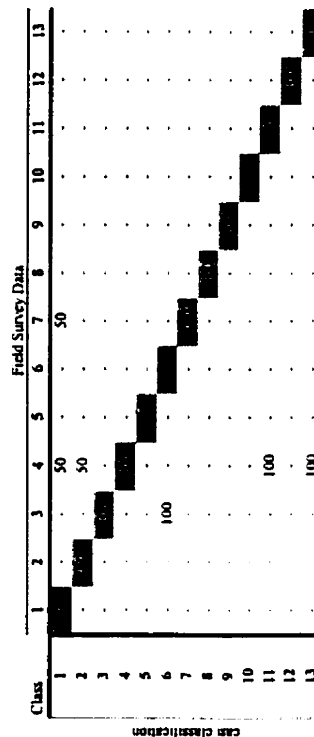
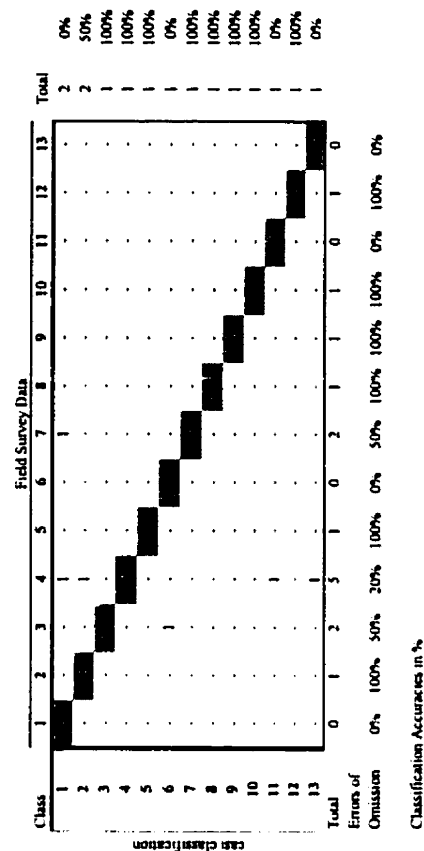
Table 5.9a. Classification results for the 13 class sample stratification using only the spectral 1m data

Results from Building of the Discriminant Function
Plot Class Assignment



63.00% of selected original grouped cases correctly classified

Results from Testing of the Discriminant Function
Plot Class Assignment



60.00% of selected original grouped cases correctly classified

Table 5.9b Classification results for the 13 class sample stratification using only the textural 1m data

Results from Building of the Discriminant Function
Plot Class Assignment

Class	Field Survey Data													Total	
	1	2	3	4	5	6	7	8	9	10	11	12	13		
1	1													4	50%
2		1												3	67%
3			1											2	50%
4				1										1	100%
5					1									3	33%
6						1								1	100%
7							1							3	0%
8								1						3	0%
9									1					4	75%
10										1				2	100%
11											1			1	100%
12												1		1	100%
13													1	2	50%
Total	2	4	1	1	2	3	1	1	5	5	2	1	2		
Errors of Omission	100%	50%	100%	100%	50%	33%	0%	0%	60%	40%	50%	100%	50%		

Classification Accuracies in %

Class	Field Survey Data													
	1	2	3	4	5	6	7	8	9	10	11	12	13	
1	25				25									
2		25								33				
3			33							50				
4				33										
5					33									
6						33								
7							33				33		33	
8								33		33				
9									25					
10										50				
11											50			
12												50		
13													50	

53.30% of selected original grouped cases correctly classified

Results from Testing of the Discriminant Function
Plot Class Assignment

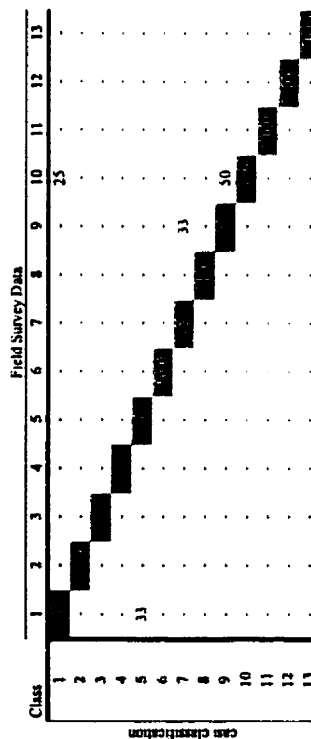
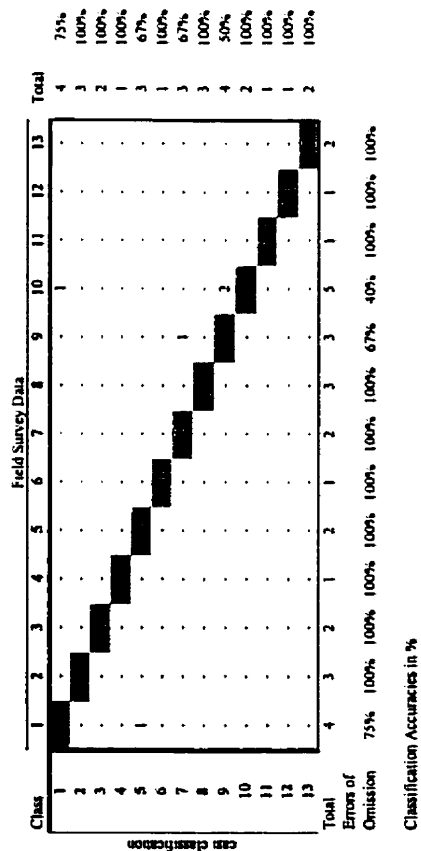
Class	Field Survey Data													Total	
	1	2	3	4	5	6	7	8	9	10	11	12	13		
1	1													2	50%
2		1												2	0%
3			1											1	100%
4				1										1	100%
5					1									1	0%
6						1								1	0%
7							1							1	0%
8								1						1	0%
9									1					1	0%
10										1				1	0%
11											1			1	100%
12												1		1	100%
13													1	1	0%
Total	1	0	3	3	0	0	1	3	0	0	1	3	0		
Errors of Omission	100%	0%	33%	33%	0%	0%	0%	0%	0%	0%	100%	33%	0%		

Classification Accuracies in %

Class	Field Survey Data													
	1	2	3	4	5	6	7	8	9	10	11	12	13	
1	50													
2		50												
3			50											
4				100										
5					100									
6						100								
7							100							
8								100						
9									100					
10										100				
11											100			
12												100		
13													100	

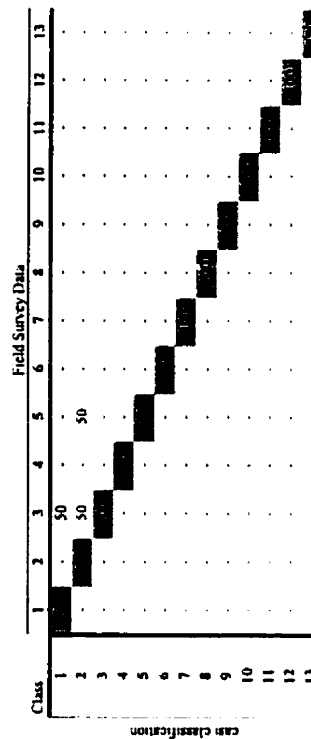
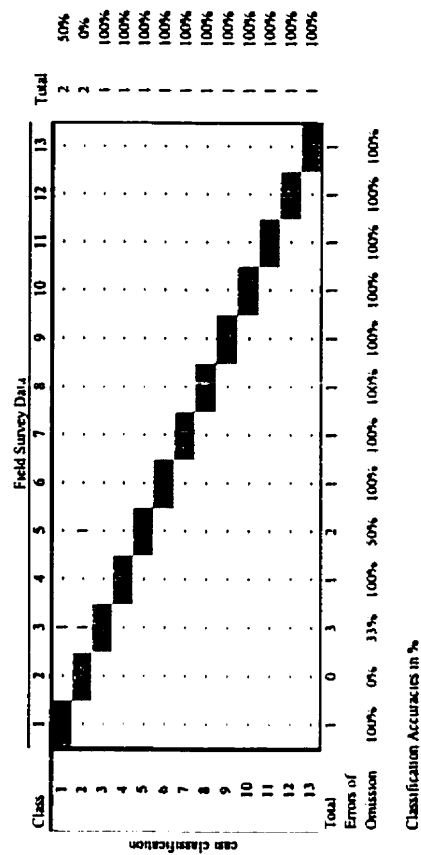
46.70% of selected original grouped cases correctly classified

Table 5.9c Classification results for the 13 class sample stratification using the combination of spectral and textural 1m data
Results from Building of the Discriminant Function
Plot Class Assignment



83.10% of selected original grouped cases correctly classified

Results from Testing of the Discriminant Function
Plot Class Assignment



80.00% of selected original grouped cases correctly classified

Table 5.10a Classification results for the 13 class sample stratification using only the spectral 2m data

Results from Building of the Discriminant Function
Plot Class Assignment

Class	Field Survey Data													Total
	1	2	3	4	5	6	7	8	9	10	11	12	13	
1	4									1				4
2		3												3
3			2											2
4				2										1
5					2									3
6						3								1
7							3							3
8								1						3
9									2					4
10										2				2
11											1			1
12												1		1
13													2	2
Total	4	4	2	2	0	1	3	4	1	5	1	1	2	
Errors of Omission	75%	75%	50%	50%	0%	100%	67%	50%	100%	40%	100%	100%	50%	

Classification Accuracies in %

Class	Field Survey Data													Total
	1	2	3	4	5	6	7	8	9	10	11	12	13	
1	4									25				4
2		3												3
3			2											2
4				2									50	1
5					2									3
6						3								1
7							3							3
8								33						3
9									25					4
10										2				2
11											1			1
12												1		1
13													2	2

63.30% of selected original grouped cases correctly classified

Results from Testing of the Discriminant Function
Plot Class Assignment

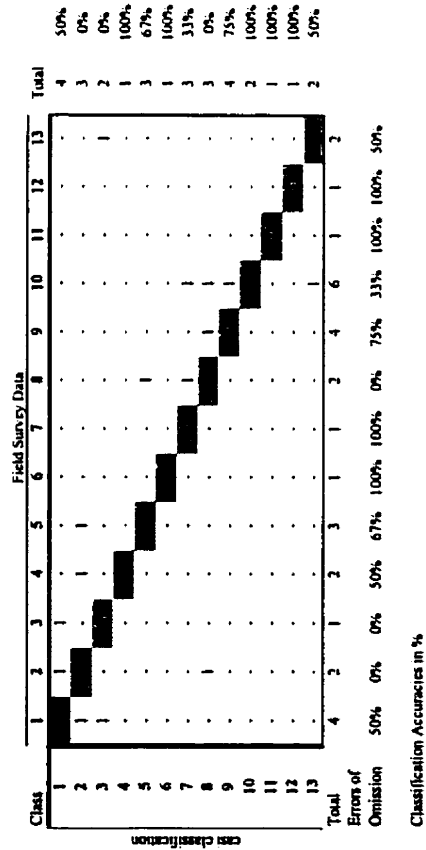
Class	Field Survey Data													Total
	1	2	3	4	5	6	7	8	9	10	11	12	13	
1	2													2
2		2												2
3			1											1
4				1										1
5					1									1
6						1								1
7							1							1
8								1						1
9									1					1
10										1				1
11											1			1
12												1		1
13													1	1
Total	0	1	2	5	1	0	2	1	1	1	0	1	0	
Errors of Omission	0%	100%	50%	20%	100%	0%	50%	100%	100%	100%	0%	100%	0%	

Classification Accuracies in %

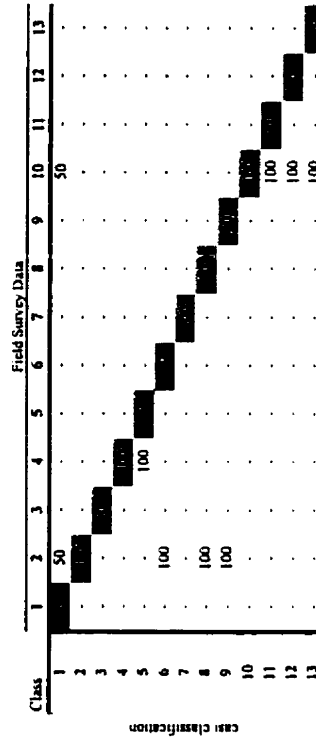
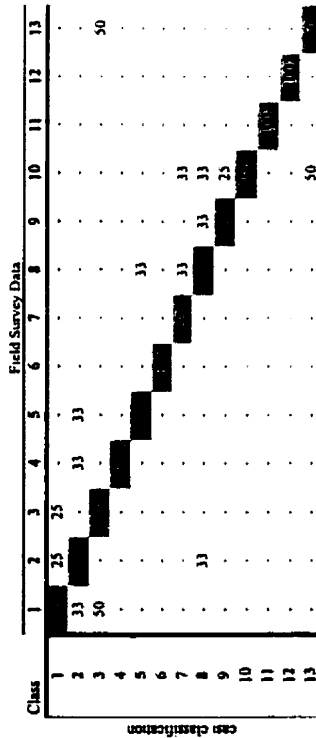
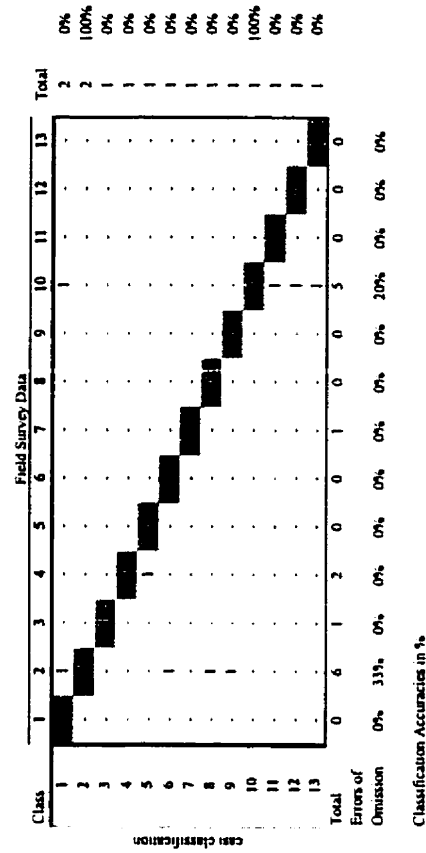
Class	Field Survey Data													Total
	1	2	3	4	5	6	7	8	9	10	11	12	13	
1	2													2
2		2												2
3			1											1
4				1										1
5					1									1
6						1								1
7							1							1
8								1						1
9									1					1
10										1				1
11											1			1
12												1		1
13													1	1

60.00% of selected original grouped cases correctly classified

Table 5.10b. Classification results for the 13 class sample stratification using only the testural 2m data
Results from Building of the Discriminant Function
Plot Class Assignment



Results from Testing of the Discriminant Function
Plot Class Assignment



50 00% of selected original grouped cases correctly classified

40 00% of selected original grouped cases correctly classified

Table 5.10c: Classification results for the 13 class sample stratification using the combination of spectral and textural 2m data

Results from Building of the Discriminant Function
Plot Class Assignment

Class	Field Survey Data													Total
	1	2	3	4	5	6	7	8	9	10	11	12	13	
1	4													4
2		3												3
3			2											2
4				1										1
5					3									3
6						1								1
7							3							3
8								3						3
9									4					4
10										2				2
11											1			1
12												1		1
13													2	2
Total	3	4	1	2	2	1	1	4	3	6	1	1	1	
Errors of Omission	67%	75%	100%	50%	50%	100%	100%	75%	100%	33%	100%	100%	100%	

Classification Accuracies in %

Class	Field Survey Data													Total
	1	2	3	4	5	6	7	8	9	10	11	12	13	
1	25									25				50
2		50												50
3			50											50
4				50										50
5					50									50
6						50								50
7							50							50
8								50						50
9									50					50
10										50				50
11											50			50
12												50		50
13													50	50

70.00% of selected original grouped cases correctly classified

Results from Testing of the Discriminant Function
Plot Class Assignment

Class	Field Survey Data													Total
	1	2	3	4	5	6	7	8	9	10	11	12	13	
1	2													2
2		2												2
3			1											1
4				1										1
5					1									1
6						1								1
7							1							1
8								1						1
9									1					1
10										1				1
11											1			1
12												1		1
13													1	1
Total	0	1	3	1	1	0	2	1	1	1	1	2	1	
Errors of Omission	0%	100%	33%	100%	100%	0%	50%	100%	100%	100%	100%	50%	100%	

Classification Accuracies in %

Class	Field Survey Data													Total
	1	2	3	4	5	6	7	8	9	10	11	12	13	
1	50													50
2		50												50
3			50											50
4				50										50
5					50									50
6						50								50
7							50							50
8								50						50
9									50					50
10										50				50
11											50			50
12												50		50
13													50	50

73.00% of selected original grouped cases correctly classified

5.6 Chapter Summary

In this chapter visual interpretation and descriptive statistics of the texture measures establish a relationship between the forest stand structural information and the *casi* imagery textural information.

The change in of the texture window size and the change in image resolution have shown that the texture derivatives image values invert from high to low or low to high based on the scale of the object is captured (from tree crown architecture to plot structure)

As forests age from immature to old stands, the canopy openness increases in the stands (Frazer *et al.* 1998). In this study area, in many cases, especially in the pioneering aspen stands, these gaps are filled by a second story coniferous canopy. The texture measure on the high resolution imagery is able to extract these structurally complex stands by detecting the shadow in the stand. However, the shadow captured by these textural measures is not only the gap shadow of the stand, but also shadows produced by large crowns of the older stands. As shown by Brandberg 1997, such shadows aid in stand type classification. Frazer *et al.* (1998) have shown that canopy openness increased more in the transition from mature to old stands (most significant after 150 years of age) than from immature to mature stands. Because the forest in the study area is still relatively young (on the succession scale) the existence of a second succession canopy in the stands is quite likely, supporting applicability of the methodology discussed in this thesis.

St.-Onge and Cavayas (1995) have shown that forest structure and texture relationships become stronger as the pixel size approaches or drops below 1 m in resolution. The findings in this thesis support the previous research, showing that the highest resolution imagery (60 cm) can produce the highest texture only classification results of plots stratified using canopy structure information. A study by Jakubauskas (1997) using low resolution imagery has also suggested that high resolution image texture would be more appropriate for forest structure classification.

The combination of the textural signatures and the spectral signatures outperforms any other type of classification, regardless of the class scheme stratification.

As spectral and spatial signatures become more generalized in the lower resolution (1 m, 2 m data) the classification accuracies are reduced.

The results show that a better stratification scheme, such as the thirteen-class sample stratification scheme, which takes into consideration the existence of the other canopy layer, is more appropriate and even increases the classification results by about 17%.

Chapter 6 Summary and Conclusions

6.1 Summary

High spatial and spectral resolution imagery (1 m and less) such as the *casi* imagery used in this thesis show potential for producing forest inventories (AVI) in shorter time intervals as compared to the traditional methods using aerial photographs (Franklin 1994; Leckie 1995). The availability of this type of resolution of imagery from satellites makes large area forest inventories logistically feasible. The methods for analyzing such imagery are being researched with the purpose of producing accurate results, which meet or exceed the standards achieved by airphoto interpretation, while at the same time retaining the classification scheme with similar or better level of detail.

To meet these goals new methods for high resolution image classification that deal with the high spatial resolution problem of spectral variability (scene noise) are being developed. The ways of dealing with this variability fall into two categories:

- Elimination of variability by individual tree crown delineation (King 1995), or automated image segmentation (Ryherd and Woodcock 1996; Lobo 1997)
- Utilization of spectral variability as an information source to be included in the classification procedure (such as texture).

Although these methods are proving to be quite successful, utilizing the high spatial resolution imagery in forest inventory classification often requires extensive field data collection, specialized software not always commercially available and an advanced understanding of the data and software. A straightforward and cost effective technique is more likely to be utilized by forest managers.

This study explored such a technique. Second-order texture readily available in commercial image analysis packages was used to represent the high spatial information content captured by the high resolution imagery. The classification procedure implemented this textural information, and forest classes outlined by the AVI standard in Alberta were digitally classified. The labels were developed using the per species basal area for each sample site.

Three resolutions of *casi* imagery (60 cm, 1 m and 2 m) collected over the study area on July 18th, 1998 were tested for best results. The sample stratification based on only the first canopy layer of the AVI label resulted in a six-class sample stratification. The second layer canopy inclusion in sample stratification provided a wide range of forest classes to be classified and resulted in a thirteen-class stratification sample scheme. A 'brightness' image was produced through Principal Component Analysis of the seven spectral bands (540–560 nm, 610–640 nm, 640–680 nm, 690–715 nm, 730–755 nm, 790–810 nm and 850–875 nm). The 'brightness' image captured the shadowed areas in the imagery which were used to establish a relationship between image shadow and the structural complexity index derived from field measurements for all plots. The relationship between the shadow and the structural complexity index was strongest at the 60 cm per pixel *casi* imagery resolution, giving an R^2 of 0.6. Signatures consisting of the mean per-plot values were generated for the seven spectral channels available at all three resolutions of the imagery and the five second-order textural derivatives (angular second moment, correlation, dissimilarity, entropy and homogeneity).

For each data set two-thirds of the sample plots were used to develop the discriminant functions, the remaining one-third was used to test the discriminant function accuracy. Three Discriminant Analyses using first only the spectral data, second only the textural data and third the combination of the two data were performed for each resolution. The KHAT statistic was used in conjunction with the co-occurrence matrices to evaluate the accuracies of the classifications.

Prior to interpretation of the results, a set of visual analyses was conducted to determine the complexity of the second order texture measures in different types of forest stands. Based on this visual analysis of the texture measure in different window sizes and different pixel resolutions, the texture of high resolution imagery (60 cm pixel resolution) appeared to contain a great deal of information on the crown architecture of individual trees. The texture was comprised of differences within crown shadows or sun-lit and shaded crowns. The texture was interpreted to contain information on stand structure such as tree distribution, species and shadows. Texture of high resolution imagery (1 m and 2 m pixel resolution) reduced the ability to detect individual tree crown architecture and was determined to be related to stand structure characteristics.

On average, the use of texture channels improved the per-plot classification accuracies by 17% compared to using the spectral channels alone. The highest per pixel resolution imagery of 60 cm outperformed the other image resolutions (1 m and 2 m) and the thirteen-class sample stratification scheme improved the classification accuracies by 14%, with results of 87% and a KHAT of 0.85, compared to the six-class sample stratification scheme results of 72% and a KHAT of 0.73.

In summary the results showed:

- The combination of the textural signatures and the spectral signatures outperforms any other type of classification, regardless of the class scheme stratification.
- As spectral and spatial signatures become more generalized in the lower resolution (1 m, 2 m) data the classification accuracies are reduced.
- The results show that a better stratification scheme, such as the thirteen-class sample stratification scheme, which takes into consideration the existence of the other canopy layer, is more appropriate and even increases the classification results by about 17%.

6.2 Conclusions and Contributions to Research

The work presented in this thesis contributes to areas of remote sensing research by demonstrating that image texture derived from high spatial resolution multispectral imagery increased the classification accuracy of multistory forest stands identified according to the AVI system as part of a forest inventory. The following conclusions can be made:

- Statistical and visual interpretation of the textural imagery was used to establish that texture could be used to express the stand complexity.
- The best classification results of 86.7 % were achieved using the highest image resolution of 60 cm, where textural and spectral signatures were combined to classify the data based on the thirteen-class sample stratification. On average, the inclusion of the textural information improved the classification by 20%; it also allowed a detailed class information to be applied.
- Sample class stratification needs to be more complex on higher resolution imagery
- Hierarchical merging of classes should be done on all AVI layer information

Supporting these conclusions:

- A relationship between stand complexity and an image component (shadow) was found;
- Visual interpretation confirmed the relationships between stand structure and image texture.

6.3 Recommendations for Further Research

There are many future research opportunities, which may be based upon the conclusions of this research:

- A quick DA showed that incorporation of the highest spatial component information (3x3 window texture) produces high accuracy; this finding should be further investigated.
- The defoliation in the aspen stands was estimated in the field. However, the effects of defoliation on the imagery have not been examined in detail. Could defoliation be causing the higher texture readings at the high resolution data in the deciduous stands? How much of an effect does it have?
- Information extracted from texture that related to forest succession has been an important area of investigation. One study (Jakubauskas 1997) has shown that on Landsat TM imagery textural data are valuable for distinguishing between quite young and very old classes, but is not successful at distinguishing between canopy classes. His work, as well as work by Woodcock and Strahler (1987), suggests that high resolution imagery texture can successfully accomplish such class distinction. The techniques introduced in this thesis could possibly be applied to the study of succession in a similar area.
- Leaf Area Index (LAI) increases with the number of layers of leaves in a canopy. The application of LAI in distinguishing of multilayer canopies has not been investigated.
- Although only second order texture measures were investigated, the comparison of other measures such as: first order texture and semivariance texture could be explored. The comparison between classifiers could also be implemented here.

- The mapping implications of these findings have not been addressed and can facilitate an area of future research.

References

- Anger, C., Mah, S., and Babel, S. (1994) "Technological enhancements to the compact airborne spectroscopic imager (casi)." *First International Airborne Remote Sensing Conference and Exhibition*, Strasbourg, France.
- Archibald, J. H., Klappstein, G. D., and Corns, I. G. W. (1996). "Field guide to ecosites of southwestern Alberta." *Natural Resources Canada, Canadian Forestry Service, Northwest Region, Northern Forest Research Centre, Edmonton, Alberta*, Special Report 8.
- Atkinson, P. M., and Curran, P. J. (1997). "Choosing an Appropriate Spatial Resolution for Remote Sensing Investigations." *Photogrammetric Engineering and Remote Sensing*, 63(12), 1345-1351.
- Avery, T. E. (1967). *Forest Measurements*, McGraw-Hill, Inc., California.
- Avery, T. E., and Berlin, G. L. (1992). *Fundamentals of Remote Sensing and Air Photo Interpretation*, Macmillan Publishing Company, New York.
- Bauer, M. E., Burk, T. E., Ek, A. R., Coppin, P. R., Lime, S. D., Walsh, T. A., Walters, D. K., Befort, W., and Heinzen, D. F. (1994). "Satellite Inventory of Minnesota Forest Resources." *Photogrammetric Engineering and Remote Sensing*, 60(287-298).
- Baulies, X., and Pons, X. (1995). "Approach to forest inventory mapping by means of multispectral airborne data." *International Journal of Remote Sensing*, 16, 61-80.
- Bobbe, T. J., Alban, J. A., Ishikawa, P., and Myhre, R. J., (1994), "An evaluation of narrow-band multispectral video imagery for monitoring forest health." *Fifth Forest Service Remote Sensing Applications Conference*, Portland, OR.
- Bowers, W. W., Franklin, S. E., Hudak, J., and McDermid, G. J. (1994). "Forest structural damage analysis using image semivariance." *Canadian Journal of Remote Sensing*, 20((1)), 28-36.
- Brandtberg, T. (1997). "Towards Structure-based Classification of Tree Crowns in High Spatial Resolution Aerial Images." *Scandinavian Journal of Forest Research*, 12, 89-96.

- Bruniquel-Pinel, V., and Gastellu-Etchegorry, J. P. (1998). "Sensitivity of Texture of High Resolution Images of Forest to Biophysical and Acquisition Parameters." *Remote Sensing of Environment*, 65, 61-85.
- Buchanan-Mappin, J., 1998, Personal Communication, Technician, Kananaskis Field Station, Barrier Lake Location, University of Calgary, Kananaskis Country, Alberta, Summer 1998.
- Butler, H., Peart, R. A., and Franklin, S. E., (1995), "Estimating canopy leaf area using aerial optical imagery in Kananaskis County, Alberta." *Proceedings of the 17th Canadian Symposium on Remote Sensing*, Saskatoon, Saskatchewan, 650-653.
- Carr, J. R., and Miranda, F. P. D. (1998). "The Semivariogram in Comparison to the Co-Occurrence Matrix for Classification of Image Texture." *IEEE Transactions on Geosciences and Remote Sensing*, 36(6), 1945-1951.
- CCFM. (1996). "Compendium of Canadian Forestry Statistics 1996, National Forestry Database Program." , National Resources Canada, Canadian Forest Service, Ottawa.
- Cohen, J. (1960). "A coefficient of agreement for nominal scales." *Education and Psychology Measurement*, 20(1), 37-46.
- Cohen, W. B., and Spies, T. A. (1992). "Estimating Structural Attributes of Douglas-Fir/Western Hemlock Forest Stands from Landsat and SPOT Imagery." *Remote Sensing of Environment*, 41(1), 1-17.
- Cohen, W. B., Spies, T. A., and Fiorella, M. (1995). "Estimating the age and structure of forests in a multi-ownership landscape of western Oregon, U.S.A." *International Journal of Remote Sensing*, 16(4), 721-746.
- Cole, W. G. (1995). *Hardwood tree crown measurement guide*, Ontario Forest Research Institute, Sault Ste. Marie, Ontario.
- Congalton, R. G., and Green, K. (1998). *Assessing the Accuracy of Remotely Sensed Data: Principles and Practice*, CRC/Lewis Press, Boca Raton, FL.
- Davis, L. S., Johns, S. A., and Aggarwal, J. K. (1979). "Texture analysis using generalized co-occurrence matrices." *IEEE Transactions on Pattern Analysis and Machine Intelligence*, PAMI-1((3)), 251-261.

- Dikshit, O., and Roy, D. P. (1996). "An Empirical Investigation of Image Resampling Effects Upon the Spectral and Textural Supervised Classification of a High Spatial Resolution Multispectral Image." *Photogrammetric Engineering & Remote Sensing*, 62(9), 1085-1092.
- Eldridge, N. R., and Edwards, G., (1993), "Continuous tree class density surfaces derived from high resolution image analysis." *GIS/LIS'93*, Vancouver, BC, 947-952.
- Felix, N. A., and Binney, D. L. (1989). "Accuracy Assessment of a Landsat-assisted Vegetation Map of the Costal Plain of the Arctic National Wildlife Refuge." *Photogrammetric Engineering and Remote Sensing*, 55(4), 475-478.
- Fish, A. K., Peart, R. A., and Franklin, S. E., (1995), "Mapping Montane forest structure using high spatial resolution *casi* data." *Proceedings of the 17th Canadian Symposium on Remote Sensing*, Saskatoon, Saskatchewan, 558-565.
- Foody, G. M., Campbell, N. A., Trood, N. T., and Wood, T. F. (1992). "Derivation and Application of Probabilistic Measures of Class Membership from Maximum-likelihood Classification." *Photogrammetric Engineering and Remote Sensing*, 58(9), 1335-1341.
- Fournier, R., Edwards, G., and Eldridge, N. (1995). "A catalogue of potential spatial discriminators for high spatial resolution digital images of individual crowns." *Canadian Journal of Remote Sensing*, 17((2)), 285-298.
- Franklin, J. T., Logan, L., Woodcock, C. E., and Strahler, A. H. (1986). "Coniferous forest classification and inventory using Landsat and Digital Terrain Data." *IEEE Transactions on Geosciences and Remote Sensing*, GE-24(139:149).
- Franklin, S. E. (1994). "Discrimination of subalpine forest species and canopy density using *casi*, SPOT PLA, and Landsat TM data." *Photogrammetric Engineering and Remote Sensing*, 60((10)), 1233-1241.
- Franklin, S. E., and Giles, P. T. (1995). "Radiometric processing of aerial and satellite remote sensing imagery." *Computers & Geosciences*, 21, 413-425.
- Franklin, S. E., and McDermid, G. J. (1993). "Empirical relations between digital SPOT HRV and *casi* spectral response and lodgepole pine (*Pinus contorta*) forest stand parameters." *International Journal of Remote Sensing*, 14((12)), 2331-2348.

- Franklin, S. E., Moskal, L. M., Maudie, A. J., Hall, R. J., and Lavigne, M. B. (1998). "Aerial texture in forest inventory classification of Canadian boreal mixed-wood stands." *International Journal of Remote Sensing*, (in press).
- Franklin, S. E., Wulder, M. A., and Lavigne, M. B. (1996). "Automated derivation of geographic window sizes for use in remote sensing digital image texture analysis." *Computers & Geosciences*, 22((6)), 665-673.
- Frazer, G., Lertzman, K., and Trofymow, J. A., (1998), "Developmental Trends of Canopy Structure in Coastal Forests of British Columbia." *Workshop on Structure, Process, and Diversity in Successional Forests of Coastal British Columbia*, Victoria.
- Gerylo, G., Hall, R. J., Franklin, S. E., Roberts, A., and Milton, E. J. (1998). "Hierarchical image classification and extraction of forest species composition and crown closure from airborne multispectral images." *Canadian Journal of Remote Sensing*, 24(3), 219-232.
- Gerylo, G. R., Franklin, S. E., Roberts, A., Milton, E. J., and Hall, R. J., (1997) "Hierarchical Alberta Vegetation Inventory (AVI) classification using aerial digital frame camera data." *Proceedings of the 19th Canadian Remote Sensing Symposium*, Ottawa, Ontario, CD-ROM.
- Getty, M. (1996). "Application of conventional and multispectral based methodology in large scale ecological classification: A case study in Dry Island Buffalo Jump Provincial Park, Alberta, Canada," Unpublished M.Sc. Thesis, University of Calgary, Calgary, Alberta.
- Ghitter, G. S., Hall, R. J., and Franklin, S. E. (1995). "Variability of Landsat Thematic Mapper data in boreal deciduous and mixed-wood stands with conifer understory." *International Journal of Remote Sensing*, 16((16)), 2989-3002.
- Gills, M. D., and Leckie, D. G. (1993). "Forest Inventory Mapping Procedures Across Canada." *Information Report PI-X-114*, Petawawa National Forest Institute, Forestry Canada.
- Glackin, D. L. (1998). "International space-based remote sensing overview: 1980-2007." *Canadian Journal of Remote Sensing*, 24(3), 307-314.

- Gordon, D. K., and Philipson, W. R. (1986). "A texture-enhancement procedure for separating orchard from forest in Thematic Mapper data." *International Journal of Remote Sensing*, 7(2), 301-304.
- Grey, L., Freemantle, J., Shepherd, P., Miller, J., Harron, J., and Hersom, C. (1997). "Characterization and calibration of the *casi* airborne imaging spectrometer for BOREAS." *Canadian Journal of Remote Sensing*, 23(2), 188-195.
- Guyot, G., Guyon, D., and Riou, J. (1989). "Factors Affecting the Spectral Response of Forest Canopies: A Review." *Geocarto International*, 3, 3-18.
- Hall, R. J. (1998). "Alberta Vegetation Inventory Methods and Applications Seminar" , Canadian Forest Service, Northern Division.
- Hall, R. J., and Crown, P. H. (1987). "Spectral classes and forest land classification: a philosophical discussion paper. Not for publication." , Canadian Forest Service, Northern Forestry Centre, Edmonton, Alberta. Department of Soil Science, University of Alberta, Edmonton, Alberta.
- Haralick, R. (1979). "Statistical and structural approaches to texture." *Proceedings of the IEEE*, 65(5), 786-804.
- Haralick, R. M. (1986). "Statistical Image Texture Analysis." Handbook of Pattern Recognition and Image Processing, R. Colwell, ed., American Society of Photogrammetry, Falls Church, VA, 793-805.
- Hay, G. J., and Niemann, K. O. (1994). "Visualizing 3-D Texture: A Three-Dimensional Structural Approach to Model Forest Texture." *Canadian Journal of Remote Sensing*, 20(2), 90-101.
- Hay, G. J., Niemann, K. O., and McLean, G. F. (1996). "An Object-Specific Image-Texture Analysis of H-Resolution Forest Imagery." *Remote Sensing of the Environment*, 55, 108-122.
- Heygi, F., Pilon, P., and Walker, P., (1992), "Replacing aerial photos in resource inventories with airborne digital data and GIS." *ASPRS/ACSM/RTI'92*, Washington, DC, 510-516.
- Hodgson, M. E. (1998). "What Size Window for Image Classification? A Cognitive Perspective." *Photogrammetric Engineering & Remote Sensing*, 64(8), 797-807.

- Hsu, S. Y. (1978). "Texture-tone analysis for automated land-use mapping." *Photogrammetric Engineering and Remote Sensing*, 44((11)), 1393-1404.
- Irons, J. R., and Petersen, G. W. (1981). "Texture Transforms of Remote Sensing Data." *Remote Sensing of the Environment*, 11, 359-370.
- Jakubauskas, M. E. (1997). "Effects of forest succession on texture in Landsat TM imagery." *Canadian Journal of Remote Sensing*, 23(3), 257-163.
- Jensen, J. R. (1996). *Introductory Digital Image Processing. A Remote Sensing Perspective*, Simon & Schuster, Upper Saddle River, N.J.
- King, D. (1995). "Airborne Multispectral Digital Camera and Video Sensors: A Critical Review of System Designs and Applications." *Canadian Journal of Remote Sensing*, 21(3), 245-273.
- Kirby, C. L. (1973). "The Kananaskis Forest Experiment Station, Alberta History, Physical Features, and Forest Inventory." , Canadian Forest Service, Northern Research Centre, Edmonton, Alberta.
- Klecka, W. R. (1982). *Discriminant Analysis*, Sage University Paper, London, England.
- Lark, R. M. (1996). "Geostatistical description of texture on an aerial photograph for discriminating classes of land cover." *International Journal of Remote Sensing*, 17, 2115-2133.
- Leckie, D. G., Beaubien, J., Gibson, J. R., O'Neil, N. T., Piekutowski, T., and Joyce, S. P. (1995). "Data processing and analysis for MIFUCAM: a trial of MEIS imagery for forest inventory mapping." *Canadian Journal of Remote Sensing*, 21((3)), 337-356.
- Leckie, D. G., and Gillis, M. D. (1995). "Forest inventory in Canada with emphasis on map production." *The Forestry Chronicle*, 71(1), 74-88.
- Lillesand, T. M., and Kiefer, R. W. (1994). *Remote Sensing and Image Interpretation*, John Wiley and Sons, Inc., USA.
- Lowell, K. E., and Edwards, G. (1996). "Modeling Heterogeneity and Change in Natural Forests." *Geomatica*, 50(4), 425-440.
- Luckai, F. (1997). *Forest measurements field manual*, Lakehead University Faculty of Forestry, Thunder Bay, Ontario.

- Mah, S., Anger, C. D., Babey, S. K., Trudeau, D., Loch, C., and Renuncio, L., (1995), "An Airborne Multispectral Imaging Spectrograph for Versatile Environmental Remote Sensing Applications." *XVII Congresso Brasileiro de Cartografia*, Salvador, Bahia, Brazil.
- Marceau, D. J., Gratton, D. J., Fournier, R. A., and Fortin, J. P. (1994a). "Remote Sensing and the measurement of geographical entities in a forested environment. 2. The optimal spatial resolution." *Remote Sensing of Environment*, 49((1)), 105-117.
- Marceau, D. J., Howarth, P. J., Dubois, J. M. M., and Gratton, D. J. (1990). "Evaluation of the grey-level co-occurrence matrix method for land-cover classification using SPOT imagery." *IEEE Transactions on Geoscience and Remote Sensing*, 28((4)), 513-518.
- Marceau, D. J., Howarth, P. J., and Gratton, D. J. (1994b). "Remote Sensing and the measurement of geographical entities in a forested environment. 1. The scale and spatial aggregation problem." *Remote Sensing of Environment*, 49((1)), 93-104.
- Maudie, A. (1999). "Forest Inventory Classification using Aerial Image Texture in the New Brunswick Acadian Forest Region," M.Sc., University of Calgary, Calgary.
- Ministers, C. C. O. F. (1997). "Criteria and Indicators of Sustainable Forest Management in Canada.", Ottawa.
- Nesby, R. (1997). "Alberta Vegetation Inventory." , Alberta Environmental Protection, Edmonton.
- Oliver, C. D., and Larson, B. C. (1996). *Forest Stand Dynamics*, John Wiley and Sons, San Francisco.
- Peddle, D.R., H.P. White, R.J. Soffer, J.R. Miller, and E.F. LeDrew, (1995). "Reflectance Processing of Field Spectrometer Data in BOREAS" *In: Proceedings, 17th Canadian Symposium on Remote Sensing*, Saskatoon, SK, Canada. Vol. I, p. 189-194. .
- Pellikka, P. (1996). "Illumination Compensation for Aerial Video Images to Increase Land Cover Classification Accuracy in Mountains." *Canadian Journal of Remote Sensing*, 22(4), 368-381.
- Peterson, E. B., and Peterson, N. M. (1992). "Ecology, management and use of aspen and balsam poplar in the prairie provinces, Canada." , Forestry Canada, Northwest Region and Northern Forestry Centre, Edmonton.

- Pitt, D. G., Wagner, R. G., Hall, R. J., Kink, D. J., Leckie, D. G., and Runesson, U. (1997). "Use of Remote Sensing for Forest Vegetation Management: A Problem Analysis." *The Forestry Chronicle*, 73(4), 459-477.
- Price, J. C. (1994). "How Unique are Spectral Signatures." *Remote Sensing of the Environment*, 49, 181-186.
- Roach, D., and Fung, K. (1994). "Fractal-based textural description for remotely sensed forestry data." *Journal of Remote Sensing*, 21(214-224).
- Robinson, C. (1981). "The logic of multispectral classification and mapping of land." *Remote Sensing of Environment*, 11, 231-244.
- Running, S. W., Peterson, D. L., Spanner, M. A., and Teuber, K. (1986). "Remote Sensing of coniferous forest leaf area." *Ecology*, 67((1)), 273-276.
- Ryerson, R. A. (1989). "Image interpretation concerns for the 1990's and lessons from the past." *Photogrammetric Engineering and Remote Sensing*, 55, 1427-1430.
- Ryher, S., and Woodcock, C. (1996). "Combining spectral and textural data in the segmentation of remotely sensed images." *Photogrammetric Engineering and Remote Sensing*, 62(2), 181-194.
- Skidmore, A. K. (1989). "Unsupervised Training Area Selection in Forests Using Nonparametric Distance Measure and Spatial Information." *International Journal of Remote Sensing*, 10(1), 133-146.
- Spanner, M. A., Pierce, L. L., Peterson, D. L., and Running, S. W. (1990). "Remote sensing of temperate coniferous forest leaf area index: the influence of canopy closure, understory vegetation, and background reflectance." *International Journal of Remote Sensing*, 11, 95-111.
- Spies, T. (1997). "Forest Stand Structure, Composition, and Function." *Creating a Forestry for the 21st Century*, K. H. a. J. Franklin, ed., Island Press, Washington, 475.
- SPSS. (1997). *SPSS Base 7.5 for Windows User's Guide*, SPSS Inc.
- Stoney, W. E., and Hughes, J. R. (1998). "A New Space Race Is On!" *GIS World* (March 1998).

- St-Onge, B. A., and Cavayas, F. (1995). "Estimating forest stand structure from high resolution imagery using the directional variogram." *International Journal of Remote Sensing*, 16(11), 1999-2021.
- St-Onge, B. A., and Cavayas, F. (1997). "Automated Forest Structure Mapping from High Resolution Imagery Based on Directional Semivariogram Estimates." *Remote Sensing of the Environment*, 61, 82-95.
- Strome, W. M., Leckie, D. G., Miller, J., and Buxton, R., (1991), "Application of high resolution remote sensing image data." *Space Commercialization: Satellite Technology*, Washington, DC.
- Tabachnick, B. G., and Fidell, L. S. (1996). *Using Multivariate Statistics*, Harper Collins College Publishers, California State University, Northridge.
- vanLeeuwen, W. J. D., and Huete, A. R. (1996). "Effects of Standing Litter on the Biophysical Interpretation of Plant Canopies with Spectral Indices." *Remote Sensing of Environment*, 55, 123-138.
- Weszka, J. S., Dyer, C. R., and Rosenfeld, A. (1976). "A comparative study of texture measures for terrain classification." *IEEE Transactions on Systems, Man and Cybernetics*, SMC-6((4)), 269-285.
- Wilson, B. A. (1995). "Estimating Conifer Forest Structure using SAR Texture Analysis," Unpublished Ph.D. Thesis, University of Calgary, Calgary, Alberta.
- Wulder, M. A. (1996). "Airborne Remote Sensing of Forest Structure: Estimation of Leaf Area Index," Unpublished Master of Environmental Studies Thesis, University of Waterloo, Waterloo, Ontario.
- Wulder, M. A. (1997). "High Spatial Resolution Remote Sensing of Forest Structure Rationale and Assessment," Unpublished Ph.D. Comprehensive Examination, University of Waterloo, Waterloo, Ontario.
- Wulder, M. A. (1998). "Optical remote-sensing techniques for the assessment of forest inventory and biophysical parameters." *Progress in Physical Geography*, 22(4), 449-476.

- Wulder, M. A., Franklin, S. E., and Lavigne, M. (1996a) "Statistical Texture Properties of Forest Structure for Improved LAI Estimates from *casi*." *18th Annual Symposium of the Canadian Remote Sensing Society*, Vancouver, B.C.
- Wulder, M. A., Franklin, S. E., and Lavigne, M. B. (1996b). "High Spatial Resolution Optical Image Texture for Improved Estimation of Forest Stand Leaf Area Index." *Canadian Journal of Remote Sensing*, 22(4), 441-449.
- Wulder, M. A., Lavigne, M. B., LeDrew, E. F., and Franklin, S. E., (1997), "Comparison of Texture Algorithms of LAI: first-order, second-order, and semivariance moment texture (SMT)." *Proceedings of the 19th Canadian Remote Sensing Symposium*, Ottawa, Ontario.
- Wulder, M. A., Mah, S., and Trudeau, D., (1996c), "Mission Planning for Operational Data Acquisition Campaigns with the *casi*." *Second International Airborne Remote Sensing Conference and Exhibition*, San Francisco, California.

Appendix A: Examples of original plot data collected in the field

119

Field Sheet - Kananaskis 1998

Crown Closure 1 Crown Closure 2

corner 1 39 43
2 42 39
3 36 33
4 41 44
centre 37 35

Plot ID:

500h

Date:

july 8/98

Time:

11:00 a.m.

Slope/Aspect:

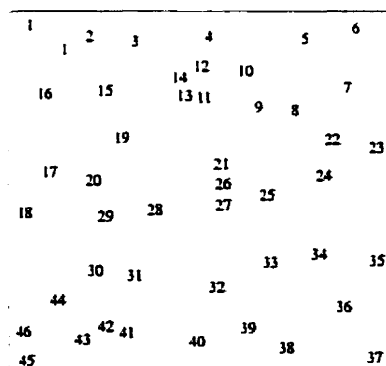
1%/200deg.

Photo #s:

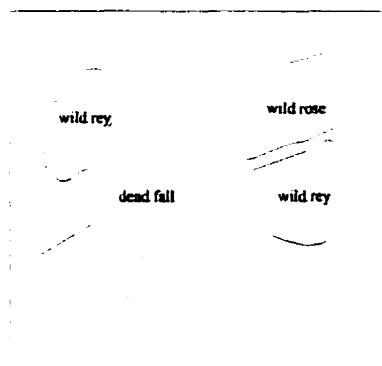
yes

Tree #	DBH (cm)	Species	Height (m)	Height to Canopy (m)	Crown Diameter at 90 degrees (m)		Comments i.e. % defoliation	GRS Crown Closure					
					Wide (m)	at 90 degrees (m)		O	M	None	O	M	None
1	11.7	Aw	7.5	6.75	2.2	1.85	80	1		x	31		x
2	25	Pl	16	9.25	4.1	4.6	na	2		x	32		x
3	23.2	Pl	16.75	9.25	3.7	2.1	na	3		x	33	aw	
4	8.5	Aw	7.75	6.5	1.2	0.76	95	4		x	34	aw	
5	17.1	Aw	10.25	8.5	3.1	2.8	25	5		x	35		x
6	8.7	Aw	8.25	6.75	1.46	1.3	95	6		x	36	aw	
7	13.5	Aw	11.25	9.5	2.58	2.61	55	7		x	37	aw	
8	5.1	Pl	3.5	3	1.59	1.47	na	8	aw		38	aw	
9	17.8	Aw	12	9.5	3.41	3.2	15	9	aw		39		x
10	12.8	Aw	12.25	9.25	1.32	2.19	60	10	aw		40		x
11	16.2	Aw	11.25	9.25	2.39	2.16	40	11		x	41		x
12	9.1	Aw	8.5	6.5	2.77	1.25	95	12		x	42		x
13	10.5	Aw	10.25	8.5	1.9	2.23	80	13		x	43		x
14	8	Aw	9	7.75	1.16	0.62	95	14		x	44		x
15	8.1	Aw	8	7.25	1.32	1.38	95	15	aw		45		x
16	11.8	Aw	10.5	8.25	2.84	1.57	70	16	aw		46		x
17	10.5	Aw	8.5	6.75	1.5	1.69	80	17	aw		47		x
18	6.9	Aw	8	6.5	0.1	0.05	90	18		x	48	aw	
19	8.8	Aw	10.25	8.25	0.84	2	95	19		x	49	aw	
20	11.1	Aw	11.25	8.5	2.58	1.51	15	20		x	50		x
21	10.4	Aw	11.25	8.75	1.55	1.28	40	21	aw		51		x
22	9.6	Aw	10	7.75	1.96	1	95	22	aw		52		x
23	9.7	Aw	12	10.5	1.87	1.28	80	23		x	53		x
24	13.8	Aw	12.75	10.75	2.79	2.24	55	24		x	54	aw	
25	7	Aw	8.25	7.5	1.43	0.96	95	25	aw		55	aw	
26	8.6	Aw	8	7.75	0.1	0.5	99	26		x	56	aw	
27	16.2	Aw	10.25	8.25	2.08	1.81	70	27		x	57		x
28	13.3	Aw	11.25	8.25	2.5	2.4	50	28		x	58		x
29	8.8	Aw	10	8	1.61	1.16	95	29	aw		59		x
30	9.3	Aw	9.75	7.75	1.81	1.35	50	30		x	60		x
31	15.7	Aw	11.5	8.25	2.7	3.13	10						
32	11.4	Aw	12.25	9.5	1.79	1.9	15						
33	12.3	Aw	12	8.75	1.43	2.19	15						
34	15.1	Aw	11.5	9	2.56	2.48	25						
35	13.2	Aw	12.25	9.25	2.46	1.62	20						
36	11.9	Aw	12.25	9.5	1.74	2.61	10						
37	7	Aw	8	6.25	1.48	0.64	95						
38	16.1	Aw	12.75	8.75	3.46	2.74	5						
39	16.3	Aw	11	9.25	1.8	1.2	35						
40	6.5	Aw	6.5	5	0.1	0.05	99						
41	8	Aw	8	7.5	0.4	0.5	95						
42	11	Aw	11	9.25	1.56	1.54	15						
43	11.1	Aw	11	9.25	1.36	1.4	70						
44	14.3	Aw	11.75	8.5	3.64	2.71	10						
45	14.4	Aw	11.75	9	1.95	1.29	80						
46	12.3	Aw	11.25	8.25	2.48	0.93	15						

O= overstory
M=midstory



tree map



understory map

N

Appendix B. Bivariate regressions for per species contributions to crown closure and per species basal area (using the first and other layers).

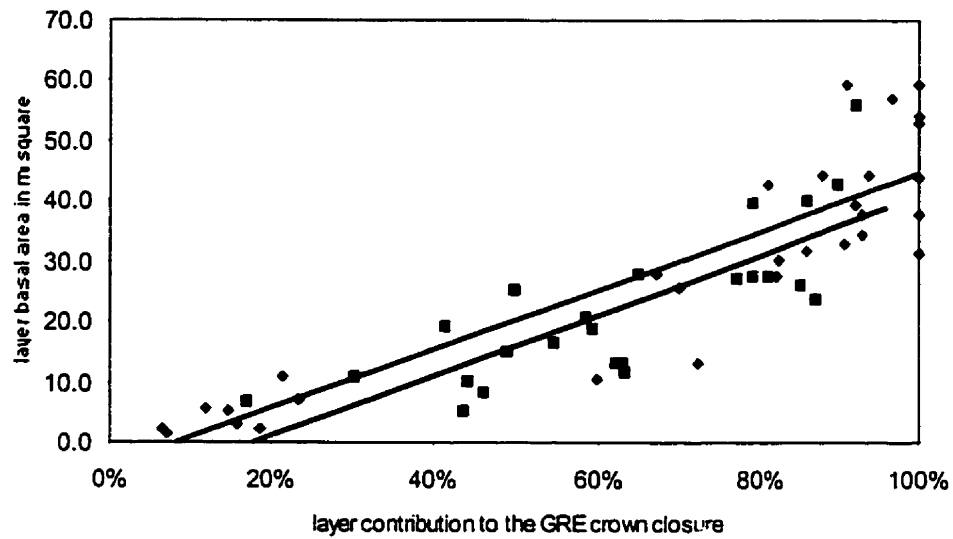
Plot ID	Per Species Contributions to GRS Crown Closure				Per Species Basal Area (m2)			
	Layer One		Other Layers		Layer One		Other Layers	
	conifer	deciduous	conifer	deciduous	conifer	deciduous	conifer	deciduous
94		100%				59.6		
500c		100%				54.2		
e2		100%				31.5		
g3		100%				52.9		
i2		100%				37.7		
i3		100%				44		
500d		91%		9%		59.4		0.2
500e		92%		8%		39.3		0.3
500hh		88%		12%		44.1		0.8
g4		86%		16%		31.8		0.7
h3		93%		7%		37.8		0.1
98		60%	16%	24%		10.7	1.9	2.9
500b		82%	5%	13%		27.7	0.4	0.9
i4		94%		6%		44.4		0.2
500i		82%	16%	2%		30.3	1.3	0.1
95		97%	20%	1%		57.1		
d3	30%	70%			11	25.8		
j1	17%	67%	1%	15%	7	27.9	0.1	1.2
500hh		72%		28%		13.1		2
f3		91%		9%		33.1		0.3
97		93%		7%		34.5		0.1
96		81%		19%		42.9		2.4
500ii	79%		21%		39.9		0.2	
500f	41%	12%			19.4	5.6		
500gg	81%		17%	2%	27.7		1.3	0.1
500k	92%		8%		56.1		0.1	
g1	50%	21%	9%	20%	25.4	10.9	1.1	2.5
500jj	43%	19%	34%	4%	5.1	2.2	2.5	0.3
99	63%	16%		21%	11.7	2.9		1
f1	58%	15%	16%	11%	20.7	5.2	0.7	0.4
1000cc	86%		14%		40.1		1	
h1	59%	7%	14%	20%	19	2.1	2.3	3.4
j2	62%	7%	3%	28%	13.1	1.5	0.3	2.6
e1	63%	7%	6%	24%	13.3	1.5	0.5	2.1
g2	96%		4%				0.3	
i1	65%		34%	1%	28.1		8.1	0.2
h2	49%		41%	10%	15.3		13.1	3.3
1000bb	44%		56%		10.1		17.6	
9	77%		23%		27.2		2.4	
500ff	55%	23%	13%	9%	16.7	7.2	1.1	0.7
19	79%		21%		27.7		2.1	
j2	85%		14%	1%	26.1		0.7	0.1
500bbb	87%		13%		23.9		0.5	
18	90%		9%	1%	42.7		0.4	
h4	46%		52%	2%	8.3		10.8	0.4

Appendix B: Per Species Contributions to Crown Closure and Per Species Basal Area Using the First and Other Layers (Data and Bivariate Linear Regressions).

Bivariate regressions between GRE crown closure and basal area for species in the first canopy layer (all significant at the 95% confidence interval)

Deciduous adjusted $R^2 = 0.804$, standard error of estimate = 0.1583

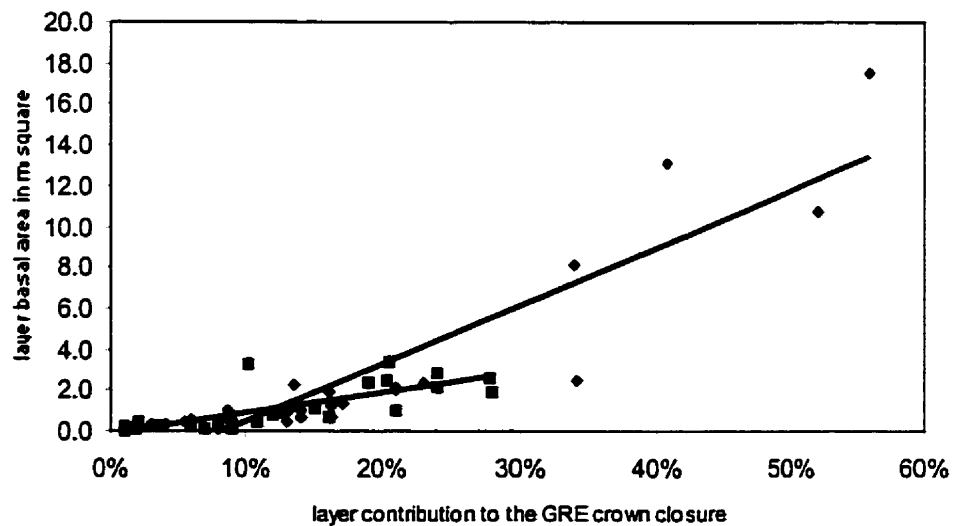
Coniferous adjusted $R^2 = 0.613$ standard error of estimate = 0.1256



Bivariate regressions between GRE crown closure and basal area for species in the second canopy layer (all significant at the 95% confidence interval)

Deciduous adjusted $R^2 = 0.574$, standard error of estimate = 0.05497

Coniferous adjusted $R^2 = 0.814$, standard error of estimate = 0.06262

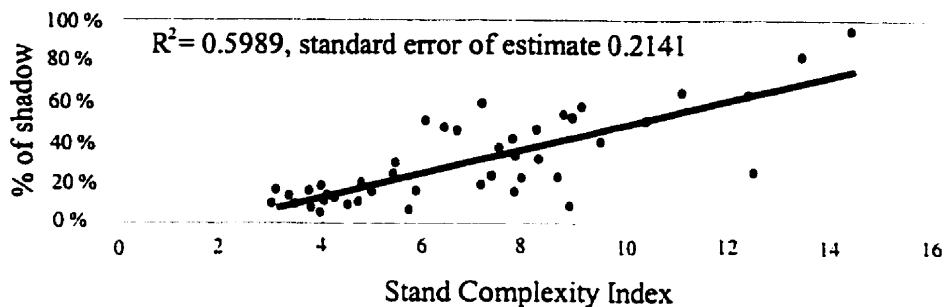


Appendix C: Per plot percent of shadow pixels and stand complexity index

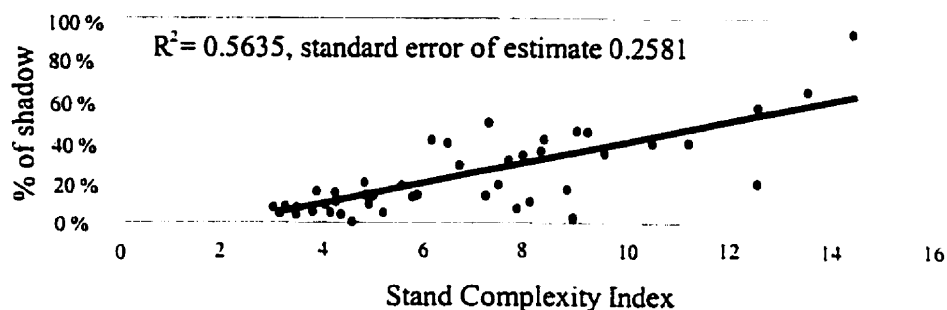
122

Plot ID	Stand Complexity Index	% per Plot Shadow Count		
		60 cm	1 m	2 m
94	3.39	13%	11%	7%
500c	3.92	5%	10%	4%
e2	3.02	11%	8%	8%
g3	7.2	17%	14%	11%
i2	5.11	15%	7%	5%
i3	4.8	12%	15%	8%
500d	7.8	15%	8%	6%
500e	3.78	15%	17%	13%
500hh	3.13	16%	10%	8%
g4	4.51	9%	3%	5%
h3	8.91	7%	2%	4%
98	4.89	17%	10%	11%
500b	8.89	51%	33%	45%
i4	4.09	12%	7%	5%
500i	5.9	15%	15%	19%
95	9.55	37%	35%	40%
d3	3.75	11%	10%	90%
j1	5.76	60%	15%	17%
500hh	4.82	20%	21%	22%
i3	4.01	14%	9%	6%
97	8.76	22%	17%	14%
96	4.25	12%	18%	22%
500ii	3.45	11%	90%	12%
500f	7.28	58%	50%	46%
500gg	8.34	32%	40%	41%
500k	8.28	45%	36%	37%
g1	9.21	55%	44%	42%
500jj	13.58	78%	63%	73%
99	7.66	37%	31%	27%
f1	6.12	49%	41%	40%
1000cc	5.48	23%	19%	19%
h1	7.84	33%	34%	30%
j2	7.43	22%	18%	18%
e1	4.25	11%	80%	10%
g2	5.54	29%	20%	25%
i1	12.58	24%	19%	13%
h2	8.05	20%	11%	18%
1000bb	10.52	48%	39%	37%
9	12.55	60%	55%	51%
500ff	9.01	50%	45%	40%
19	6.48	47%	39%	40%
f2	14.52	90%	88%	69%
500bbb	6.7	45%	30%	27%
18	7.88	39%	33%	27%
h4	11.23	63%	40%	41%

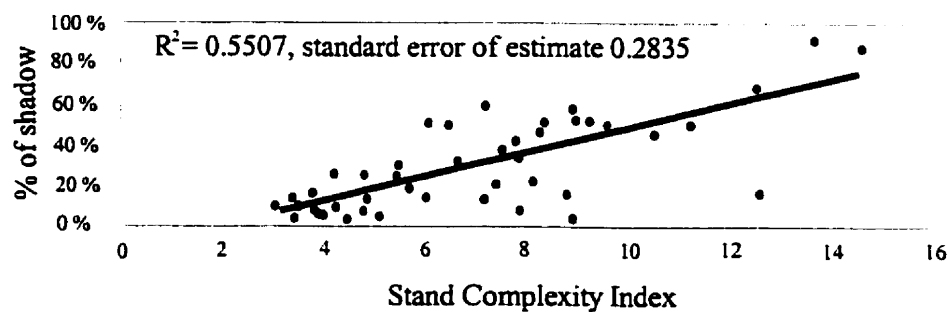
Per plot % of shadowed pixels and the Stand Complexity Index for the 45 plots on 60 cm casi imagery (all significant at the 95% confidence interval).

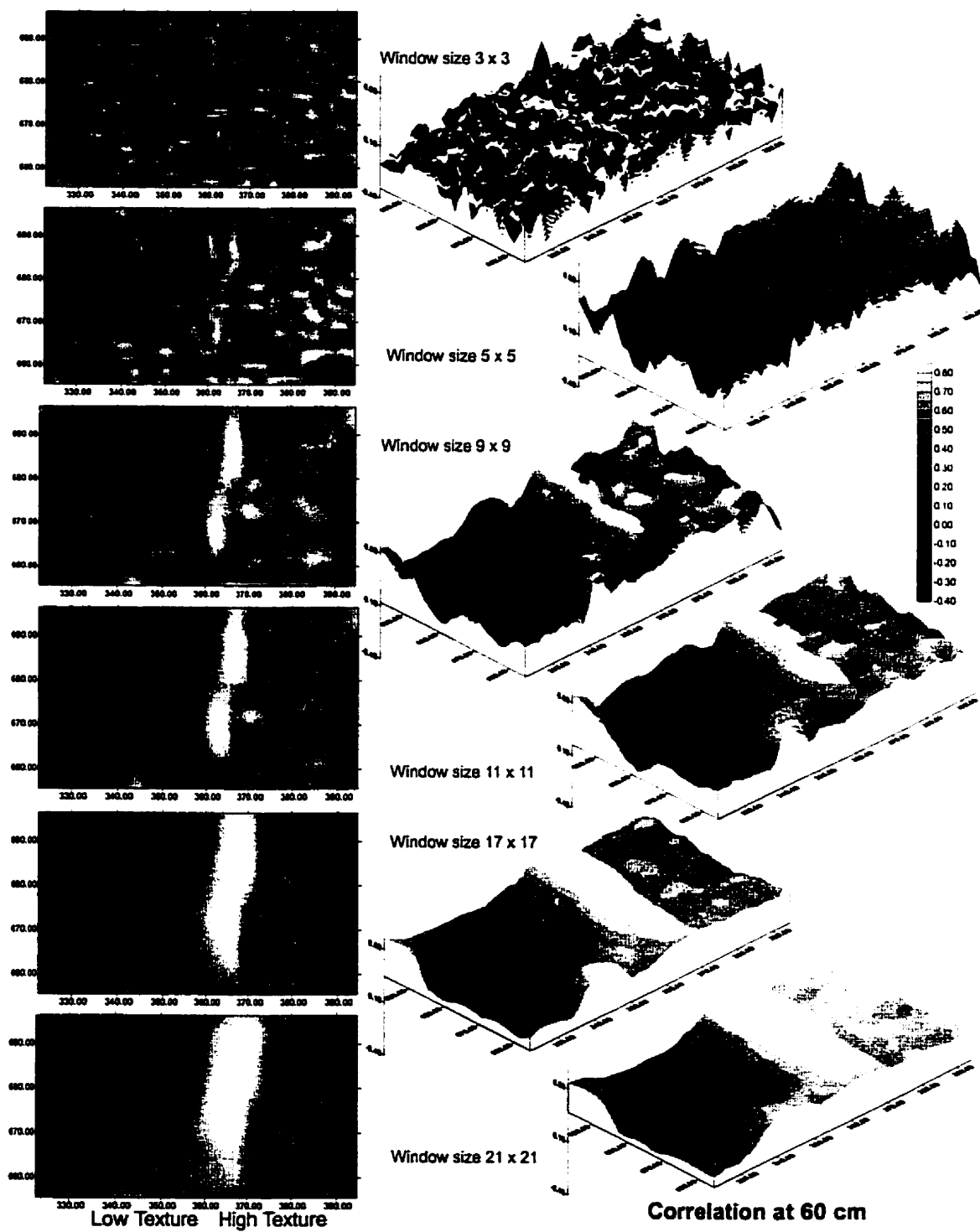


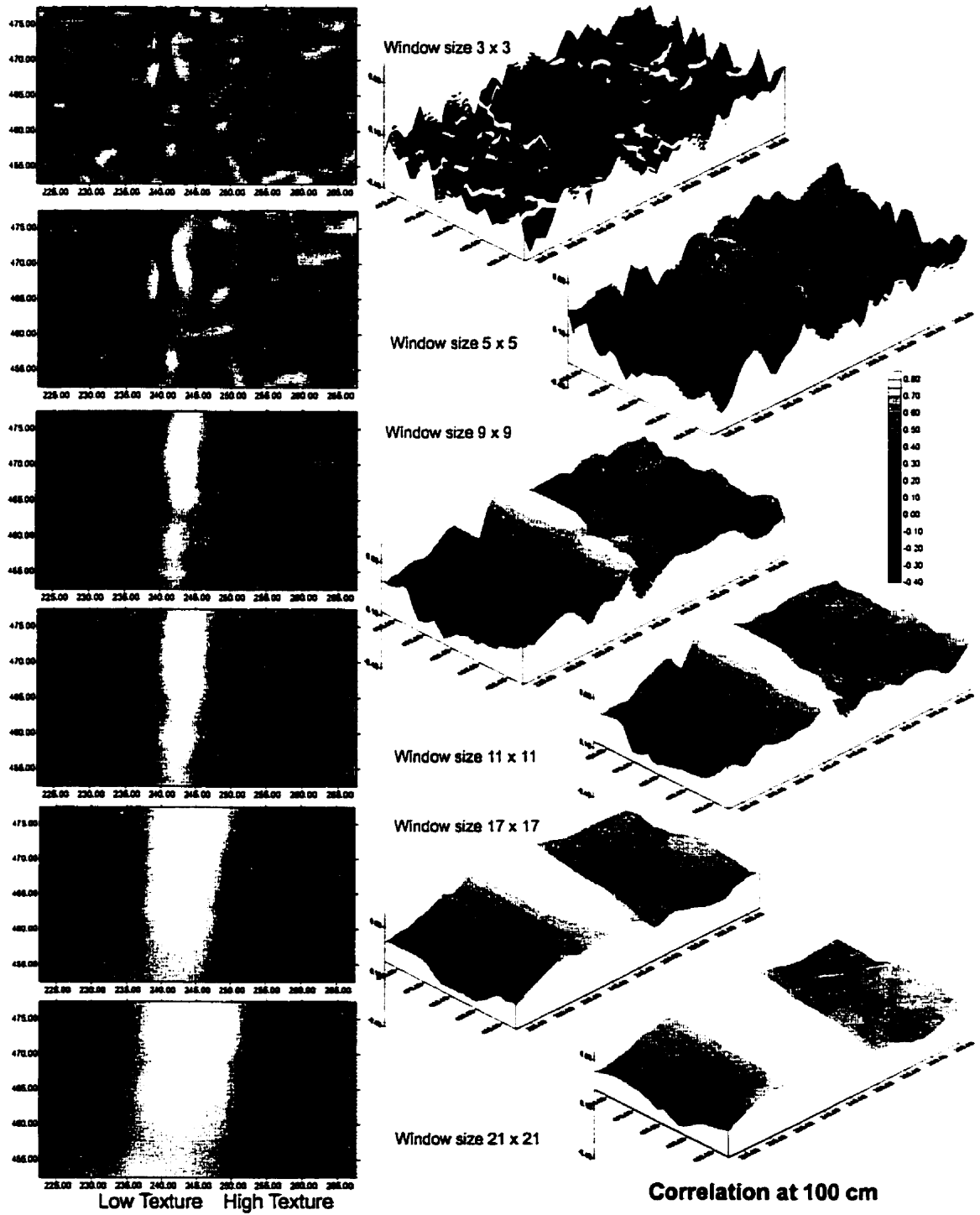
Per plot % of shadowed pixels and the Stand Complexity Index for the 45 plots on 1 m casi imagery (all significant at the 95% confidence interval).

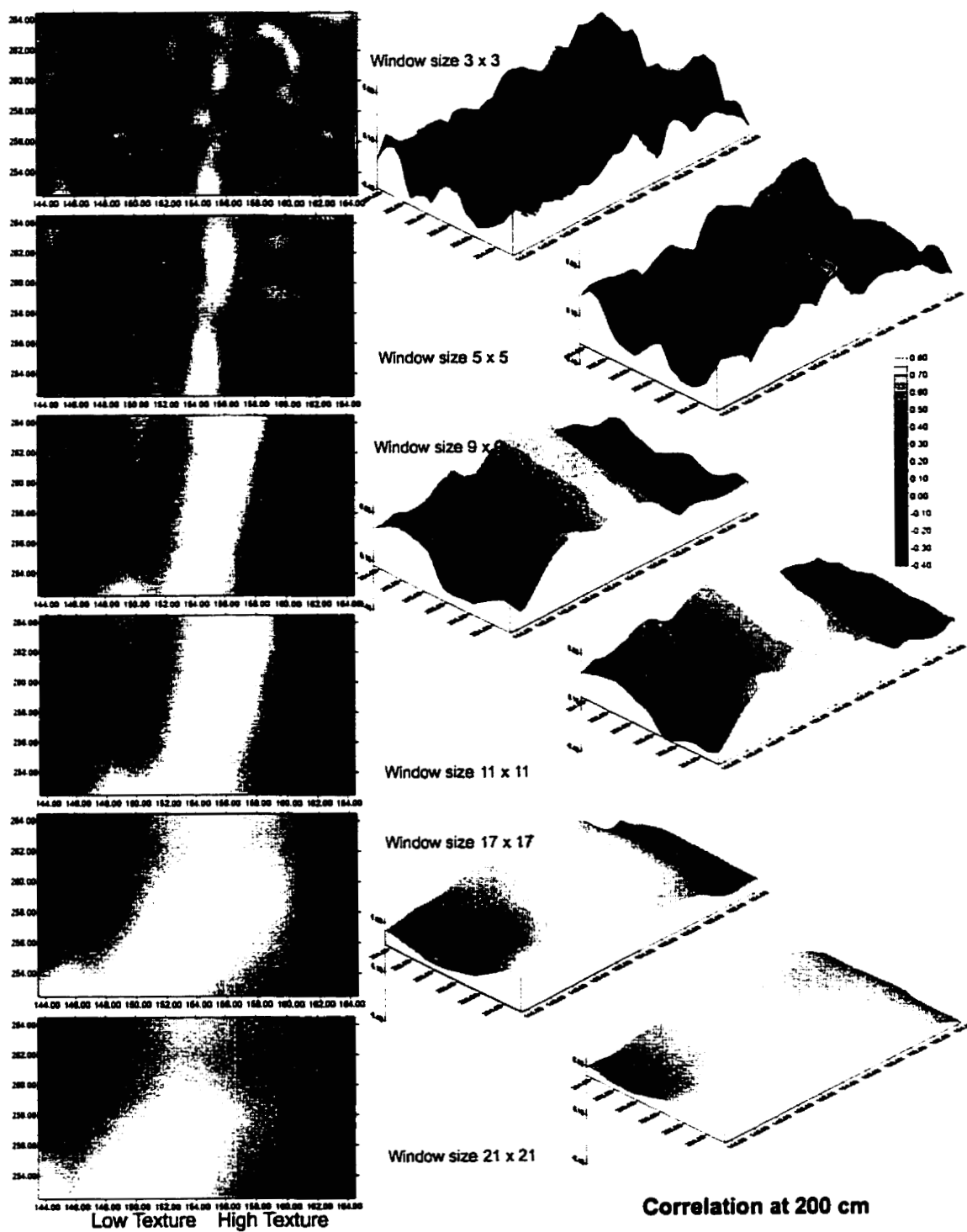


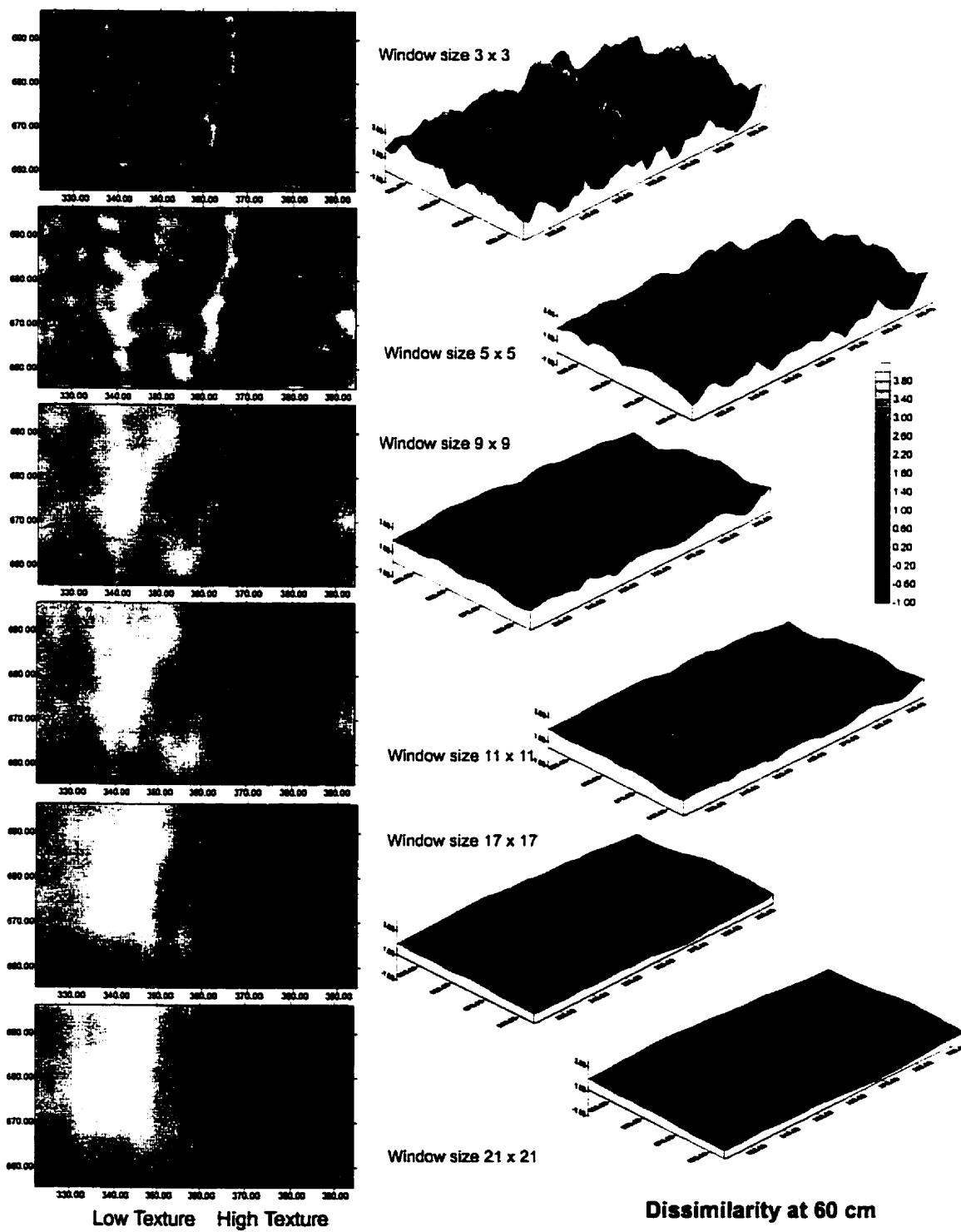
Per plot % of shadowed pixels and the Stand Complexity Index for the 45 plots on 2 m casi imagery (all significant at the 95% confidence interval).

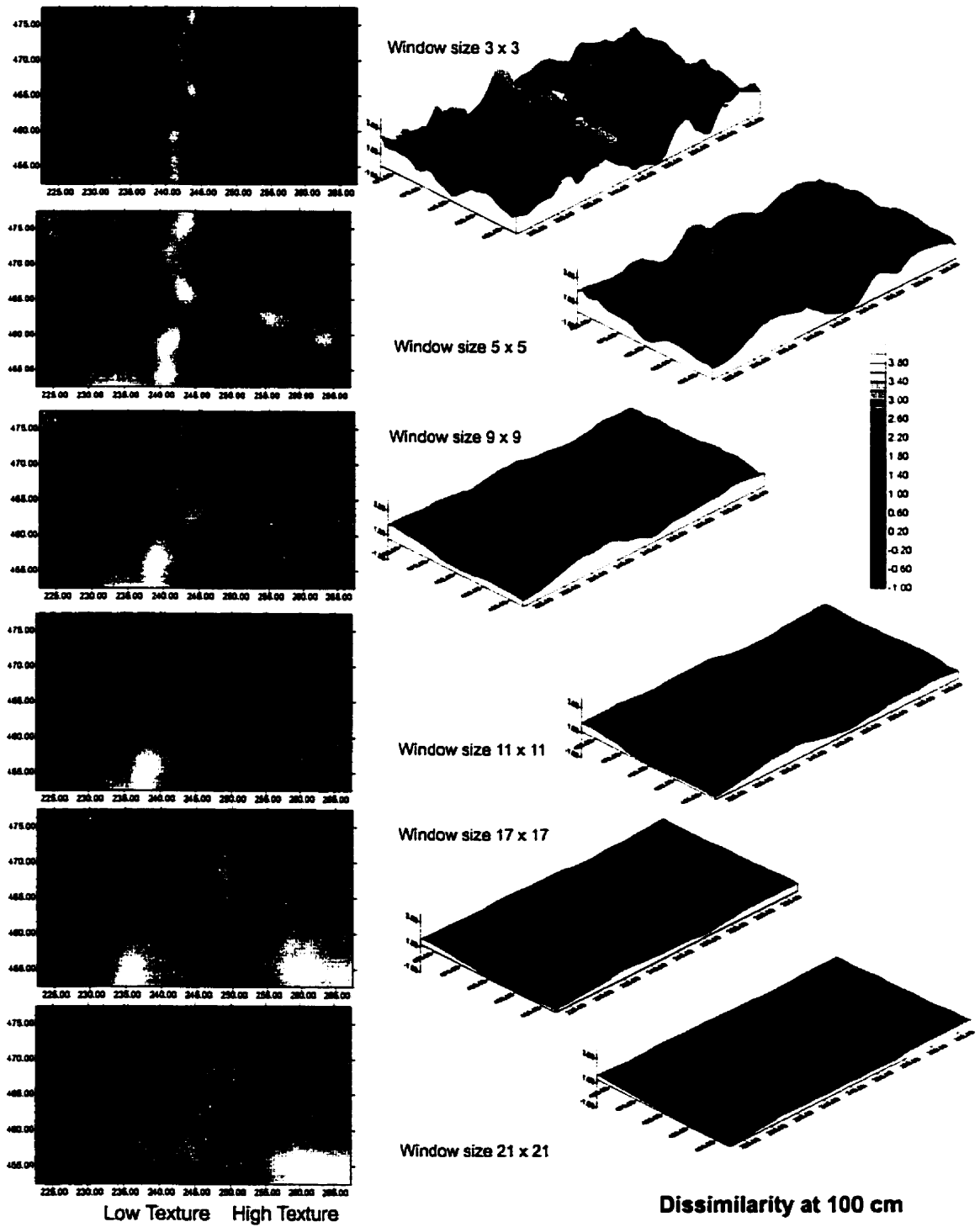


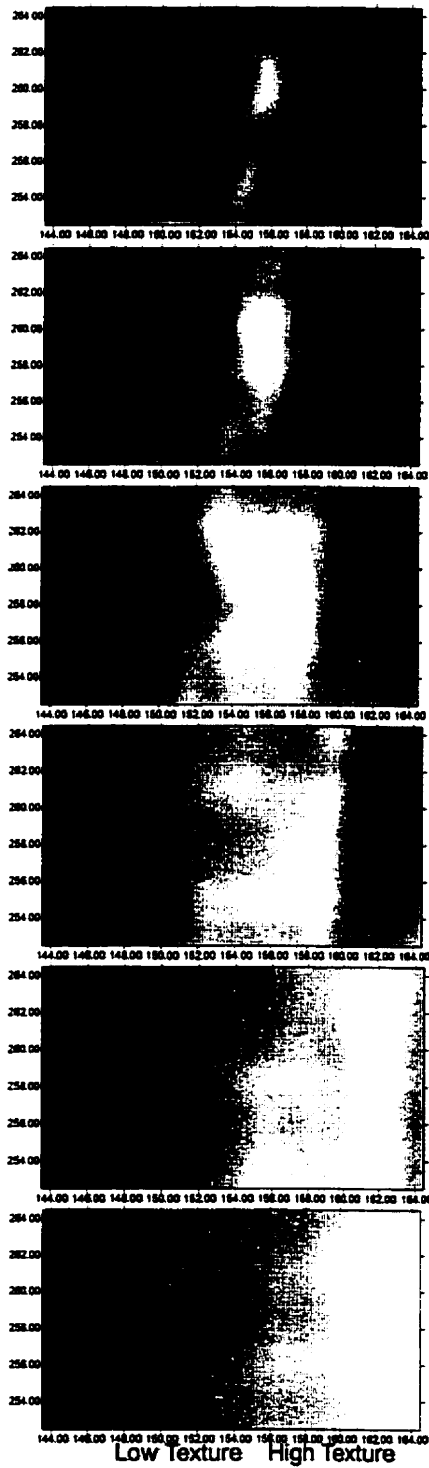




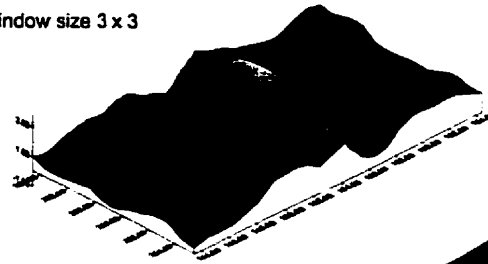




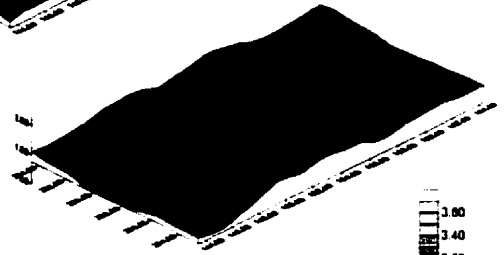




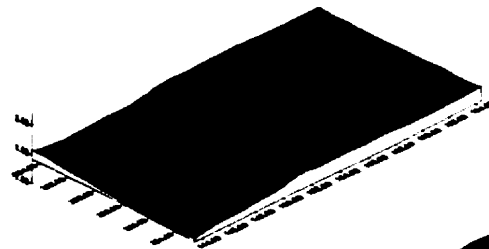
Window size 3 x 3



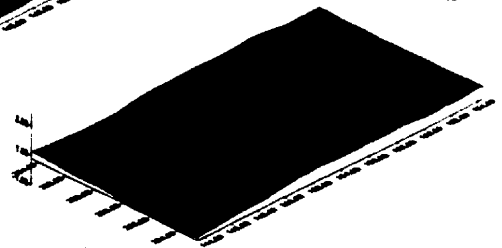
Window size 5 x 5



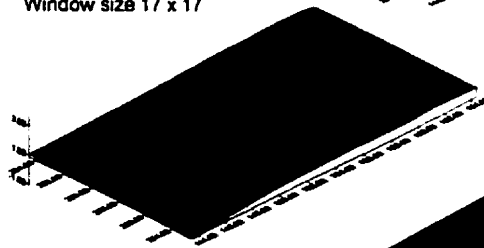
Window size 9 x 9



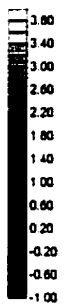
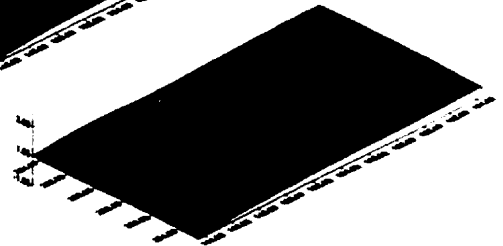
Window size 11 x 11



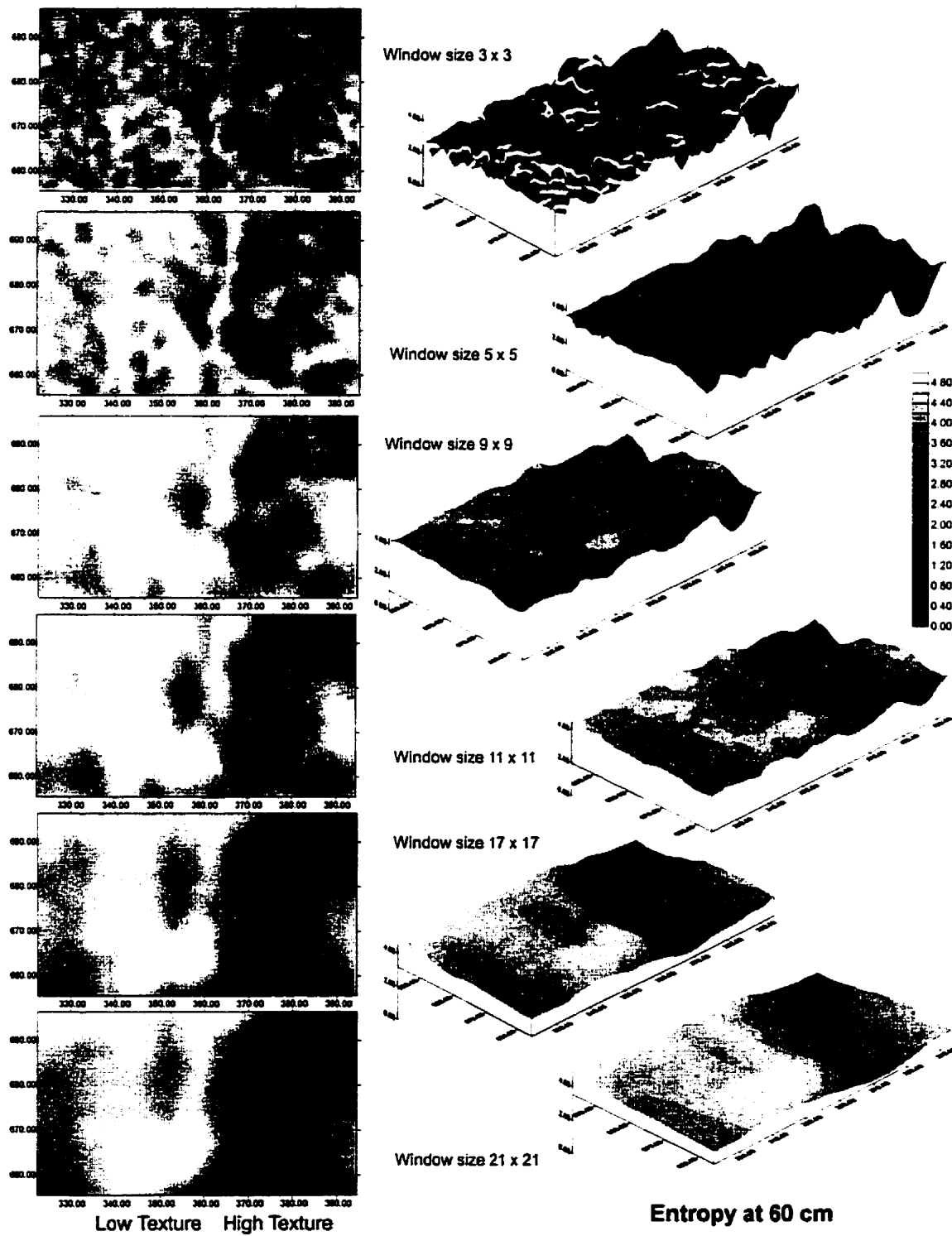
Window size 17 x 17

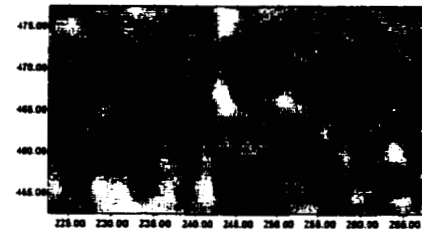


Window size 21 x 21

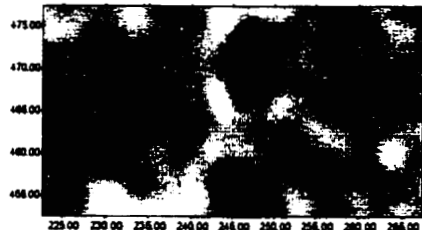
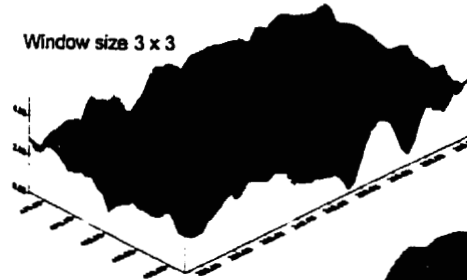


Dissimilarity at 200 cm

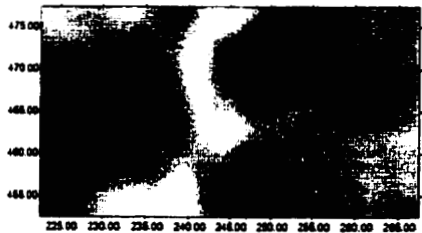




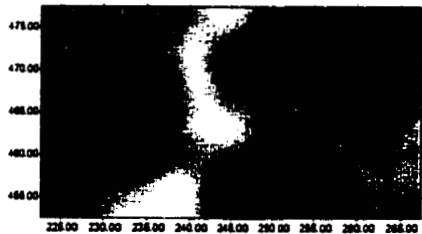
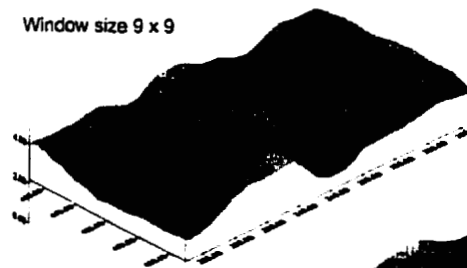
Window size 3 x 3



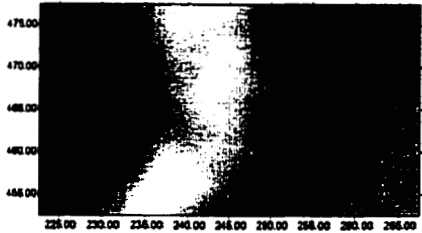
Window size 5 x 5



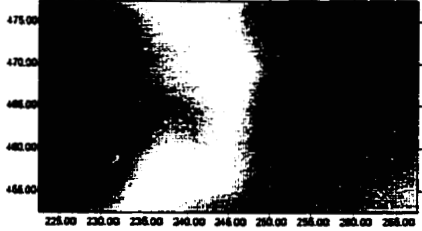
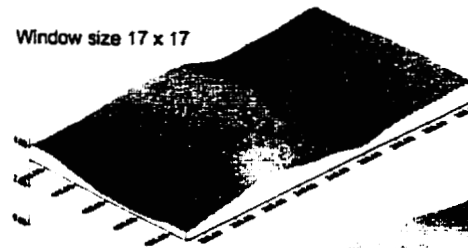
Window size 9 x 9



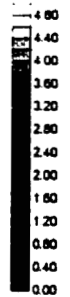
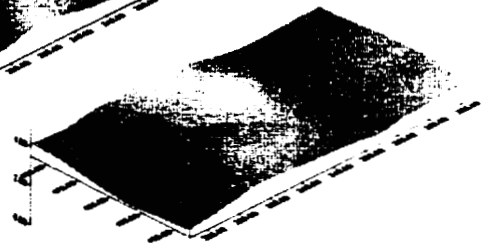
Window size 11 x 11



Window size 17 x 17

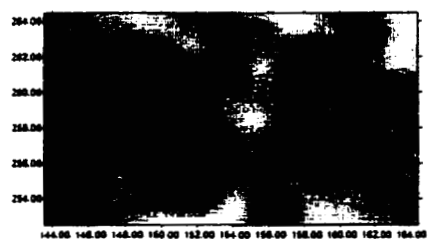


Window size 21 x 21



Low Texture High Texture

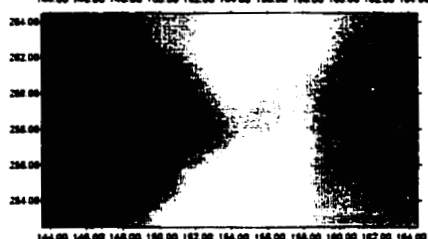
Entropy a 100 cm



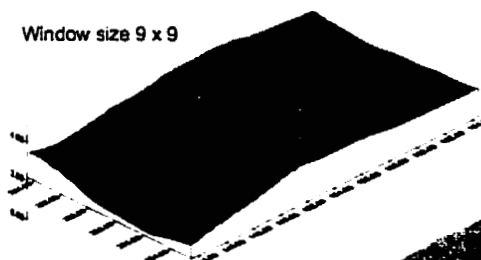
Window size 3 x 3



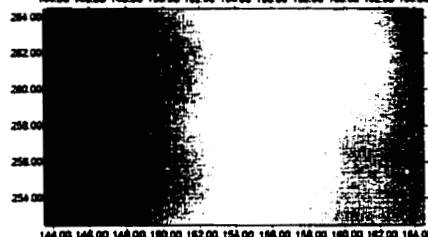
Window size 5 x 5



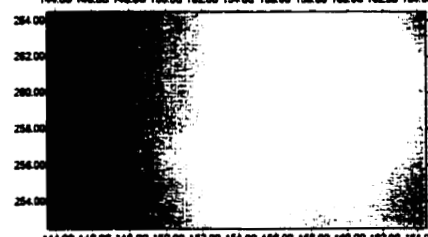
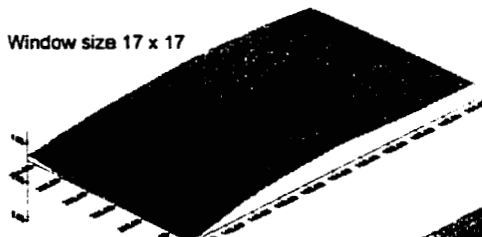
Window size 9 x 9



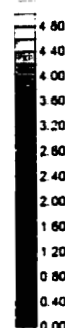
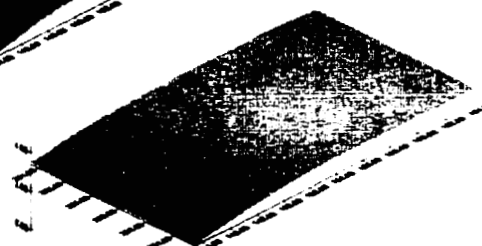
Window size 11 x 11



Window size 17 x 17

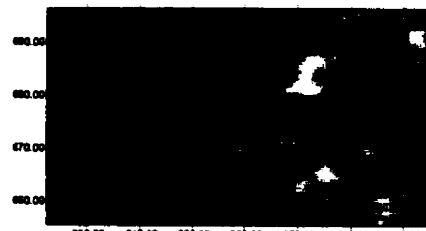


Window size 21 x 21

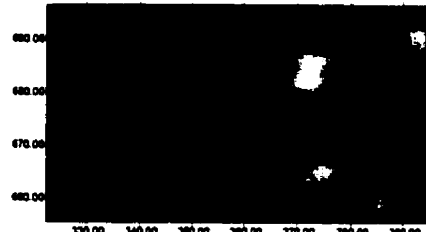


Low Texture High Texture

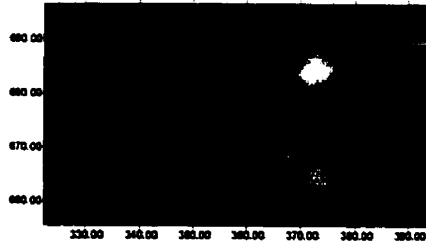
Entropy a 200 cm



Window size 3 x 3



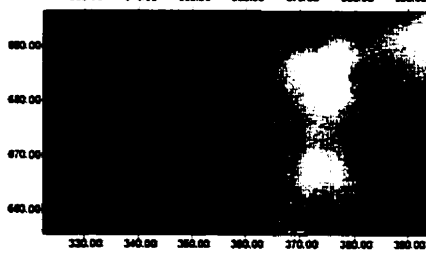
Window size 5 x 5



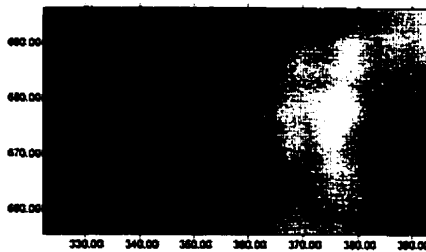
Window size 9 x 9



Window size 11 x 11

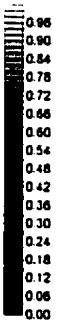
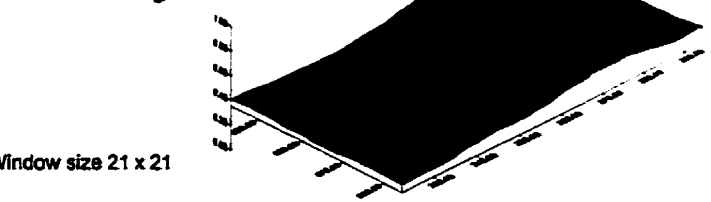
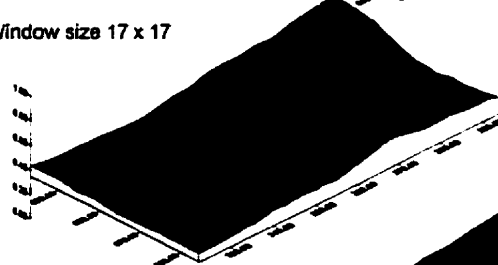
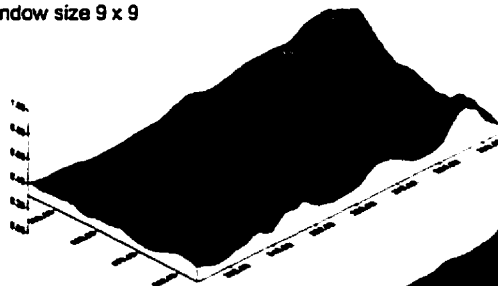
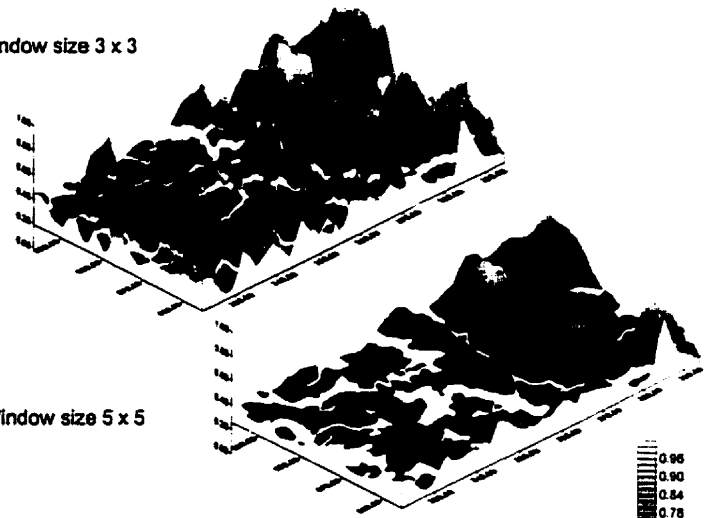


Window size 17 x 17

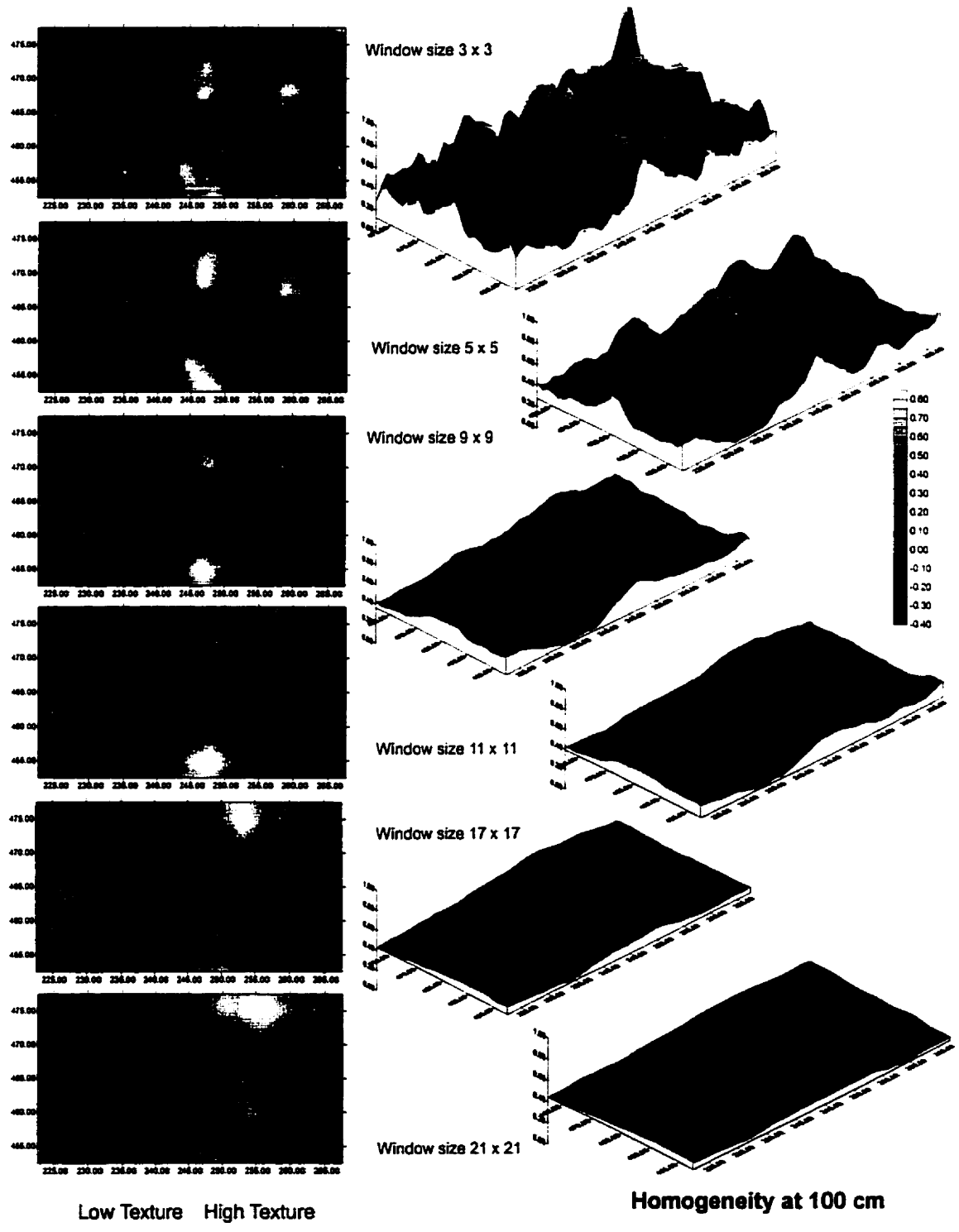


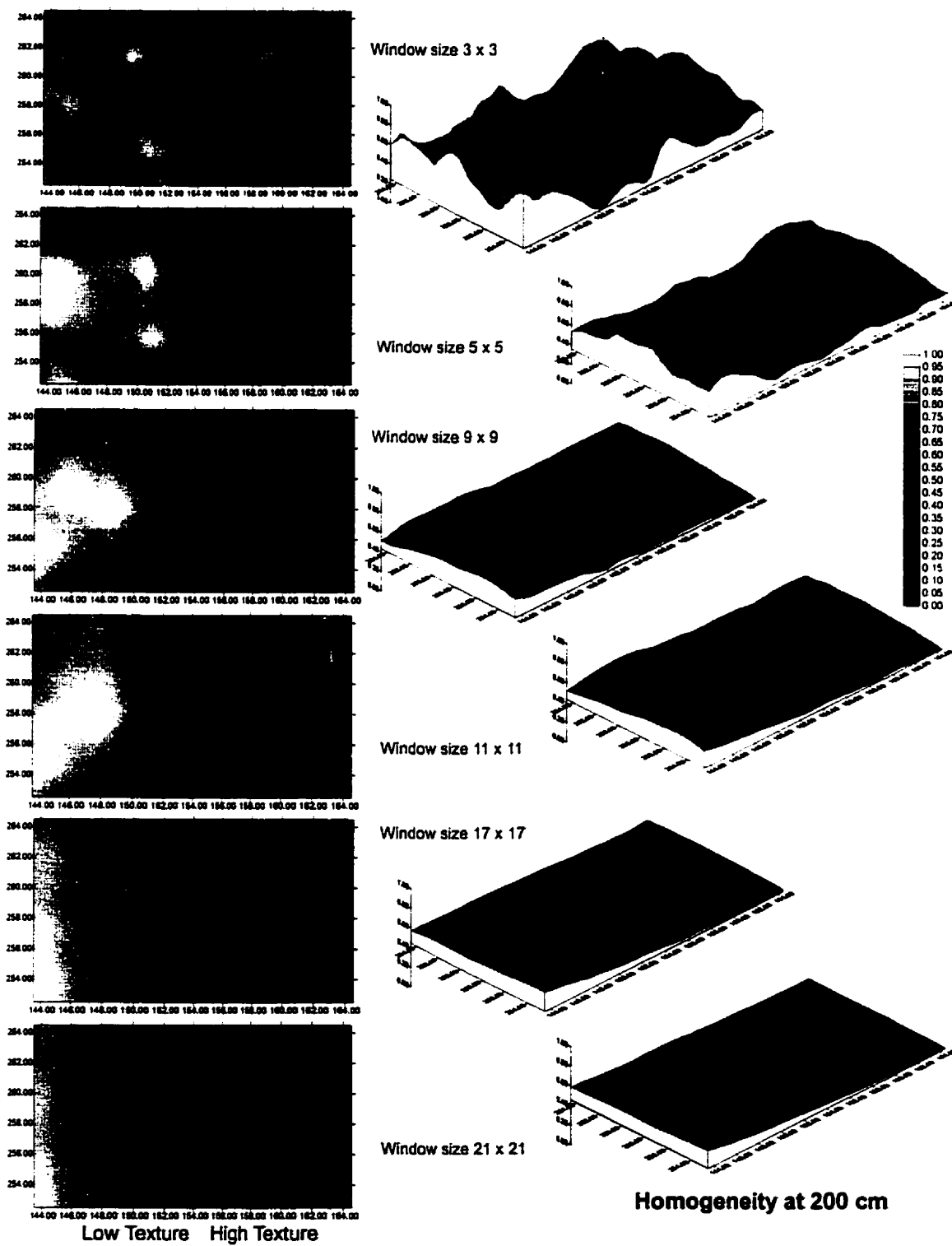
Window size 21 x 21

Low Texture High Texture



Homogeneity at 60 cm





Appendix E. Radiance for aspen (showing range of defoliation) and conifer stands using 60 cm *casi* data

*Radiance for aspen (showing range of defoliation) and conifer stands using 60 cm *casi* data*

